The University of Salford

School of Computing, Science and Engineering

MSc by Research in Robotics

Design and Development of an Anthropomorphic Metamorphic Robotic Hand

Dissertation submitted to the University of Salford in complete fulfilment of the requirements for the degree of Master of Science by Research in Robotics.

By

Olegs Marcenko

@00370152

Supervisor

Dr. Guowu Wei

November, 2018

Contents

The List of Figures

The List of Schematics

DECLARATION OF ORGINALITY – CONDUCT OF ASSESSED WORK

ASSESSED WORK WHICH DOES NOT HAVE THIS FORM ATTACHED WILL NOT BE ACCEPTED

Research Degree Programme……

Assessment Title ……..……..

Title of the report ……...

Family name of candidate ……..
(in BLOCK CAPITAL LETTERS)

Given name of candidate……....
(in BLOCK CAPITAL LETTERS)

ID number: ……

In presenting my Interim Assessment / Internal Evaluation (please delete as appropriate) I declare that I have read and understood the University Policy on Academic Misconduct

(available at http://www.salford.ac.uk/about-us/corporate-information/governance/policies-and-procedures/browse-by-theme/2) and that:

1. this work is my own
2. the work of others used in its completion has been duly acknowledged
3. I have been granted the appropriate level of ethical approval for my research

Signature of candidate: …… Date: ……

Acknowledgements

I would like to express my gratitude to my supervisor Dr. Guowu Wei for his patience and knowledge. I am very happy that I was able to get involved into challenging robotics theory and improve my understanding of the field. Also, I would like to thank Catriona from postgraduate office for her support and understanding. My family was supporting me during studies and I would like to thank them for everything they have done for me.

Abstract

This work presents analysis of the 4-fingered robotic hand and is a continuation of the Bachelor's thesis "*Design and Development of an Anthropomorphic Metamorphic Robotic Hand*". First, general comparison between scientific and commercial robotic hands is introduced. Specification and structure of the hands are studied. Noted tendencies are discussed. After that, kinematic analysis of the proposed manipulator is produced. Based on kinematics, dynamic model of the hand is investigated and then programmed in MatLab software for numerical simulations. Therefore, description of capabilities and properties of the proposed robotic hand is given. In addition, control techniques are discussed and SimMechanics tool of the MatLab software is used for providing supplementary data. In the end, FEA of vulnerable areas is briefly examined.

Chapter 1
Introduction and Objectives

1.1. Introduction to Robotics

Science and engineering today make complicated designs possible and ideas from the past decades can eventually find realization. Manufacturing technologies continuously improve, allowing key parts to be transferred into small scale. Robotics industry will be one of the first to experience new capabilities.

In terms of robotic manipulators, when the first industrial robot was introduced by Dr. Engelberger[1], manipulator patterns represented simple grippers with two or three elements to compress an object. In course of time, more demanding tasks to robotic hands were given. Then, anthropomorphism of the robotic hands has proven that the approach is viable and prospective if precision grasping of complicated objects is considered. Unlimited interest in anthropomorphic designs was then expressed and various prototypes were developed.

It is not only the industry that benefits from the advances in robotics sphere, but also medicine and prosthetics. Artificial body parts were developed even centuries ago, there are evidences that survived the time.[2] It was important for people with lost limbs to look the same as others – to feel themselves 'complete'. Nothing has changed since then in terms of understanding completeness. Although ancient prostheses were rather cosmetic improvements than functional models, with higher level of technological progress it is now possible to almost fully retrieve natural limb functionality.[3]

While being an industry with a long historical background, robotics field gained significantly more attention in last few years, which resulted in increased funding and rapid growth of the sector. There are two main points of research interest – industrial robots and prosthetics. As the society tends to focus on automatizing most of the processes for both convenience and safety purposes, industrial robotic demand significantly increased. The International Federation of Robotics (IFR) states that the worldwide supply of industrial robots increased

by approximately 15% each year since 2017 and by 2020 is expected to be almost twice the number of robots supplied in 2016.[4]

As the competition increases, robotics industry attracts more scientist from various fields to improve the quality of the product, its functionality and safety of operation. Industrial robotics is focused on the simplification of production process, however, most of the robots still lack the artificial intelligence for complete autonomy and hence require the supervision of a professional to minimize the number of mistakes made during the manufacturing process. Therefore, robotics industry also attracts AI specialists, apart from material scientist, engineers and others, making it a high demanding interdisciplinary sector with plenty of development opportunities.

Another robotics discipline which deserved attention in last decades – is prosthetics. While attracting researchers from all physical disciplines, it is closely related to medicine and human psychology. If for industrial robots it is important mostly just to be able to functionate in a time- efficient and safe manner, usually regardless of size and complexity of the mechanism, then for prothesis requirements are stricter. Main points of concerns in prosthetics are the size and weight of the body part. Due to the size restrictions for customer satisfaction, production of a highly functional and sophisticated body part becomes a complicated process. Despite the market having a well-fitting to human needs prothesis for arms and legs, there is always more to be achieved with the development of medicine and physical sciences.

The minor part of robotics research is focused purely on producing functional stand-alone robots, with no direct relation to any of the discussed industries. For example, these can be surveillance, delivery, bomb disposal, rescue, animal-like or space robots. However, research in this field is vital too as it increases overall understanding of robotic systems and allows advanced methods to be employed in other sectors of robotics.

As a general idea, any robotic system is meant to improve human life – artificial autonomy in secondary daily tasks, autonomy in difficult repetitive manipulations, research of other planets, body performance enhancement (exoskeleton) or simply limb replacement.

1.2. Objectives

This work presents the metamorphic anthropomorphic robotic hand, which utilizes the principles of gear transmission and actuator integration. In order to fully analyse its structure and performance, the following objectives were set:

- Produce the literature review and assess the common tendencies that are present on the market and in the research society.
- Provide detailed description of the robotic hand CAD model and discuss the features it has.
- Assess the kinematics and dynamics of the proposed design; develop and simulate the dynamic model.
- Describe the strategies of how the robotic hand may be controlled.
- Evaluate the weaknesses of the design and produce the FEA of vulnerable areas.
- Based on the retrieved overall results, suggest improvements for the design and future work.

Chapter 2

Literature Review

In order to rightfully compare modern robotic hands and identify their unique design points, it is necessary to introduce two categories into which they will be split. Most of the robotic hands (quantity, not types) are made with ideas of high pragmatic approach – final product is based on profit and high production volume criteria. That said, durability and simplicity are main factors to be considered. Usually those hands have particular market and specific area of competence. Hence, they fit in commercial category. The other robotic hands, however, represent various prototypes to show maximum performance and abilities, broad potential and application, and, sometimes, just to acknowledge possibility of concept materialization. Those specimens are often made regardless of price matter, weight and aesthetics. Therefore, such robotic hands are closer related to scientific category. Scientific hands are a basement for the future commercial products.

2.1. Background of Commercial Hands

- Bebionic hands [A]
- Vincent Hand [D]
- The i-Limb hands [C]
- Michelangelo Hand [E]
- DLR hands [B]
- Body powered or electric fingers as partial hand options from Advanced Arm Dynamics [F, G]
- BarrettHand [H]
- Robotiq adaptive gripper hands (2-3 fingers) [J]

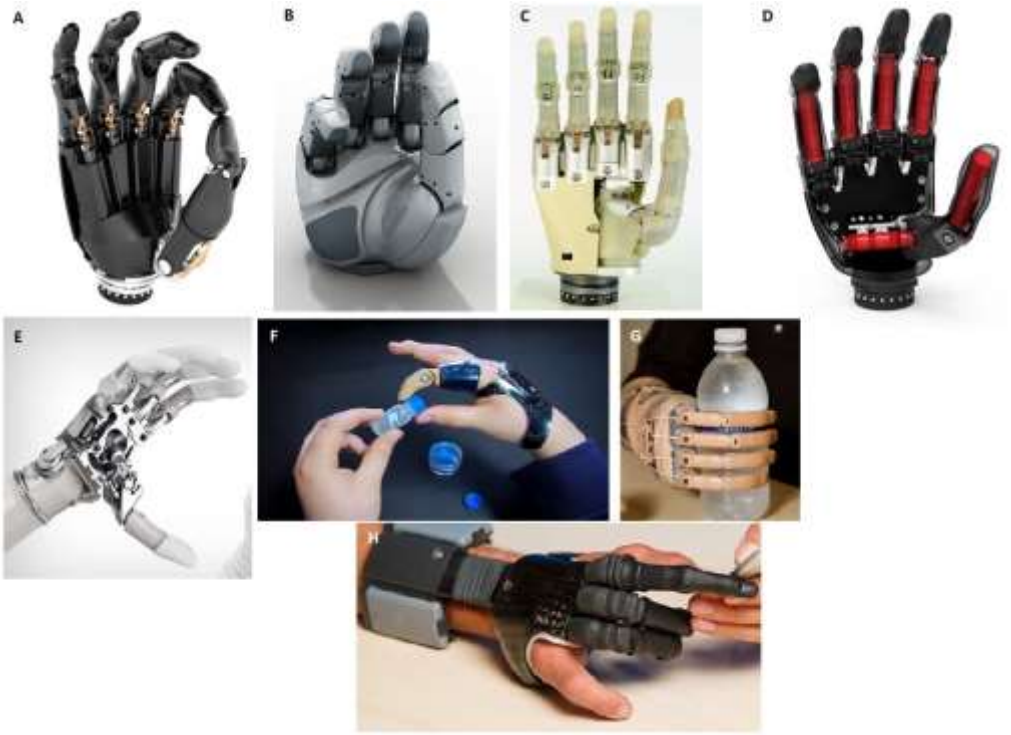

Figure 2.1. Commercial robotic hands for prosthetics and other uses

Figure 2.2. Commercial robotic manipulators for industrial applications

2.1.1. The i-Limb hands

Presented in 2007, i-Limb hand by Touch Bionics was first electrically driven multi-joint prosthetic hand.[5] Since each joint was powered individually, movement freedom has significantly increased in contrast to other prosthetic hands available at that time. For such breakthrough in prosthetic field, i-Limb hand won the MacRobert Award for Engineering and Limbless Association's Prosthetic Product Innovation Award in 2008.[6,7] In 2010, Touch

Bionics introduced the i-Limb pulse, the hand had more anatomically correct design, improved durability and increased pulsing grip strength.[8] Starting from the i-Limb pulse hand, patients could modify the hand via a special software. Over the next few years, company focused on improving the grip strength, durability and the shape of the prosthesis. The i-Limb quantum was launched in 2015 with a revolutionary simple control of the grips.[8] The hand is easy to operate and modify for the patients (via mobile application) and also offers faster speed and longer battery life than previous Touch Bionics products.

2.1.2. Bebionic hands

First Bebionic hand by RSLSteeper was introduced in 2010. During the presentation of the hand in Leipzig, amputees had an opportunity to try the prosthesis in action. The appearance of the Bebionic hand is one of the key points that company focuses on as it makes patients more confident about their choice. In 2011, RSLSteeper launched Bebionic Hand v2, which came in large and medium sizes. It showed overall performance improvement, including speed, accuracy and durability. Significantly, several new grip patterns were added.[9] New Bebionic3 was presented in 2012. It offered greater precision with faster speed and grasp strength. Bebionic3 comes with several wrist options, including multi-flex wrist that allows more natural wrist movement and positioning (up to 30°).[10] This year (2017), Bebionic was bought by Ottobock company and all further progression will be led by the new company.

2.1.3. Vincent Hand

Vincent Hand was first presented in 2010, at the same conference as Bebionic hand. It had the size and shape similar to the natural human hand. An option of production different hand sizes was also present without anatomical proprotions.[5] The hand allows various types of basic grips: cylindrical, precision, lateral, hooking and key. There are, however, more options available for professional use.[11] In 2014, Vincent Systems GmbH presented Vincentevolution 2 – first prosthetic hand with touch sensing.[12] The hand allows amputee to feel the force feedback, which makes gripping much safer and natural. Vincentevolution 2 has anatomically correct size and shape of the hand, natural skin-like cover and ability to feel how strong one is holding an object.

2.1.4. Michelangelo Hand

Michelangelo hand is the prosthesis produced by Ottobock (German manufacturer) in partnership with Advanced Arm Dynamics (American company), that joined the research in 2008. The hand has anatomically correct shape and low weight. The main drawback of the hand is that only thumb, index and middle fingers are actively moved: ring and little fingers

just follow the driven ones. Thumb, however, can be moved separately and as a result, more hand positions are possible.[13] The Michelangelo hand has a special, stretchable wrist joint (AxonWrist) that allows two possible modes: flexible and rigid. The flexible mode allows greater movement freedom and therefore provides the hand with an opportunity of more natural behavior.

2.1.5. DLR hands (Commercial)

DLR is a national aeronautic and space research center of Germany. Its division – Robotics and Mechatronics Center – is a competitive developer of various robotic hands. DLR Hand I – one of the first robot hand in which all the motors and electronics were housed within the space of the hand – was presented in 1997 and induced active research in integrated mechatronics.[14] DLR Hand II is an improved multisensory hand produced in 2001. Second DLR hand also has fully integrated actuators and electronic, but the shape of the hand was changed and amount of cabling was greatly reduced.[14] Designed multisensory hand is mostly oriented on service use, such as teleoperation.[15] The DLR Hand II is used on Rollin' Justin – a humanoid robot for various service operations including both household use and assistance to astronauts.[16]

DLR Hand II application require high precision of finger position and applied force. Great control is achieved by utilizing multiple sensors, including three motors and three joint position sensors on each finger, three torque sensors and several temperature sensors. [17] Since actuators and electronics are integrated into the hand, it can be easily employed on various robots. Design of the hand allows fingers to be bend backwards, which provides more grasping options.[15] DLR Hand II has reconfigurable palm that adds one more DOF (additional to 3 DOF in each finger). Such palm allows different grasps to be effectively obtained.[16]

Based on DLR Hand II, a commercial DLR/HIT hand was produced in 2004, in cooperation with Harbin Institute of Technology (HIT). DLR/HIT hand is also a 13 DOF (degrees of freedom) four-finger hand with 3 DOF in each finger apart from thumb, which has an extra DOF for grasping and better manipulation functions. Hand has integrated actuators and amount of cables is reduced to four excluding power supply (in comparison to 400 in DLR Hand I and 12 in DLR Hand II).[18] Sensor system was also improved in comparison to DLR Hand II. Amount of sensors did not change, however, Hall effect based (contactless) joint position sensors were used instead of potentiometers.[18] In 2007, DLR/HIT hand gained IF Design Award.

With further development, DLR/HIT hand II was produced. It has five (instead of four) fingers with 3 DOF each (15 DOF in total). Despite having more fingers, hand is smaller and lighter than the previous version due to use of smaller and flatter motors and drivers.[19] Second generation of the hand has become more human-like as the overall weight and size were reduced. An extra DOF from the thumb was removed, as it had no particular impact in the manipulation.[19] The DLR/HIT hand II is used on humanoids for telemanipulation.[20] This hand also gained iF Design Award in 2009.

2.1.6. BarrettHand

BarrettHand is a multi-fingered grasper that is used in multiple fields including component assembly, food industry, handling of various materials and others. The hand has enough dexterity to operate with objects of different shape, weight and size. Flexibility and high precision allows such applications as glass handling and even bomb disposal.[21]

2.1.7. Body powered or electric fingers as partial hand options from Advanced Arm Dynamics

There are many partial hand options available from various manufacturers, including i-digits by Touch Bionics and VINCENTpartial. Advanced Arm Dynamics, is an American company that works with multiple prosthetic hand developers to supply amputees the prosthesis they require. One of the products is partial hand prosthesis that is designed for people who miss only some of the fingers. There are various options, including body powered and electric fingers.

An example of body-powered prosthetic finger is an M-finger. It comes in two versions: full finger and partial M-finger. These fingers are designed to restore the functionality of the hand, not the appearance. Full M-finger is mounted at MCP joint and are moved via Spectra cables (special cables with low friction coefficient) on the wrist.[22] Partial M-fingers are fixed at residual phalanx if sufficient length is present. Both partial and full M-fingers come in different lengths and colours to suit patient's requirements. Electric fingers are built specifically for the patient in order to match other fingers and specific requirements.[23]

Although many options are available for partial prosthetics, the best option is selected according to the activity and work requirements, some medical indications and desired appearance of the finger.

2.1.8. Robotiq adaptive gripper hands (2-3 fingers)

Robotiq is Canadian company that focuses on production of service robots. Company produces two types of grippers: two-fingered and three-fingered. Two-fingered hand has several application fields, oriented on human-work replacement with automation. It is used for machine loading and unloading, automated assembly and in quality control.[24] The gripper is reported to be simple in installation and control, ensuring compatibility with most of industrial robots.

The three-fingered hand gripper has similar application fields with an option of use in advanced manufacturing, as it is more dexterous and precise in comparison with two-fingered gripper. The hand is suitable for all industrial robots and is designed to pick object of any shape with maximum recommended payload of 10 kg.

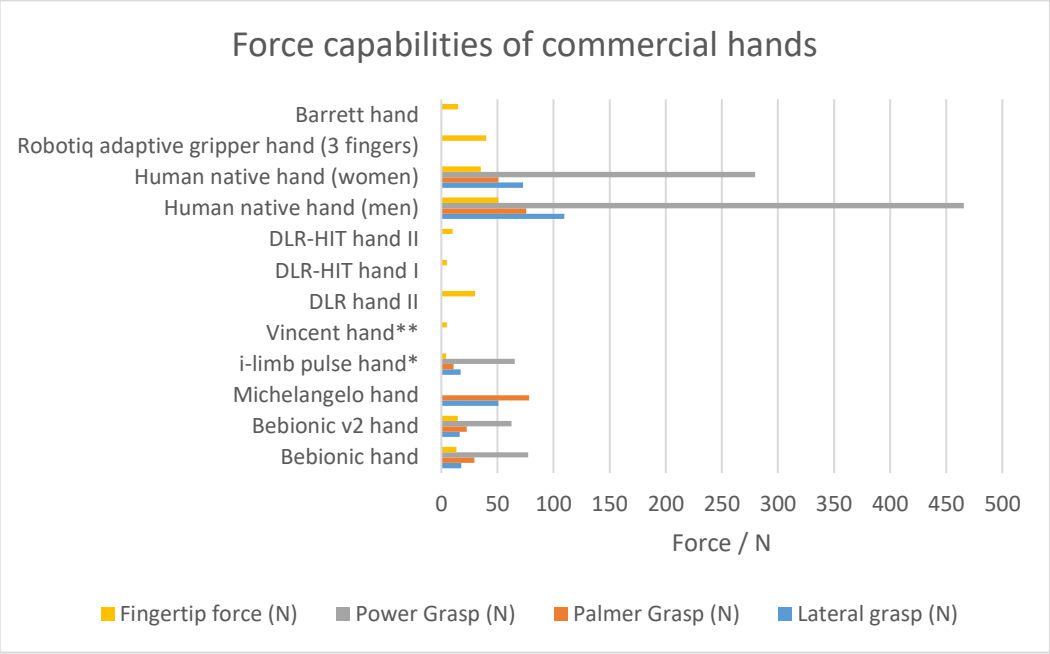

Figure 2.3. Force capabilities of commercial hands

Unfortunately, not all the manufacturers provide the full force capabilities of their hands, however, it is still possible to compare some of them based on the information summarised on figure 2.3.

Among the prosthetic hands available for purchase, the Bebionic hand shows the greatest potential of providing enough grasp force for everyday life. It's power grasp force is still dramatically lower than the potential grasp force of human hand, but not all of the grasp strength is used in everyday life, unless there are specific requirements for individual. Bebionic hand also provides reasonable palmer grasp force, but not the lateral grasp.

The hardest point to achieve is the similar fingertip force as the human hand can provide. None of the commercially available prosthetic hands can provide sufficient fingertip force, which may make it harder for user to use their prothesis fingers to full extent.

The robotiq adaptive gripper hand is the only hand which provides similar fingertip force and hence can be effectively used in manufacture field or factories.

The lateral grasp can hardly be implemented by prosthetic hand. Michelangelo hand provides only half of the potential male human hand lateral grasp force, whereas the other hands cannot produce even a quarter of a human hand potential.

Despite the force capabilities limitations of prosthetic hands, they still provide sufficient strength for most of everyday tasks and hence simplify life of injured individuals and increase the overall standard of living.

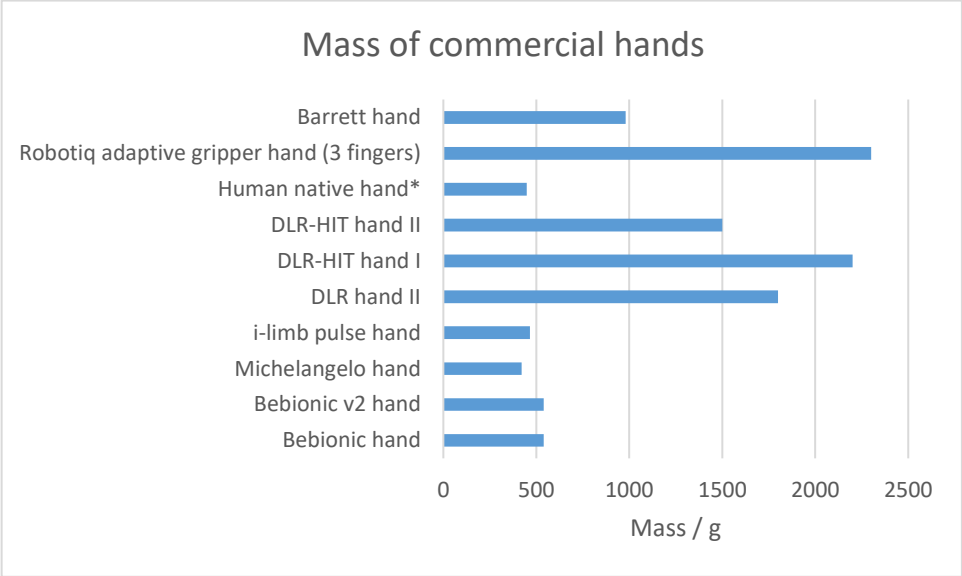

Figure 2.4. Mass of commercial hands in grams

Masses of commercially available hands are in reasonable range based on the areas of application. So the prosthetic hands are in a range of 460-550 grams, which is similar to the approximate average mass of human hand. Any other prosthetic hand, which is not included in the report, should also fall in the given range as it is the standard requirement for medicinal purposes.

The non-medicinal robotic hands are much heavier due to the requirements of the application field. So the Robotiq gripper hand, which is more likely to be used in factories, is the heaviest

of the listed hands: just above the 2.25 kg. The second heaviest hand is DLR-HIT hand, which reduced the size and mass in the second generation.

The weight of the commercially available hands differs dramatically based on application, however, the mass of the particular hand is always likely to be in an acceptable range for the robot utilisation field.

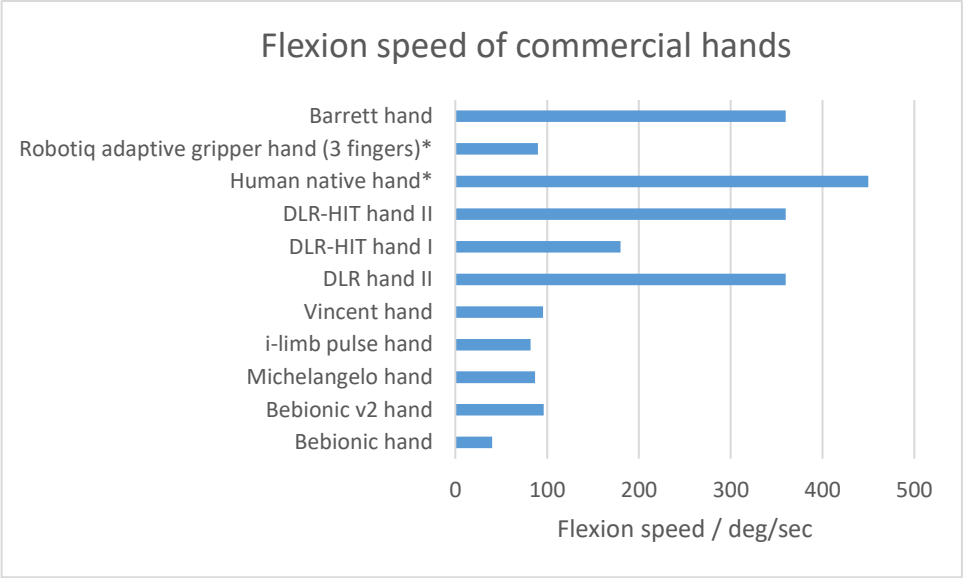

Figure 2.5. Flexion speed of commercial hands

Another point of comparison robotic hands is the flexion speed they provide. Based on the figure 2.5, the main drawback of the commercially available prosthetic hand can be identified to be the flexion speed. The second generation of Bebionic hand provides the fastest flexion speed of all the prosthetic hands, however, it is still less than ¼ of the human hand capability.

The lack of flexion speed affects person performance in emergency situations, such as inability of catching the falling object. This is the common situation in everyday life and hence the small flexion speed will affect the performance of disabled person quite dramatically. However, apart from the unexpected situations of objects falling, the flexion speed is acceptable in most of the activities. The process of flexion is still much slower than for human hand, but the ability to do so already improves the quality of life of disabled person.

Other robotic hands, such as second generation of DLR hands and Barret hand, provide a comparable flexion speed to human hand potential. The Robotiq gripper hand, which was leading in previous points of comparison, has flexion speed similar to prosthetic hands. But in

case of the gripper, the precision and strength of grip are more important than the speed of flexion.

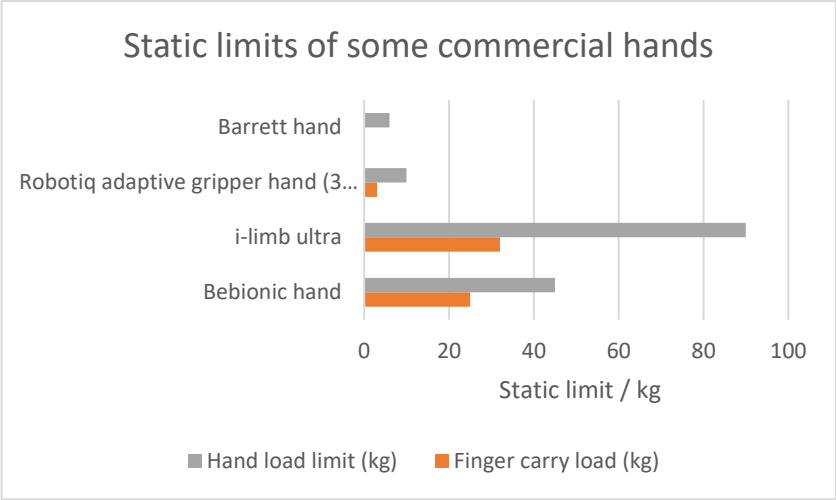

Figure 2.6. Static limits of commercial hands

Static limits are rarely provided by the manufacturer; however, it is an important parameter, especially for the prosthetic hands. Based on figure 2.6, it can be concluded that i-limb ultra prosthetic hand, greatly outstrip the Bebionic hand. This may be an advantage for individual who requires a high load limit to be present. On the other hand, the hand load limit of approximately 45 kg in Bebionic hand, should be sufficient for most of the everyday activities. Considering other advantages of Bebionic hand listed above, it may still show the great performance in heavy loading.

The finger carry load is nearly similar for both of the available prosthetic hand, with i-limb ultra being about 10 kg further.

The non-prosthetic robotic hands have much lower static limits, which seriously affects the range of fields where these hands can successfully be used.

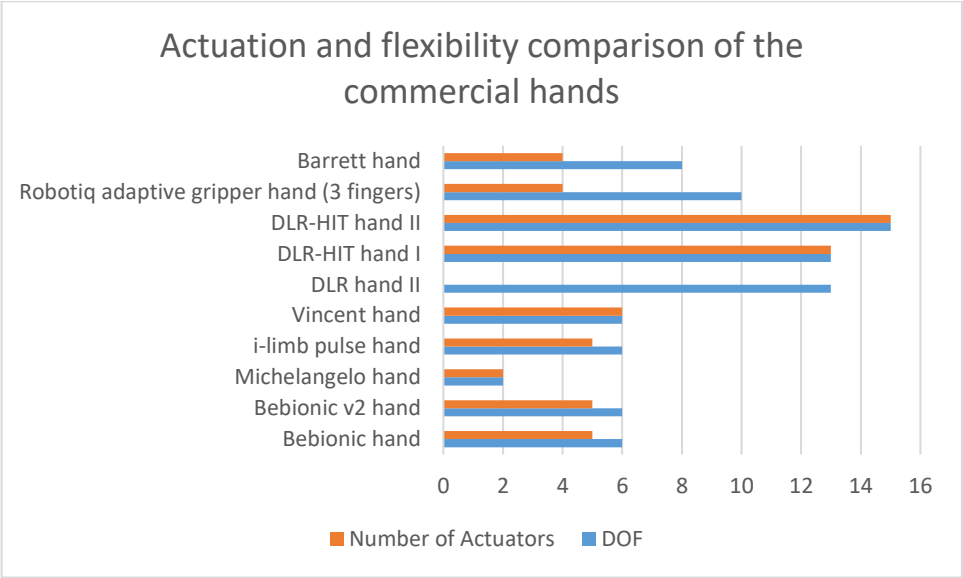

Figure 2.7. Actuation and flexibility of commercial hands

As shown on figure 2.7, commercially available hands are either underactuated or fully actuated. Most of the prosthetic hands are underactuated, which slightly affects the ability of the hand to follow the commanded arbitrary trajectory. The fewer number of actuators, however, reduces the weight of the prothesis, which is more desirable than exceptionally accurate motion control for everyday use. The number of degrees of freedom (DOF) is similar for most of the prosthetic hand, which is expected as it should obey the human hand characteristics.

The DLR hands have much larger number of DOFs and are fully actuated, therefore, they are much more precise in motion. This also explains the large mass (up to 2.25 kg) of the prototype and provides an idea of why there cannot be many actuators in prosthetic hands at this stage of the robotics field development.

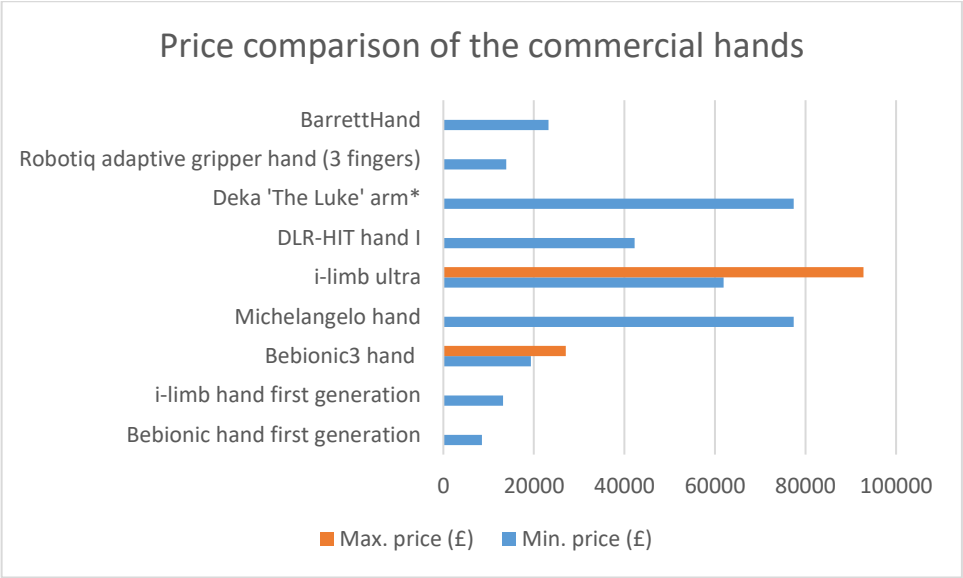

Figure 2.8. Prices of the commercial hands

The final point of comparison is the price of the discussed hands. As expected, the range of prices is huge due to the various reasons including the materials used, performance characteristics and application field.

Prosthetic hands prices differ mostly based on similarity of visual appearance of the prothesis to human hand: the more alike the prothesis is, the higher the price. Due to the human nature, individual is more likely to prefer the weaker hand but which looks similar to the natural hand, rather than a high-performance but dissimilar to human hand prothesis.

The non-prosthetic hands also differ in price, mostly based on the performance characteristic: the more efficient hand is, the higher the price. Therefore, DLR hand is much more expensive than Robotiq gripper or Barrett Hand.

*Although the Deka Arm (‘Luke Arm’) is a system that includes more parts than just a hand (literature review aims to observe hands, not arms), it is still considered for the reference purposes. Deka arm was a scientific project and only recently in 2014 was approved by FDA (U.S. Food & Drug Administration)[25], making it commercial product. It is important to note that mentioned price is set for the product which has the latest technologies integrated and allows user to have sensitive feedback. It also supports targeted muscle reinnervation (TMR)[26] that vastly enhances control of the arm.

2.1.9. Comments

Prosthetic robotic hands that are currently present on the market tend to have a rigid palm structure to store actuators. Their number of DOF is optimised in the way that the size of the

hand would be human-like, but at the same time providing considerable force and grasp variety for daily operations. In addition, excessive number of actuators leads to increased weight of the prosthesis, extra power requirement (battery), enlarged proportions and less acceptable shape. Distinctive characteristics dramatically influence production costs and final price of the product.

As for industrial applications, anthropomorphism is not required for basic manipulations with objects, so therefore grippers are mostly used as an inexpensive and reliable solution.

2.2. Review of Scientific Robotic Hands

- Biomimetic anthropomorphic hand by Zhe Xu and Emanuel Todorov [A]
- DLR hands [David's Hand – B]
- Elu-2 Hand [C]
- KCL 3-finger metahand [D]
- Modular soft robotic gripper [E]
- RBO Hand 2 [F]
- Multifingered metamorphic hand by G. Wei et. al. (has options of 4 or 5 fingers) [G]
- The Robonaut Hand [H]
- UB Hand I-IV [I]
- The SmartHand [J]
- The Shadow Hand [K]

Figure 2.9. Scientific robotic hands

2.2.1. Biomimetic anthropomorphic hand by Zhe Xu and Emanuel Todorov[27]

The idea of this hand strongly relies on the desire of many engineers to replicate human natural hand. Introduced on the 18th of February 2016[28], the robotic hand represents an outcome of the mentioned aim and elastic materials. Its structure includes tendon-based actuation with cooperation of unique and novel parts like elastic pulley mechanisms, laser-cut extensor hood, artificial joint capsules and crocheted ligaments. In terms of bones re-creation, laser/MRI scanner was used to carefully capture shape of bones. In order to prevent abnormal sideways bending of each joint of the hand, artificial ligaments as strong fibrous tissues are applied. Also, index finger, as well as middle finger and thumb, is actuated with more than two servo motors ensuring extra control. Human hand similarity ensures high number of DOF (Degrees of Freedom).

To evaluate hand prototype's efficiency and kinematics in action, it was tested using telemanipulation technique with sensory glove. Manipulations with the prototype evaluated drawbacks that will have to be carefully studied further. Underactuation of the fingers may put some of them into unknown postures between full flexion and extension. Good point of it is additional level of compliance and automatic object shape adjustment. In general, empirical research has shown acceptable percentage of finger motion (trajectory) repeatability, which means that the prototype is successful. Novel hand design makes real complicated

manipulations with objects, grasps; and overall it is an important contribution to the prosthetic science. As for minor drawbacks, servo motors are housed outside the hand, so that additional space for the actuation system is required. Also, tendon-based systems are known for the relative durability.

It would be important to point out that this hand is a working prototype that shows possibility of the concept, so further development will take place.

2.2.2. DLR "David's" Hand

DLR hands were discussed in details in commercial hands section. However, DLR has produced an unusual robot hand that is not available commercially. The David's Hand is the same size and shape as human hand. The hand has five separately movable fingers with each joint being actuated with two motors.[29] Fingers are controlled with 38 tendons, which results in 19 DOF. Flexion speed of each joint is described as 720 deg/sec. Apart from structure similarity, hand was designed to function as a natural hand: to withstand collisions with heavy objects without breaking.[30] High durability is achieved because of the controllable stiffness due to the produced tension in tendons. Therefore, David's hand can endure large impacts. The hand utilizes strong Dyneema tendons.[29] The production of such durable hand can reduce the risks of significant damage dealt to the robotic hand during its application in real world. The David's hand is part of DLR Arm System, which is presented in form of David – robot developed in 2010 in order to achieve more human-like dexterity, dynamics and robustness.[31]

2.2.3. Elu-2 Hand

Elu-2 Hand is a multi-articulated robotic hand produced by Elumotion Ltd. The hand has five fingers with 9 DOF. It was designed to produce movements at human-like speed and therefore may easily interact with people and various tools and object in the environment.[32] Elu-2 Hand is also known as Servo-electric 5-Finger Gripping Hand SVH and is distributed by SCHUNK. The hand comes in left- and right-handed versions, both of which can be fitted to most of light industrial robots.[33]

2.2.4. KCL 3-finger metahand

The first metamorphic robotic hand was produced by Professor Jian Dai in 2003. The concept of the palm made complicated dexterous grasp and manipulations possible.[34] Metamorphic hand is foldable with several DOF and therefore adds more dexterity to the hand. Because the palm is not rigid, motion of fingers must be combined with folding of the palm, which was a unique robotic hand system at that time.[35] The metahand has three underactuated fingers

which orientation is dependent on the palm's motion.[36] The foldable hand adapts to various shapes of the object and hence has wide range of possible applications.

2.2.5. Modular soft robotic gripper[37]

Soft robotics is entirely new approach in robotics and it is a totally new direction in the history. There are not yet many systems engineered using this technology, but the modular soft robotic gripper is one of them. It was introduced in a scientific paper in 2015. Main contrast and advantage of the soft robotics compared to solid designs lies in the pursue of many scientists to obtain perfect compliance of their robotic mechanisms. Main industrial solutions represent designs like already mentioned BarettHand and Robotiq grippers with corresponding limitations. Aim of the modular soft robotic gripper is to successfully grasp objects of the unknown shape. Gripper's specifics allows interaction with very fragile, delicate objects. Therefore, this area of research is remarkably, supremely advanced and prospective. As a general downside of the soft manipulators, it is pointed out that due to extra compliance it would be problematic to predict particular pose of the soft gripper or hand, although very likely to obtain object's shape. The study was manly focused on enveloping and pinch grasps.

Presented soft robotic gripper is underactuated with pneumatics. It is currently made with main idea to be attachable to fingers of the solid hands or manipulators. Presented work outlines serious superiority over solid manipulators in terms of grasp tenderness.

Drawbacks evaluated during the study list sensor readings being unacceptably noisy. Further research will also involve additional attention to sensorial classification of the objects for better grasp accuracy. In addition, slippery and heavy objects do represent certain level of problem and should face an engineering solution in the future.

2.2.6. RBO Hand 2[38,39]

While some soft robotic systems are tested and addressed more for industrial use, meanwhile there are interesting examples of anthropomorphic soft robotic designs intended for future prosthetic use. RBO Hand 2 is one of them. It was fully described in 2015.

RBO hand 2 has underactuated pneumatic system. This means simpler control of the hand. In comparison to solid designs of the anthropomorphic hands, RBO hand 2 represents better cost-effective option with optimized number of sensors and actuators, while showing high performance. Conducted research shows tendency for the passively compliant parts to be more advanced than actively elastic. RBO hand 2 is very light – 178g overall. It is capable

handling load more than 0.5 kg with certain adjustments, while being able to produce 31 grasping motions described in Feix grasp hierarchy. Obvious disadvantage of the soft robotic designs is restriction from the interaction with sharp objects that can damage the hand. But due to seriously decreased cost price, it may not be classified as a defect of the design. Moreover, such hands could be used under hazardous conditions, because the overall risk does not involve loads of money.

As to grasping capabilities, it was detected that distal type grasp and light tool grasp of scissors and pencil respectively cause problems. But these are minor fails for the first prototypes in this area. Hand is able to apply 6-8 N forces and that is enough for most of the daily objects. A harder rubber is suggested for making higher forces involved in grasping operations. Also, slippery problems that were already discussed in a different section are present here as well. All in all, for a hand worth only 77 pounds – presented efficiency is for sure a breakthrough in financially optimal robotic anthropomorphic designs.

2.2.7. Multifingered metamorphic hand by G. Wei et. al.[40]

The best example of the practical application of the metamorphic hand developed by G. Wei et.al. could be considered the DEXDEB project. The successful prototype was tested in serious environment alongside with the Shadow Hand.

The four-fingered metamorphic hand has 15 DOF overall, its palm is formed by five-bar linkage based on spherical principles. Since the hand is metamorphic and highly flexible, for simplification, weight reduction and contradiction prevention underactuated tendon-based external actuation is integrated. Each finger is actuated by two motors, making overall actuator number of 10, including two actuators for the palm.

Deboning research has evaluated that occurring friction and wear of the tendons should be carefully studied further. Recommendation for the metamorphic hand weight reduction was made.

In general, outstanding results of the metamorphic hand were presented and it is possible to predict demand in designs based on the metamorphic principles in the nearest future.

2.2.8. The Robonaut Hands[41,42]

In May 1999, anthropomorphic robotic hand, The Robonaut 1 Hand, of the human scale intended for space activity was presented. It is obvious that aeronautics department has very high requirements for robotic devices; moreover, tasks assigned to space robotics involve manipulations with heavy tools and serious force application while doing repairing works.

Also, specific conditions of working area should be mentioned – all electronics and actuators have to be perfectly sealed and pressurized in order to work in vacuum. The robonaut hand (as part of the proper robot) is designed to reduce (or to completely replace) human presence outside a space station. Back then it was the most advanced hand engineered for space considering several other hands under development and even some grippers already tested in space conditions. To list some of the stated requirements: force of 88.9 N and torque of 3.39 N.m should be achievable (for the whole arm module). Variety of grasps is dictated by necessary compatibility with EVA (extra-vehicular activity) interfaces at International Space Station. Strict restrictions are applied to materials and motors: extreme temperature level change withstanding ability, contamination prevention standard fulfilment, lubrication certified for space use, etc. Overall DOF number of the hand is fourteen, including 2-DOF wrist. The forearm is carrying all fourteen motors with necessary electronics and is of 10.16 cm by 20.32 cm size. Leaving hand empty of actuators is justified by limitations applied to its required overall size. As a more reliable and durable competitor than tendon actuation, flex shafts are used. Leadscrews attached to the fingers provide final linear motion. For outstanding control, more than 43 sensors are used. Each finger has not common extra durable 7-bar linkage system and there are special elements integrated in the fingers and hand that reduce backlash and vibration. Since this robotic piece of art was first in class, only the following minor disadvantages could be mentioned: most of the parts have complicated geometry, leadscrew actuation is done only one way in order to save the tool in the power loss scenario – otherwise extra forces required for finger back extension will overheat the motor and damage it.

Second generation of the robonaut hand, The Robonaut 2 Hand, introduced in 2011 is expected to have serious advantages over its previous generation. Major differences involve increased DOF number of the thumb for better grasping at certain positions and improved reachability, overall durability increase and optimization where possible. Number of conductors was decreased from 80 to just 6, meaning better utilization of the limited space. In addition, while hand module above forearm is now designed to easily be taken off, the Cutkosky's grasping possibility evaluation shows 40% efficiency improvement due to more dexterous thumb in comparison to the robonaut hand 1 taxonomy. Hand overall length with all electronics is just above 30.4 cm. The weight of it is 9 kg. Speed of the joint rotation is given as 200 mm/sec. While number of DOF remained fourteen, actuator number is now sixteen in comparison to the previous fourteen. Also, fingers are now relied on four-bar linkages. Index and middle finger are independently controlled by four tendons, while thumb

by five. Remaining fingers are underactuated. It is important to note that now design has polymer tendon system for better finger shape optimization and simplification purposes. Special 'Vectran' material is used for tendons; its breaking force is 1775.61 N at diameter of 1.2 mm. Each actuator is able to provide pull force of 225.63 N. But now due to tendon system the hand is compliant, so therefore there is a risk of losing a tool in space. As a solution and substitution of the leadscrew technology, gloves of whether low or high flexion friction are now used. This means that in case of the emergency, fingers will not extend back due to high friction. They will only be able to do so when additional torque overcoming the friction will be applied.

It is concluded by researchers that 'Spectra' polymer material for tendons is better for abrasion resistance and durability properties than 'Vectra' material, but the latest is chosen only because of the limited compatibility. It is also highlighted that abrasion prevention is improved with Dupont Krytox lubricant for tendons and leaded phosphor bronze as finger material. New tendon material and overall actuation system design allowed increased level of break strength overall durability with considerable factor of safety. Elastic actuation is recognized as a positive innovation and further development will continue to replace solid parts where it is rightly.

2.2.9. UB Hand IV

University of Bologna is working on robotic hand since 1988, when the first three-fingered UB Hand I was produced. The hand had two parallel fingers, thumb and a palm all controlled by tendons, driven by DC-motors and controlled by complex electronic equipment. Later a modernized UB Hand II was developed introducing the wrist articulation. The structure and working mechanism was simplified in the third generation of UB Hands. In 2008, new approach was applied to produce the UB Hand IV also known as DEXMART Hand.[43] UB Hand IV is based on endoskeletal model with non-hollow structure. The hand involves tendon transmission system with adapted tendon path in order to reduce the curvature and resulting friction.[43] The hand uses twisted-string actuation system that minimizes the friction and simplifies the mechanism as no intermediate hardware is required. As most of the robotic hands, UB hand has various position and velocity sensors, force and tactile sensors.[43] While producing the hand's prototype, scientists explored and offered various solutions to the existing and expected problems, which was later used in further research for range of robotic hands.

2.2.10. The SmartHand[44]

The SmartHand is a prosthetic hand developed by Scuola Superiore Sant'Anna (SSSA, University in Pisa, Italy). The hand has five underactuated fingers, 16 DOF and 40 different sensors. Hand is actuated only by 4 motors and is bent with single tendon.[45] Only thumb and index finger are separately actuated, whereas middle to little finger are actuated with one DC-motor. *The last actuator is used for thumb abduction/adduction.*[45] Moderate flexion speed is assured: 90 deg/sec. Such design does not allow complicated grips and movement, although power, precision and lateral grasps are possible along with pointing and counting. The aim of the SmartHand, however, was just to make possible basic everyday gestures, which was achieved with weight and speed characteristics comparable to that in commercial prostheses.[45]

2.2.11. The Shadow Hand[46,47,48,49]

Another example of solid design that is close to human hand functionality is the Shadow Hand. Initially, its prototype was presented in 2002 in Japan. The first commercial version with pneumatic muscles was introduced in 2004, but in 2008 option with electric motors became available. One of the aims of the whole project was to investigate and develop advanced tactile sensors. In general, the hand is intended to serve as a test system for intelligent manipulation and grasping. Therefore, it is not designed for non-professional public, but rather for research institutions. Prototype that could be bought and tested by various research groups.

Research on tactile sensing has led to the shadow hand's most unique selling point – it was equipped with special novel sensor placed on the fingertip that has 34 tactile regions and is vulnerable even to 3g of applied weight. Other advantages are also mentioned: fast construction time, high compliance (which back then was not very common) for interaction with humans, outstanding dexterity and significant maneuverability ensured by 25 DOF producing 24 different movements. The fact that the hand became a product out of the prototype means that it was a serious contribution to the overall robotics field and particularly general purpose robotics. One of the research groups have tested and positively identified hand's functionality[50].

The Shadow Hand has several models: c6 and c6m, 3-fingered C6F1F3T and 1 finger test unit FTU-C6. Various additional features are offered. C6 hand has 20 DOF with 40 air-muscle actuators, while C6M has optimized 20 electric actuators. C6F1F3T has 11 DOF and 22 air-muscle actuators. As a final determination of the Shadow Hand capabilities, the Shadow Robot Company states that the hand provides force output similar to human hand.

Furthermore, the hand has been involved in neural control, industrial quality control and brain computer interface research.

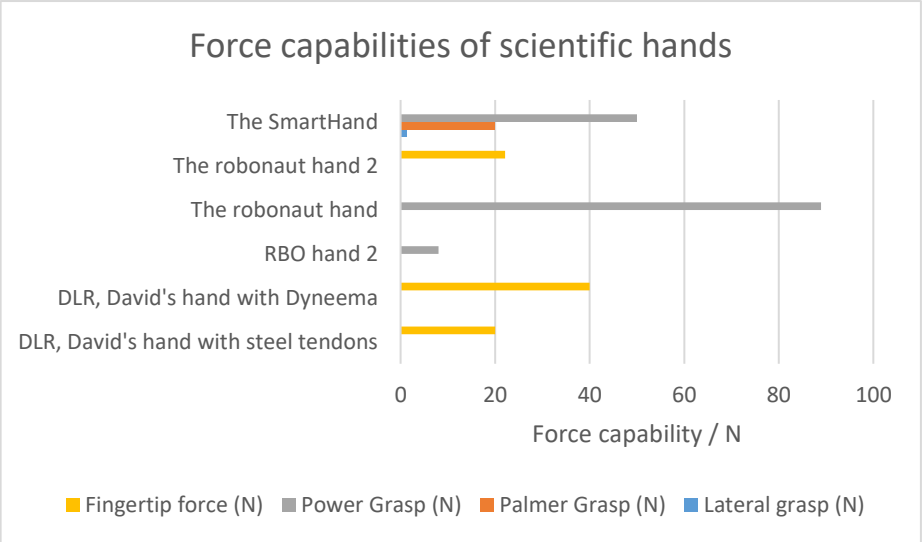

Figure 2.10. Force capabilities of scientific hands

Unfortunately, only few force parameters are provided by scientists on their hands. The main point of interest is therefore the fingertip force and the power grasp. DLR hand provides twice higher fingertip force when Dyneema fiber is used instead of steel tendons. The robonaut hand uses the polymer tendons and provide just a bit higher fingertip force than DLR hand with steel tendons.

The power grasp information is provided only for three scientific hands, with the first generation robonaut hand unquestioningly leading. It may be assumed that the second generation robonaut hand should have similar properties, as the force capability tends to improve in every next version of the hand, both commercial and scientific.

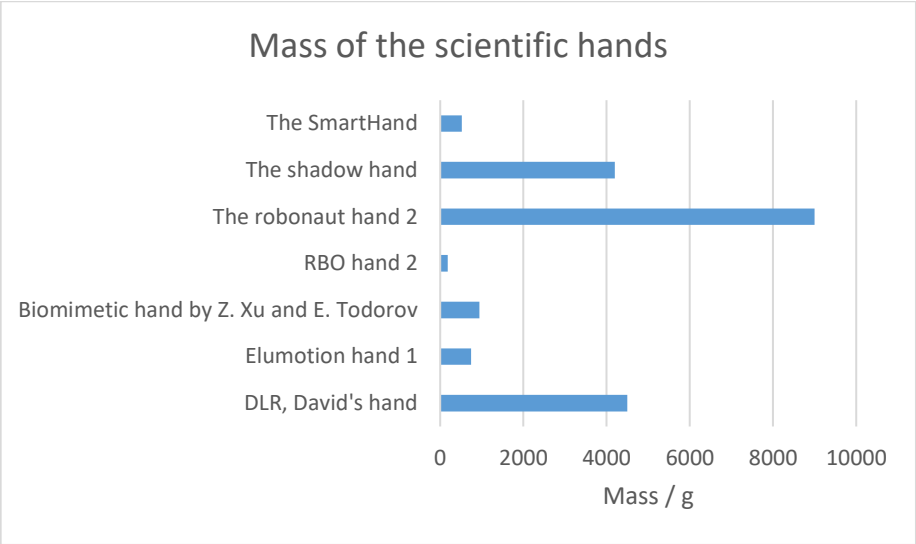

Figure 2.11. Mass of scientific hands

Scientific hands are much heavier than commercial hands, as they do not require the similarity to human hand and only focus on the precision and performance efficiency. The mass of the hand mostly is affected by number of actuators, materials and size of the hand. The mass range is clearly visible on figure 2.11 and does not require any further explanation.

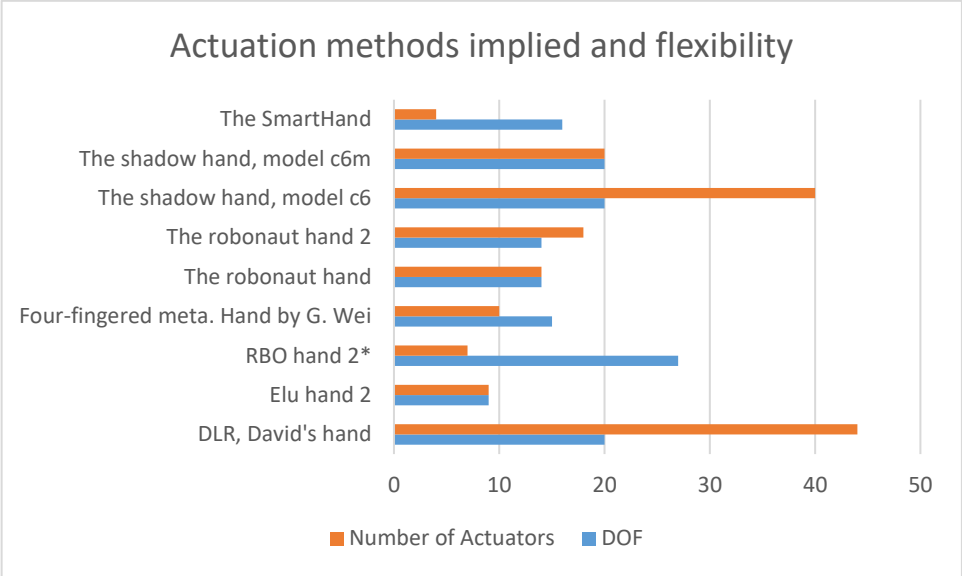

Figure 2.12. Actuation and flexibility of scientific hands

As expected from scientific hands, were the accuracy and control of movements is usually the most desirable parameter, most of the hands are overactuated. There are, however, plenty of examples of underactuated (RBO hand 2, Elu hand, The SmartHand) and fully actuated hands. Due to the nature of scientific research, all three types of robotic hands must be studied in order for robotic field to develop further.

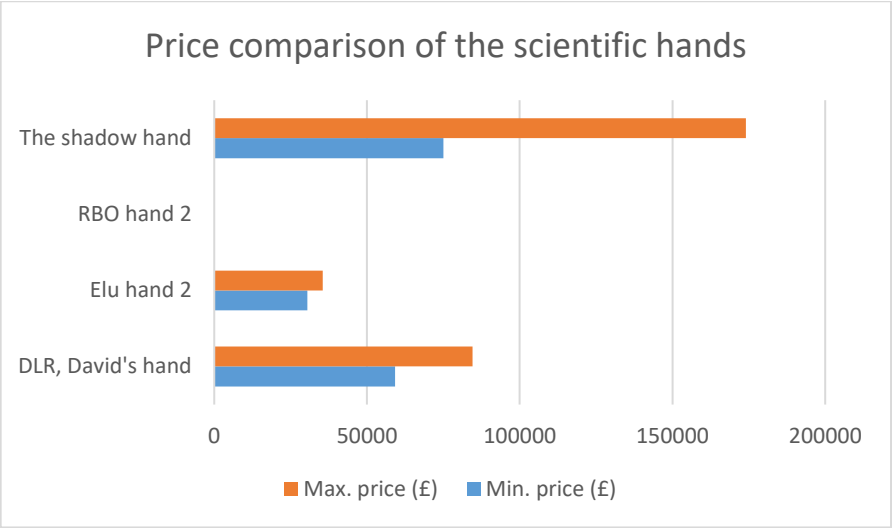

Figure 2.13. Prices of scientific hands

Not many of scientific hands are available for purchase as it is usually the only exemplar and is only studied within particular research group. The hands that are available, however, are mostly expensive. The price depends on the performance, material and size of the hand, similar to commercial robotic hands. The RBO hand 2 is being the most cost-effective due to the lack of efficiency in comparison to other hands described above.

2.2.12. Comments

Scientific hands are mostly task-specific rather than commercial general-purpose hands. Hence, desired performance is obtained regardless of price, weight, dimensions, etc. Improvements that were made by scientific hands, problem solution ideas and a novel approach lead to better commercial products in the future. It was also noted that scientific hands typically represent prototypes and are rarely produced with quantities higher than 1. However, developers of the Shadow Hand have made their product available for research groups and universities, but the public access is highly limited due to the price, which is only affordable by large organizations/corporations.

2.3. Summary

The commercially available hands have been compared purpose-wise and reasonable price to quality ratio was observed. Unfortunately, not all the manufacturers provide full characteristics of their product and not all of commercially available hand could be discussed. More detailed research and comparison of commercial hands characteristics may be performed in future work.

There exist a huge number of scientific robotic hands as this is the main research ground for all further development of commercial products. With the range of hands with different properties including type of actuation, material of tendons or other driving mechanism presence, robotic hand scientific research remains the main drive for robotic industry development.

It is important to highlight that in recent research articles and conferences, new generation of robotic manipulators was introduced. While metamorphic mechanisms are considered as advancement in solid solutions, soft robotics is now becoming a key research interest for many developers. There is no unified theory yet as this field of study is still new, but it can be predicted that in the nearest future commercial soft robotics products will appear on the market.

Chapter 3
Robotic Hand Design

3.1 Introduction

Design is an irreplaceable part of engineering project. It is a complex process which combines certain sequence of tasks, where some parts are constantly repeated for design improvement purposes. Design is a fundamental part of engineering, without which accomplishment of required task could not be achieved. The final result of design is a set of specifications from which the final product can be built.[51]

Design is a process in which variety of factors must be considered: environment in which the final product will operate, existing standards and requirements for the designed product, target audience, etc. Therefore, the purpose of the designing process is to find the optimal interception between the physical properties, environment requirements and ease of application.[52] Design complexity is also affected by the fact if the product is modernised or invented at first place. However, regardless of the initial task, design procedure can be divided into several parts to simplify the task.

Mechanical design involves variety of mathematical calculations prior to the production of the designed product. As obtained results can prove design mistakes, changes to specifications are made constantly throughout the design period and after the first tests of the built product.[52] In help comes programming software, which simplifies introduction of changes to the final results. Most of the design engineering software nowadays are connected between each other so that the designer can interconvert new mathematical calculations to the change of specifications in a least time-consuming way.

This leads to one of the design criteria obedience.[52] It is essential for the design to be slightly adjustable even in the latter stages of development. Other standards, which design must obey are cost-efficiency, reliability, safety and marketability. Therefore, design must produce the

product with both efficiency in terms of fulfilling the required function and at the same time cost reasonable of money to produce for the company to make profit in long-term perspective.

Design is not purely technical and scientific process, as creativity of designer and their ability to gather and separate certain information about the final product simplify the core of all the design projects – identification of the need. Design is an iterative process, where at every step new information about the product is gained and hence the design may change. Some of the issues might be found at the mathematical calculation stage, some at simulation stage and some can only be identified when the product is built. It is vital to understand that mechanical design, in particular, combines all mechanical engineering disciplines, and therefore requires the designer to have certain level of engineering literacy.

This chapter gives a description of what is the mechanism behind the achievement of various hand postures. Design complexity and possible areas of manipulator application are discussed. Furthermore, grasping of different shape objects is introduced to demonstrate capabilities and evaluate downsides of the design. Conclusions of this chapter will make a ground to the overall structure simplification and future work.

3.2 Design Overview

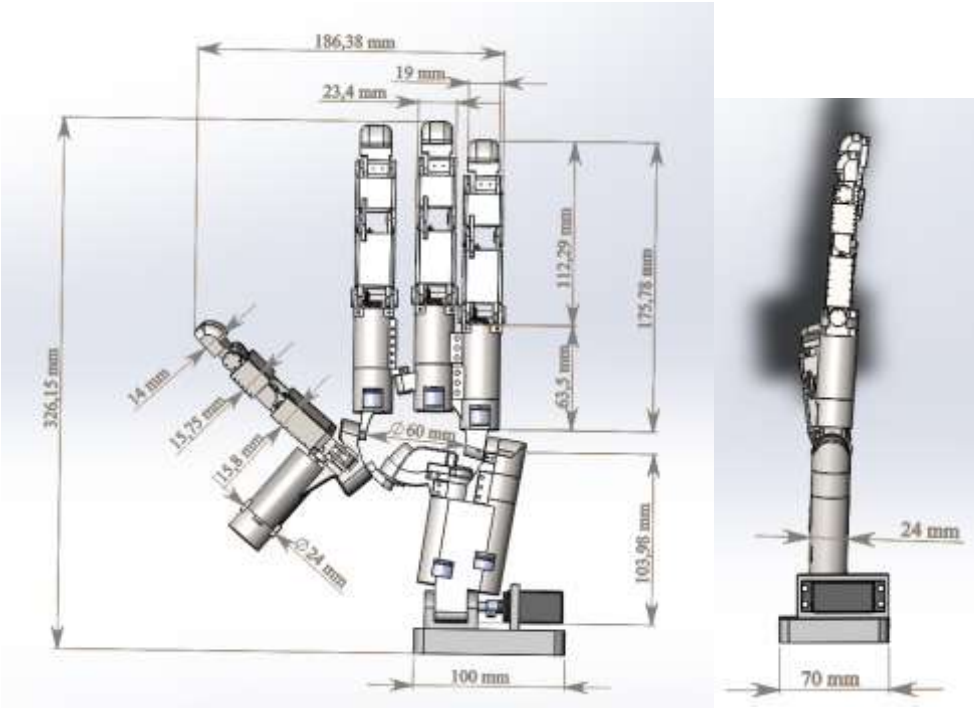

Figure 3.1. The principal dimensions.

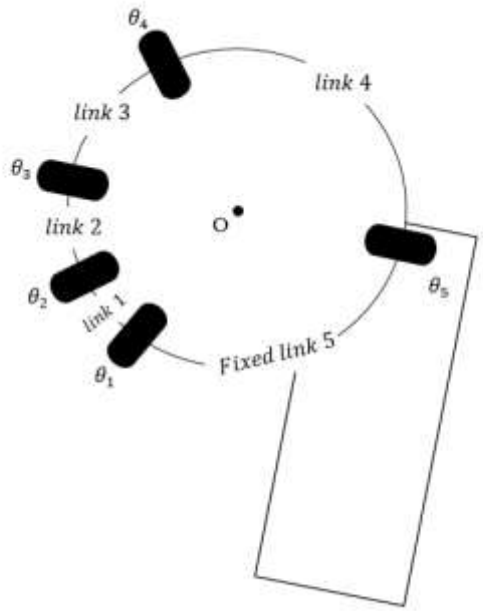

Figure 3.2. Schematics of the palm.

In general, structure of the mechanism can be split into several sections (figure 3.2):

- The supporting unit that is meant to be attached to the robotic arm. The unit is carrying the robotic hand and wrist actuator.
- The lower section of the palm (link 5), which stores its two actuators. As the whole palm spherical mechanism has only 2 DOF, the other links have only actuators for the fingers.
- The upper section of the palm (link 4), which is carrying the middle and the ring fingers, as well as their DC motors. It is actuated with a DC motor.
- The ring finger's palm section (link 3), which is a passive link, containing a DC motor.
- The thumb's palm section (link 2) – passive link with a DC motor inside.
- The small crank (link 1), which is actuated through a double universal joint.
- Individual fingers. Index, middle and ring fingers have a similar structure. Thumb's lower part has a unique design due to the four-bar actuation mechanism.

Principal dimensions make it possible to compare this anthropomorphic manipulator with the human hand. Of course, the idea of implementing actuators inside the palm is not novel – it is found in most of the commercial prosthetic hands with rigid palm. However, the same approach applied to the metamorphic palm leads to significant impact.

As it is seen on the figure 3.1., the overall height of the robotic hand with its attachment module is 326.15 mm. Thickness is 24 mm maximum, excluding the attachment module. Length of the 3 phalanges is 112.29 mm, increasing to 175.78 mm with the DC motor and gearbox. Inner breadth is 60 mm.

According to the anthropometric survey[53], length of the natural hand varies from 158.9 mm to 205.0 mm and from 172.8 mm to 219.0 mm for women and men respectively. Hand's breadth differs from 80.7 mm to 100.4 mm for men, but for women is about 10 mm less on average.

Hence, it is not likely that the proposed manipulator would be able to fit into the commercial prosthetics category. Although addition of the fifth finger would make the manipulator more attractive, the robotic hand is still beyond the expected dimensions for prosthetics. Nevertheless, it can be suitable for minority of people that prefer to show to the public that they have an artificial and non-standard limb. In this case, larger proportions of the robotic hand outline its uniqueness. As for the industrial applications like meat deboning[40], developed manipulator would perfectly fit – the gear transmission is superior than the tendon principle in terms of accuracy and durability, while oversized and irregular shape does not have a significant impact on the operation and task fulfilment.

The tendon principle requires actuators to be stored outside of the manipulator – this factor greatly optimizes the shape and proportions, but meanwhile complex mechanisms with many DOFs will have all actuators stored inside the forearm. This may not be convenient in cases when the forearm is required to be small or available space is mostly occupied by other electronics like sensors and controllers.

Since the proposed robotic hand has only 4 fingers, it is important to understand how exclusion of fingers influences the grip performance of the hand. In relatively recent research of the grip strength[54], 100 hands in total (variously aged women and men) were analysed. It was found that the exclusion of both ring and small fingers relates with 54% decrease in grip strength. In particular, little finger contribution was 33%, whereas ring finger – only 21%. Although all five fingers contribute to grasping abilities of the human hand, their strength contribution is uneven and with enough power supported to 4 fingers, the robotic hand is capable of successfully securing most of the grips/pinches and producing demanded operations without severe limitations of the fifth finger absence.

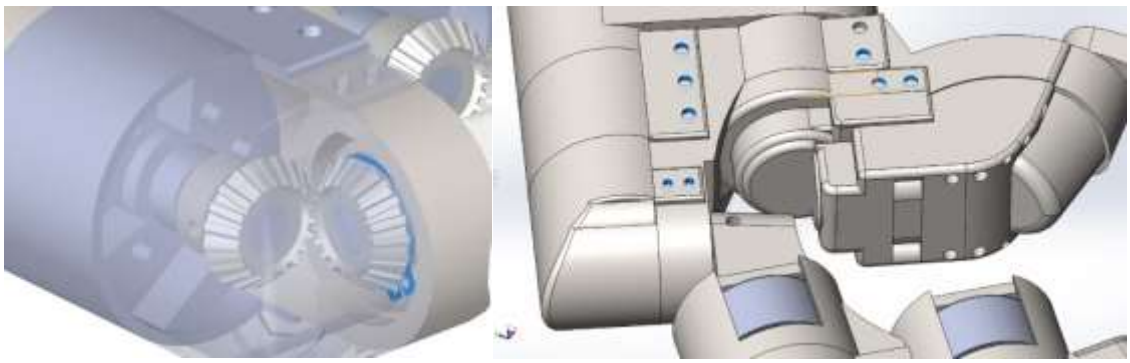

Figure 3.3. Lower part of the palm, i.e. fixed link 5.

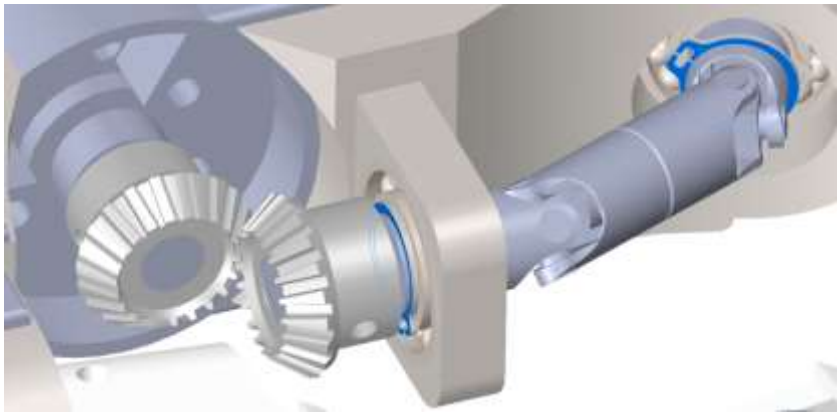

Figure 3.4. Double universal joint transmits the motion.

The palm, which is represented by the five-bar spherical linkage, can be controlled by 2 DC motors. In order to have as much unconstrained motion of linkages as possible, the inner area of the palm is left empty. Hence, space limitations obliged one of the palm's DC motors to transfer its motion through 2 universal joints. The total angle of motion transfer is 156 degrees. The bearings are securely blocked with the highlighted retaining rings. The lower section of the palm, link 5, has circular cavities for DC motors to be fitted in. It can also be seen on the figures 3.3 and 3.4 that the attachments to the palm provide fixation of actuators and cover from external interferences. The ones that have to hold an actuator are meant to be made out of aluminium or steel, whereas the others that act as a cover are intended to be made out of plastics to avoid manufacturing complications (difficult to reproduce shape) and not necessary weight.

It is beneficial for the hand closure strategy to have a gear transmission, because the grasping and handling of the object becomes secure and reliable. Unfortunately, non-compliance is considered as a disadvantage when the human interaction takes place. For example, although the Bebionic Hand does not have a tendon motion transfer, but is intended for interaction with

humans, – it has some compliance. When impact takes place, linkages that connect linear actuators with fingers are folding and therefore allow fingers to freely move backwards to certain extent. This is something to think about if the proposed manipulator would be required to be adapted for prosthetics applications.

Steel bevel gears that are used in the palm and fingers have a 10.7 mm diameter and offer 1:1 transmission. Although the overall size and teeth dimensions are modest, nevertheless, the gears are capable of withstanding torque up to the 3.9 N.m according to their specification. Higher transmission ratio to increase the torque is not available due to strict space limitations.

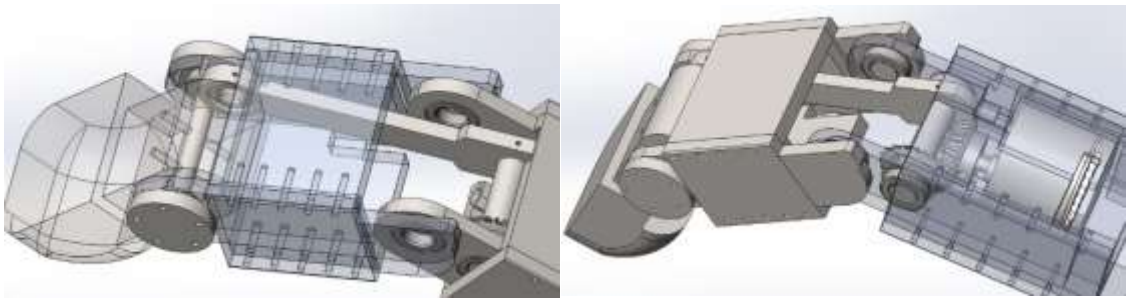

Figure 3.5. Structure of the finger.

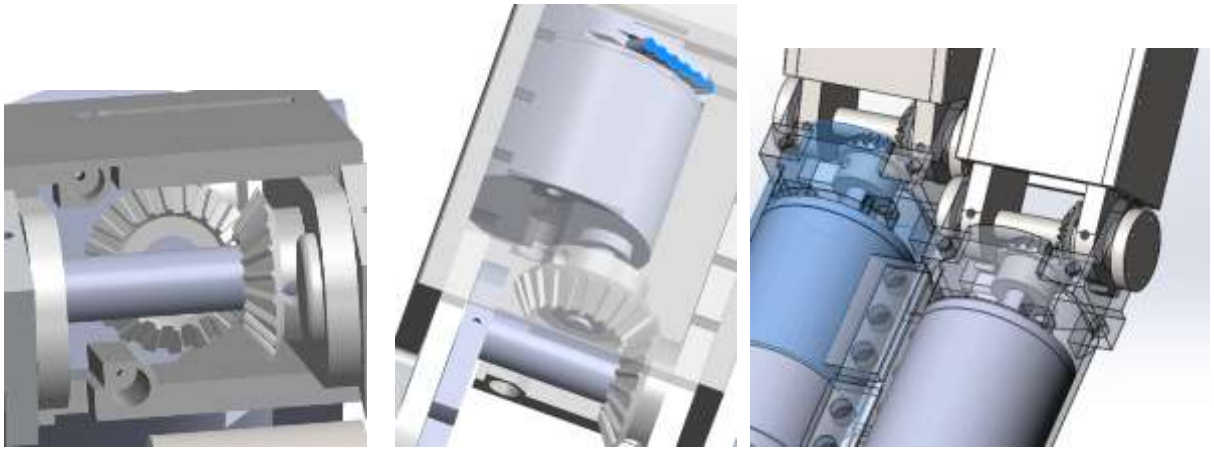

Figure 3.6. Structure of the finger.

The articulated fingers have 2 DOFs each and are represented by 3 types of phalanges, i.e. distal phalanges (the upper), middle phalanges and proximal phalanges (the lower). The upper phalange is rigid. The middle and lower phalanges are assembled from three separate parts each. The complexity of the lower phalange is the highest among the other phalanges due to the following requirement - actuator storing and sealing, while the overall phalange structure's stress resistance is not significantly influenced. Both middle and lower phalanges have

additional material support from the side walls in order to reduce the load from the screws when decompression takes place.

Figures 3.5 and 3.6 help to understand how the finger was assembled. It can be seen that the bearings are covered only for four joints. Circular protrusions of the middle phalange in the lower section act as shafts. Other parts that are placed on shafts have set screws where possible to provide additional fixation. The role of the small DC motor is to force the middle and the upper phalanges to acquire certain posture, before the final torque from the finger's main actuator (which is located inside the palm's link for each finger) is applied. In terms of joints, rivet joints may be suggested as a cost-effective alternative, if the maintenance is not expected in the nearest future of manipulator service. This is also a way how to reduce manufacturing complexity of the middle phalange.

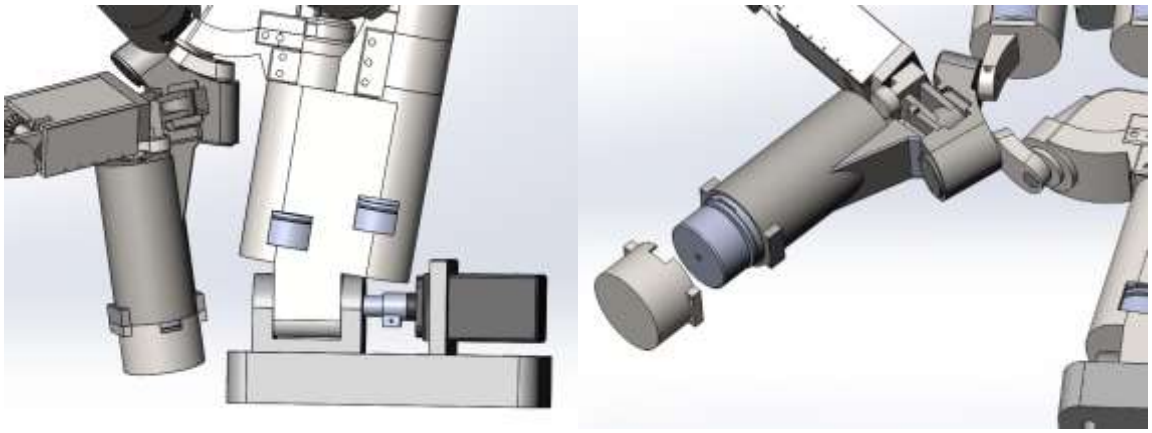

Figure 3.7. Thumb and lower area of the hand.

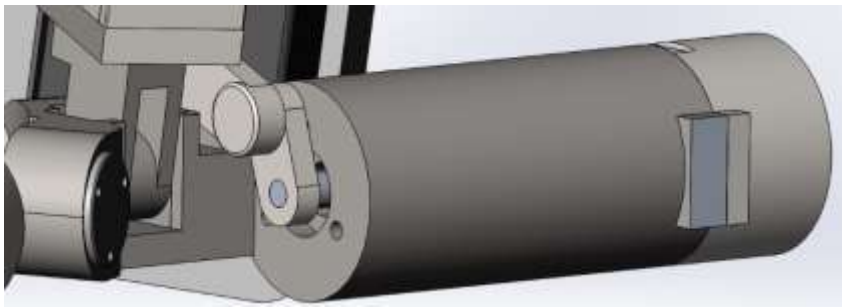

Figure 3.8. Four-bar mechanism of the thumb.

Figure 3.7 illustrates that the palm's crank is turned 180 deg. Neither link 1 or link 2 is not interfering with the attachment module or link 5. Cavities left in the parts are necessary for the cables that would go from the motors to the control unit to provide data from hall sensors.

Four-bar mechanism is used inside all fingers and is also actuating the thumb. It was already proven by Bebiobic Hand that this principle is efficient, convenient and reliable way of motion transfer. Belt transmission would have been harder to implement when available space is very limited. Especially with the fact that belts are installed on pulleys. However, it may be considered as an option inside the arm as gears are more expensive.

Specifications of DC motors:

- DC motors inside the finger: Faulhaber 1512_012 SR, reduction 324:1, max. 50 mNm.
- DC motors in the palm links: Maxon EC 20 flat A (351100) with planetary gearhead GP 22 C (143989), reduction 157:1, max. 1.9 N.m.
- Servo motor is included for reference purposes. It can be of any size, depending on the application and size affordability of the attachment module. CAD model is based on the Hitec servo motors.

3.3 Grasping Capabilities

Object grasping is the most important test of the anthropomorphic manipulator. It is the easiest way to assess if the proposed robotic hand has enough performance to meet the requirements. This process outlines design flaws that have to be eliminated and advantages that should be advertised.

Most difficulties with grasping arise when the hand has to have more than two contact points with a small object. While the commercial hands are able to provide these two contact points, necessity of the third contact may become a problem. As the literature review states, two-split and triple-split hands are not very common – the rigid palm is a suitable way to provide small size of the hand and yet sufficient grasping power. Unfortunately, this approach has obvious limitations. The thumb is the only finger that is circulating in front of other fingers. In natural hand, it might be noted that the basements of thumb, index and little fingers are able to turn inside the inner area of the palm. Described kinematic versatility allows the natural hand to make unachievable postures from the solid link robotics point of view. In spite of this, the metamorphic palm mechanism of the developed manipulator grants the robotic hand unique and unprecedented flexibility.

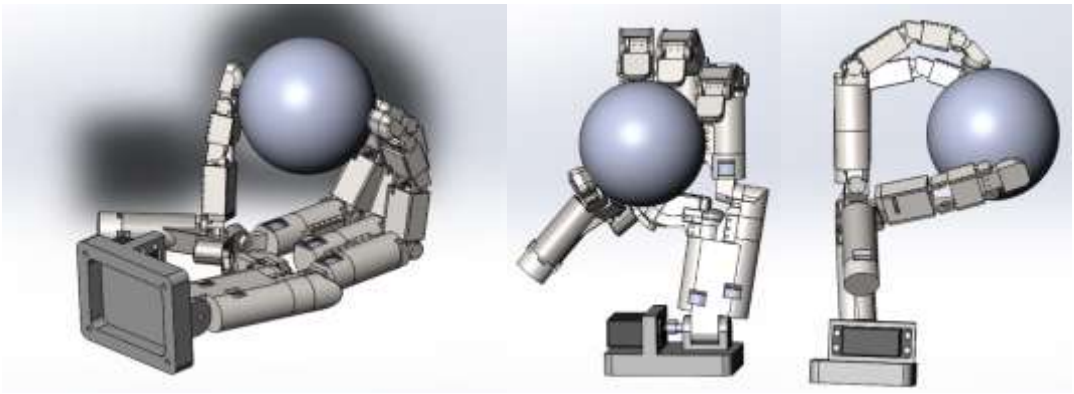

Figure 3.9. Holding a medium-sized ball.

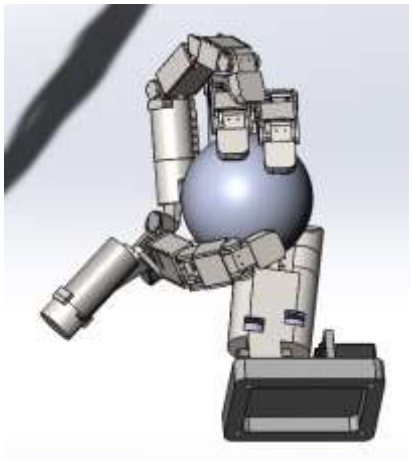

Figure 3.10. Holding a medium-sized ball.

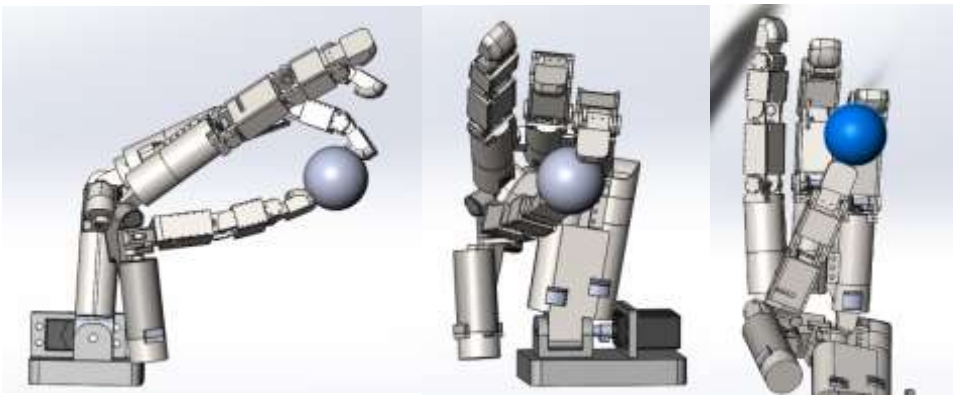

Figure 3.11. Holding a small ball.

The reason why the ball can be considered as an object of advanced shape is the fact that it has no planes. If it is assumed that the ball's surface is slippery, it is highly unlikely that the ball would be grasped with only two contact points. When the ball is relatively large as in figures 3.9 and 3.10, it takes no additional effort to hold it. Figure 3.10 shows secure grasp - the index finger is able to support the middle and ring fingers. Figure 3.11 clearly indicates

the possibility of providing at least three contact points. Popular commercial hands have a special movable platform for the thumb in order to provide various hand posture support. However, the metamorphic anthropomorphic robotic hand is capable of rotating the basement of index finger in addition to the thumb's. Moreover, with only 1 DOF in commercial hands, the fingers are forced to bend all three phalanges altogether. 2 DOFs of the proposed manipulator give extra workspace and posture variety.

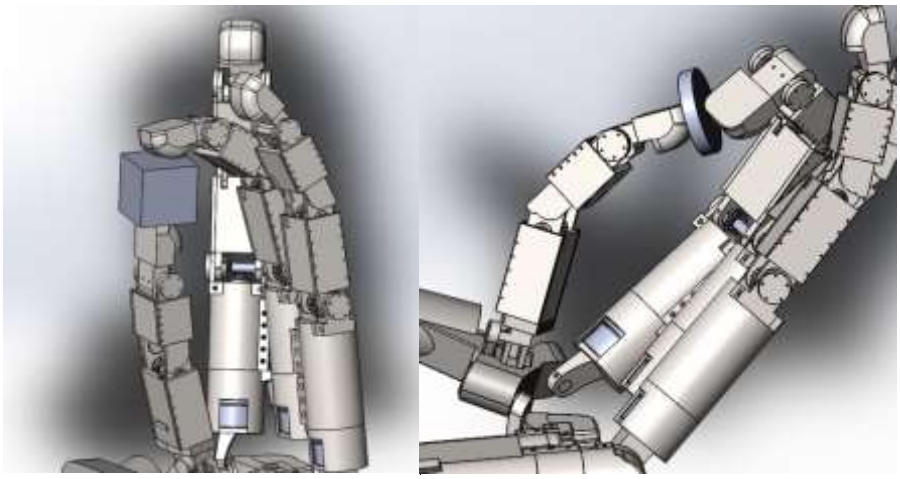

Figure 3.12. Holding a small cube and a coin.

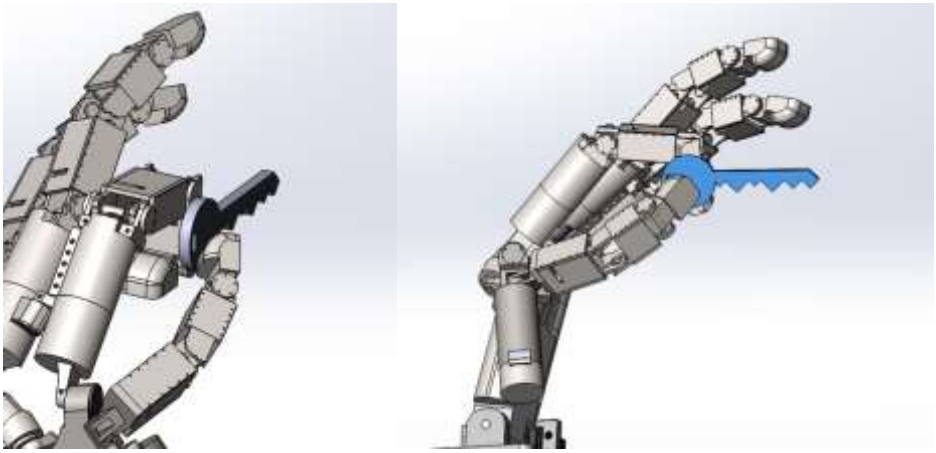

Figure 3.13. Holding a key.

A coin and a key (figures 3.12 and 3.13) are typical items that are used on daily basis. Grasping a coin can be sometimes challenging even for the human hand. Robotic hands use pinch technique to handle different small things, including needles too.

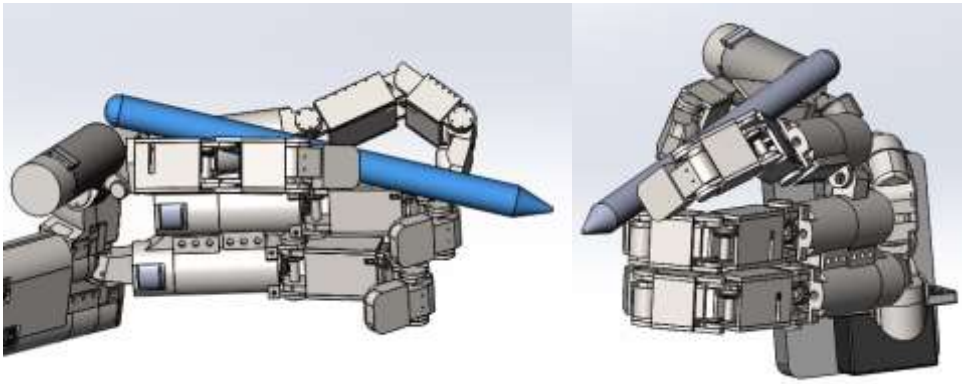

Figure 3.14. Pencil handling 1.

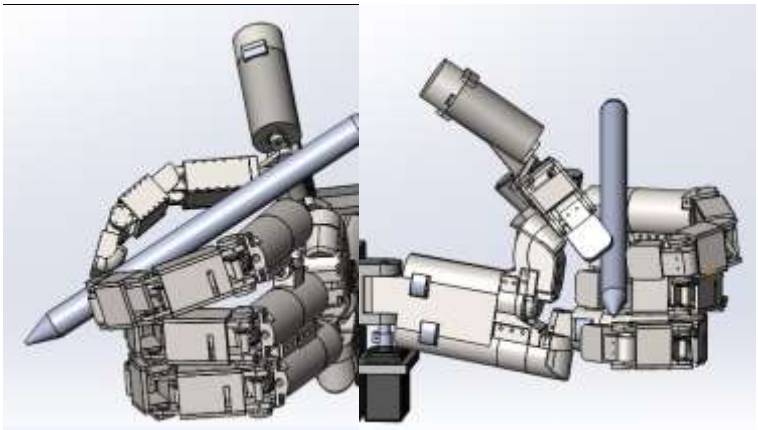

Figure 3.15. Pencil handling 2.

Since the advancement of technology, with the invention of computers, the habits of humans have changed. A large amount of time is now spent using hand-held portable devices, such as: laptops, mobile phones and tablets. Hands and fingertips are required to adapt to the new circumstances - to grasp and grip smaller objects.

Pencils (figures 3.14 and 3.15) and pens used to be objects with higher frequency of utilization in comparison to any others. Nowadays all documents are maintained electronically, however people continue to apply manual signatures, write notes and draw sketches or paintings. The typical handling strategy of the pencil represents control provided by index finger and thumb, as well as support of other fingers from beneath.

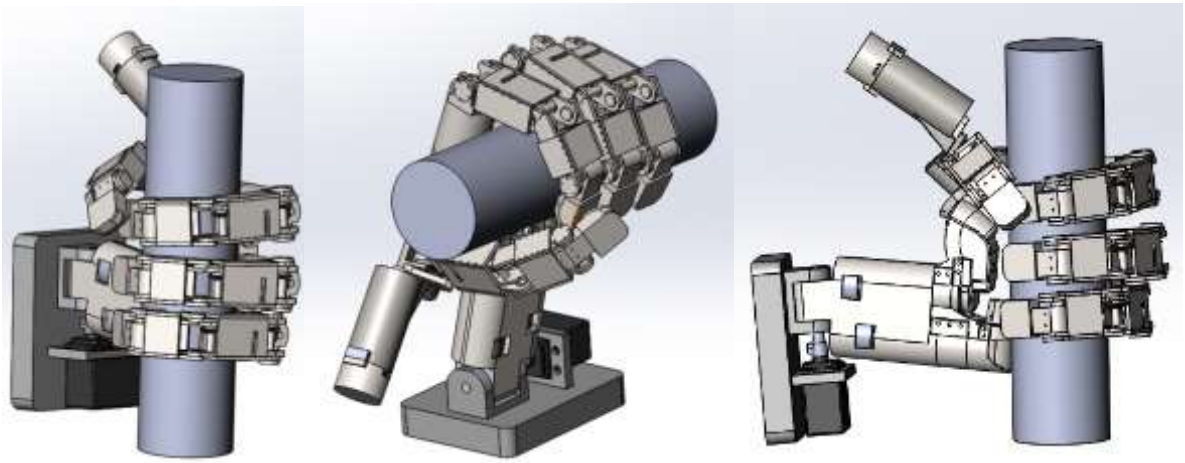

Figure 3.16. Holding a bar.

A bar is often encountered in buses and stairs. The same closure pattern is applied to any bags that should be carried. As seen from the figure 3.16, the robotic hand is able to successfully hold a bar.

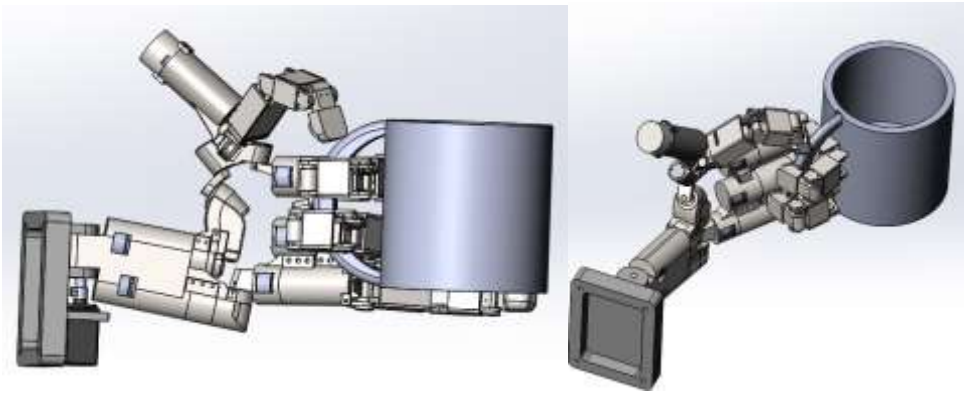

Figure 3.17. Holding a mug 1.

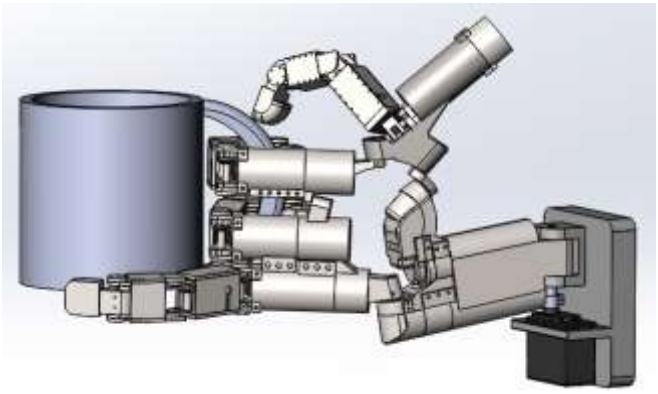

Figure 3.18. Holding a mug 2.

Objects like mug have a handle to ease the manipulation process. Handle is supposed to provide comfort and support, but as for the robotic manipulators, the problem is that they are

obliged to maneuver the mechanical links around the handle to grip and lift the mug. It can be observed on the figures 3.17 and 3.18 that thumb also plays a key role in securing the stable grasp. Thumb prevents the mug from deviating down. Ring finger can be used as an additional support underneath the mug.

Another aspect of the object manipulation is friction. It is necessary to note that the steel or aluminium materials on their own are not improving grasping. There are situations when slippery objects should be handled. Absence of high friction does not affect the function, but it might influence the performance. There are a lot of cover materials with high friction coefficient that can be (or should be if there is such demand) applied to the fingertips and other parts, so therefore it is inconsequential to address it in more detail.

3.4 Summary

Overall, design is a complex interdisciplinary part of engineering, which is mainly based on decision-making. Then, the decisions are modified with every new information obtained in order to optimize the final product. There is no completely final point of the design as it is extremely flexible and hence, should be easily adjustable for further needs of the research or consumer. Design starts with a specific idea and set of requirements that can be achieved in a variety of ways, which are only limited by the chosen approach. And this is what makes design a fundamental unit of the progress.

Although the developed robotic hand might be of a limited value to prosthetics, there is a limitless demand in the industrial applications. Provided evidence of the robotic hand's grasp potential shows that the manipulator is capable of being used in operations involving objects of intricate shapes or procedures that require complex postures.

Structure of the proposed hand and actuating mechanisms have some areas that can be improved. Rivet joints should be considered as a cost-effective alternative to bearings and their sealings. For some sections of the design, like outer four-bar linkage driving the thumb, they are a must. Also, in case of the manipulator adaptation to prosthetics use, it is necessary to address a way how make the mechanisms compliant. On the other hand, the manipulator is an advanced mechanism that can be successfully used in industrial applications.

Chapter 4

Kinematics

4.1. Introduction

Forward kinematics represents a set of transformation matrices that leads to the end effector of manipulator. Obtained result shows position and orientation of the end effector.[55, 56]

Inverse kinematics is a mathematical technique which finds the joint properties based on the desired end-effector (or fingertip) position. The IK approach is rather complicated as there exist various joint position combinations at which desired fingertip position is achieved. The presence of more than one suitable combinations comes from the fact that transformation matrix (^0T_n) is composed from trigonometric functions of joint variables.[5] Which by definition have infinite number of solutions. In order to suit a particular case, several analytical and numerical methods for solving inverse kinematics problems are known. These include such approaches as decoupling technique, inverse transformation technique and iterative method.

In this chapter, method of obtaining kinematics equations is described.

Although sections containing equations of accelerations are mostly reviewed in dynamics chapter of books, for convenience purposes and better information representation, they will remain in kinematics chapter.

4.2. Preliminary Theory

4.2.1. Orientation and Translation. Position in Space[57]

Before the kinematics can be considered, it is necessary to define a coordinate system to show the way how results will be presented. Although there are various options available, in this work, everything is based on the Cartesian coordinate system.

The first step in obtaining kinematics of mechanisms is establishment of the reference frame. The frame itself gives description of where the point is located and how it is oriented. It is

also vital for the further kinematic equations to be based on correct reference point, because sometimes later on there might be a requirement to attach new system of coordinates to the existing one in order to present motion in global coordinates. Hence, reference frame coordinates have to be carefully chosen.

When the reference frame is determined, transformation matrix is used to move from point to point (usually, from one joint to another joint) through the kinematic chain to the end point, which is whether fingertip, finite link or some gripper's part. Transformation matrix consists of two elements: 3 x 3 set of vectors that are describing an orientation and 3 x 1 position vector. Consider transformation matrix T that represents a homogeneous transform:

$$ {}^{A}_{B}T = \begin{bmatrix} r_{11} & r_{12} & r_{13} & p_x \\ r_{21} & r_{22} & r_{23} & p_y \\ r_{31} & r_{32} & r_{33} & p_z \\ 0 & 0 & 0 & 1 \end{bmatrix} \qquad (4.1) $$

where 'r' and 'p' stand for coordinates of orientation vectors and position vector accordingly.

The row [0 0 0 1] can be thought of as a convention that is related to the position vector representation. In other words, that vector could be 3 x 1 or 4 x 1 if multiplied by 3 x 3 or 4 x 4 matrix. As rotation matrix is defined to be orthogonal(squared), zeros take place. There are cases when the last row is not [0 0 0 1] - for example, scaling operations.

Separation of the T matrix elements is also an option. In this way, rotation matrix, R, and position vector, P, equally substitute the transformation matrix T and now route to the end point may represent specific number of rotations and translations instead of 4x4 transformations. That form of notation is more applicable to computer calculations.

Form of rotation matrix depends on the axis around which motion is occurred. Therefore, rotation matrices are specified:

$$ R(\xi_n, x_n) = \begin{bmatrix} 1 & 0 & 0 & 0 \\ 0 & \cos(\xi_n) & -\sin(\xi_n) & 0 \\ 0 & sin(\xi_n) & cos(\xi_n) & 0 \\ 0 & 0 & 0 & 1 \end{bmatrix} \qquad (4.2) $$

$$ R(\varphi_n, y_n) = \begin{bmatrix} \cos(\varphi_n) & 0 & \sin(\varphi_n) & 0 \\ 0 & 1 & 0 & 0 \\ -\sin(\varphi_n) & 0 & \cos(\varphi_n) & 0 \\ 0 & 0 & 0 & 1 \end{bmatrix} \qquad (4.3) $$

$$R(\theta_n, z_n) = \begin{bmatrix} \cos(\theta_n) & -\sin(\theta_n) & 0 & 0 \\ \sin(\theta_n) & \cos(\theta_n) & 0 & 0 \\ 0 & 0 & 1 & 0 \\ 0 & 0 & 0 & 1 \end{bmatrix} \quad (4.4)$$

General form of rotation matrix, R = $\begin{bmatrix} c\theta_i & -s\theta_i & 0 \\ s\theta_i c\alpha_{i-1} & c\theta_i c\alpha_{i-1} & -s\alpha_{i-1} \\ s\theta_i s\alpha_{i-1} & c\theta_i s\alpha_{i-1} & c\alpha_{i-1} \end{bmatrix}$ (4.5)

Scheme 4.1 illustrates how the transformation of point A to point B represents both translation and change of orientation with respect to the reference frame. Coordinate systems are always attached to the points in kinematic loops regardless of the point quantity, so that consequences of movement are taken into account.

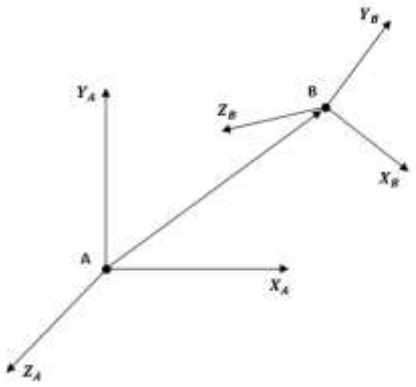

Scheme 4.1. Position Transformation

Denavit-Hartenberg parameters are often used to give a general characteristics of the mechanism. Based on the principle shown in scheme 4.1, it is possible to move from joint to joint, from link to link and correctly assign values. This is a geometric approach leading to a better understanding of the mechanism. The following principle variables are present on the scheme 4.2: a_{i-1} – the distance between neighbour joints; θ_i – the angle that describes deflection of the $link_i$ with respect to the $link_{i-1}$; d_i – the distance between joints measured about the axis $\hat{Z}_i$ which is perpendicular to the a_{i-1}; α_{i-1} – the angle that represents the difference between neighbour joints axis of rotation.

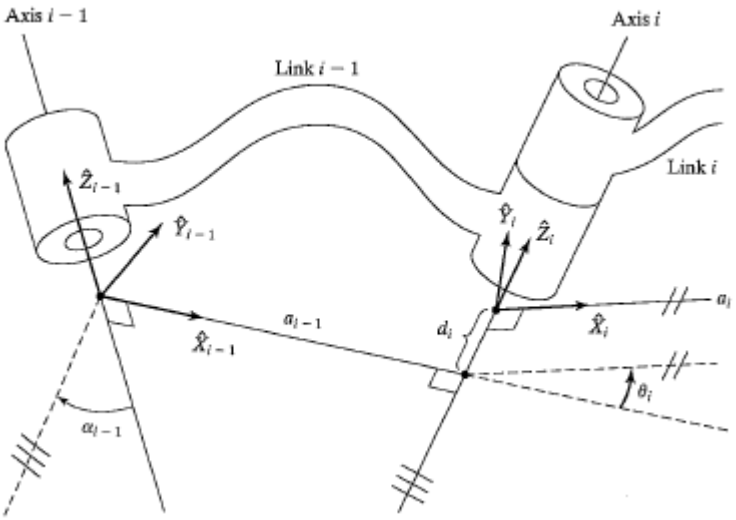

Scheme 4.2. DH approach[58]

4.2.2. Alternative Methods of Transformation in Space. Screw Theory Fundamentals

Although it was already mentioned that global coordinates are defined as Cartesian, other ways of representation within defined coordinate system can still be used without contradiction in some areas as a necessity in order to solve specific problems that occur during derivation of equations. That said, principal concepts[59,60] of the screw theory are introduced.

While in Cartesian coordinates rigid body in space has 6 DOF, a simple line would have just 4 DOF – rotation about itself and translation in its own direction do not change the line. If the line in space is defined by direction, 'l', and a point that it crosses, 'p', the Pl$\ddot{u}$cker coordinates[61] (or special case of Grassmann coordinates) of that line will have 2 components – vector 'l' and the moment vector 'm', which is equal to the 'p' and 'l' vector cross product. Therefore, line 'L' consists of six dimensions (l, m) and can be noted as a screw. Scheme 4.3 illustrates this concept:

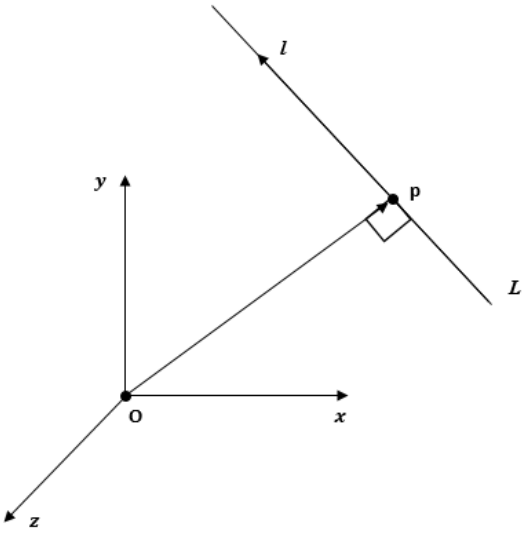

Scheme 4.3. Alternative coordinate system

Common notation for the screw is \$, (S;S_0). When 'S' is a unit vector, moment vector 'S_0' will define the magnitude of vector 'p'.

When a screw has assembled velocity in it, it is called a twist (scheme 4.4):

$$\omega\$ = \omega(S; S_0) = (\omega S; \omega S_0) = (\omega; v_0) \qquad (4.6)$$

where 'S' is a unit vector, 'ω' and 'v_0' are angular velocity and linear velocity (or tangent linear velocity) of the point,'p', that is coincident with the origin.

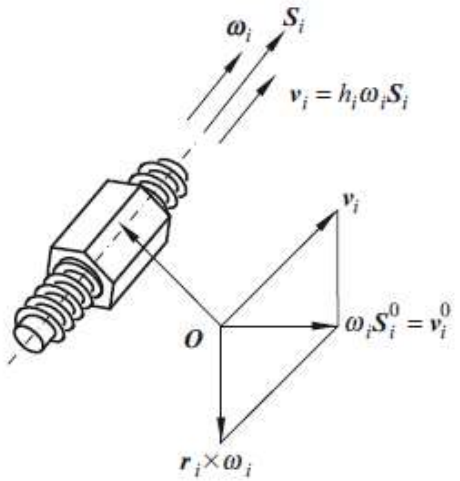

Scheme 4.4. Twist motion ('ri' is vector 'p' in scheme 4.3)[62]

In case the origin is crossed by the rotational axis,

$$\omega\$ = (\omega; 0) \qquad (4.7)$$

Otherwise, if sliding/prismatic kinematic pair is present, then translation has the following representation,

$$v\$ = (0; v) \tag{4.8}$$

For combined motion, i.e. rotation and translation,

$$\omega_i(S_i; S_{i+1}^i) = (\omega_i S_i; \omega_i S_{i+1}^i + h\omega_i S_i) \tag{4.9}$$

where 'h' denotes the pitch.

The pitch itself could be found by equation 4.10,

$$h = \frac{S_i \,.\, S_{i+1}^i}{S_i \,.\, S_i} = \frac{\omega_i \,.\, v}{\omega_i \,.\, \omega_i} \tag{4.10}$$

Likewise, the force and torque vectors also could be integrated into a screw representing a wrench,

$$f\$ = (fS; fS_0) = (f; C_0) \tag{4.11}$$

where $'C_0'$ is force moment f about the origin, i.e. $C_0 = f.p \times S_0$. Moment will not be present when force f will cross the origin, so therefore $(f; 0)$.

Important properties of screw theory that have high relevance to the spherical palm[63]:

1) If the origin is crossed by the line, the Plücker coordinates of that line are (S;0).
2) System of screws for the open chain serial linkages: twist of the end joint equals sum of all joint twists, $T_{end}=T_1+T_2+T_{n-1}+T_n$ (4.12)
3) System of screws for the closed chain serial linkages: sum of all twists for all joints in the loop equals zero, $T_1+T_2+T_{n-1}+T_n=0$ (4.13)
4) Particular joint twist in the closed loop can be expressed by summation or subtraction of other joint twists in the loop.
5) Acceleration analysis[64] of the closed chain serial linkages:

$$\dot{\omega}_1\$_2^1 + \dot{\omega}_2\$_2^1 + \dot{\omega}_n\$_n^{n-1} + L_n = 0 \tag{4.14}$$

where L_n represents the simplified derivation of grouped Lie products.

The Lie screw of acceleration, $L_n = [\omega_1\$_1 \quad \omega_2\$_2 + \omega_3\$_3 + \ldots \omega_n\$_n] \ldots$

$$\ldots + [\omega_2\$_2 \quad \omega_3\$_3 + \omega_4\$_4 + \ldots \omega_n\$_n] \ldots$$

$$\ldots + [\omega_{n-1}\$_{n-1} \quad \omega_n\$_n]. \tag{4.15}$$

6) The product of two screws is dictated by the Lie algebra[65]:

$$[\$_1 \quad \$_2] = \begin{bmatrix} \hat{\$}_1 \times \hat{\$}_2 \\ \hat{\$}_1 \times \$_{0(2)} - \hat{\$}_2 \times \$_{0(1)} \end{bmatrix} \tag{4.16}$$

4.2.3. Velocities and Accelerations[66]

Regarding velocities and accelerations,

$$^{i+1}v_{i+1} = {}^{i+1}_{i}R(^{i}v_i + {}^{i}\omega_i \times {}^{i}P_{i+1}) \tag{4.17}$$

$$^{i+1}\dot{v}_{i+1} = {}^{i+1}_{i}R(^{i}\dot{\omega}_i \times {}^{i}P_{i+1} + {}^{i}\omega_i \times \left({}^{i}\omega_i \times {}^{i}P_{i+1}\right) + {}^{i}\dot{v}_i) \tag{4.18}$$

$$^{i+1}\dot{v}_{C_{i+1}} = {}^{i+1}\dot{\omega}_{i+1} \times {}^{i+1}P_{C_{i+1}} + {}^{i+1}\omega_{i+1} \times \left({}^{i+1}\omega_{i+1} \times {}^{i+1}P_{C_{i+1}}\right) + {}^{i+1}\dot{v}_{i+1}) \tag{4.19}$$

$$^{i+1}\omega_{i+1} = {}^{i+1}_{i}R\,{}^{i}\omega_i + \dot{\theta}_{i+1}\,{}^{i+1}Z_{i+1} \tag{4.20}$$

$$^{i+1}\dot{\omega}_{i+1} = {}^{i+1}_{i}R\,{}^{i}\dot{\omega}_i + {}^{i+1}_{i}R\,{}^{i}\omega_i \times \dot{\theta}_{i+1}\,{}^{i+1}Z_{i+1} + \ddot{\theta}_{i+1}\,{}^{i+1}Z_{i+1} \tag{4.21}$$

4.2.4. Jacobian of the Manipulator and Inverse Jacobian[66]

In general, the Jacobian is a matrix that consists of partial derivatives of the joint functions. It is mainly used to relate joint velocities and end-effector linear and angular velocity. After mentioned in previous section velocities are propagated through the kinematic chain, it is then possible to extract $\dot{\theta}$ out of the final matrix. Therefore, Jacobian is obtained:

$$\begin{pmatrix} \upsilon \\ \omega \end{pmatrix} = J(\theta)\dot{\theta} \tag{4.22}$$

Nevertheless, it is often required for the Jacobian to be inverted. That allows to set velocities of the final part in the kinematic structure as an input and automatically program joint velocities using basic algorithm.

$$\dot{\theta} = J^{-1}(\theta)\begin{pmatrix} \upsilon \\ \omega \end{pmatrix} \tag{4.23}$$

Complexity of the inverting procedure depends on whether matrix is squared or non-squared. Inverse of the squared matrices is straightforward in terms of accuracy, but with non-squared matrices accuracy may be the problem. Non-squared matrices are inverted using pseudo-inverse technique. After that, in order to reduce deviations in calculations, Newton-Raphson method is used.[67] This approach is very useful but computational resources demanding since forward velocity and acceleration determination should be implemented in it. Moreover, considerable number of iterations should take place until desirable result would be acceptable. Newton-Raphson method is described in the next section.

As for accelerations, they are computed in the following manner[68]:

$$\begin{pmatrix} \dot{v} \\ \dot{\omega} \end{pmatrix} = J(\theta)\ddot{\theta} + \dot{J}(\theta)\dot{\theta} \qquad (4.24)$$

$$\ddot{\theta} = J^{-1}\left(\begin{pmatrix} \dot{v} \\ \dot{\omega} \end{pmatrix} - \dot{J}(\theta)\dot{\theta}\right) \qquad (4.25)$$

4.2.5. Four-bar Linkages Used in the Robotic Hand

Four-bar linkages are often used in robotics and provide reliable transmission ratio and durability. Schemes 4.5 and 4.6 show typical crank-rocker mechanism that drives the thumb.

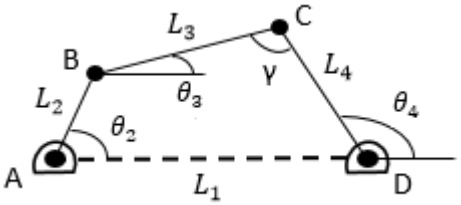

Scheme 4.5. Four-bar linkage (standard quadrants) 1

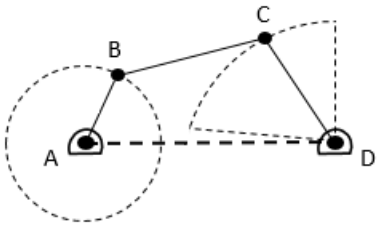

Scheme 4.6. Four-bar linkage (standard quadrants) 2

Position equations:

$$BD = \sqrt{L_1^2 + L_2^2 - 2L_1L_2\cos\theta_2} \qquad (4.26)$$

$$\gamma = \cos^{-1}\left(\frac{L_3^2+L_4^2-BD^2}{2L_3L_4}\right) \qquad (4.27)$$

$$\theta_3 = 2\tan^{-1}\left(\frac{-L_2\sin\theta_2+L_4\sin\gamma}{L_1+L_3-L_2\cos\theta_2-L_4\cos\gamma}\right) \qquad (4.28)$$

$$\theta_4 = 2\tan^{-1}\left(\frac{L_2\sin\theta_2-L_3\sin\gamma}{L_2\cos\theta_2+L_4-L_1-L_3\cos\gamma}\right) \qquad (4.29)$$

Velocity equations are:

$$\omega_3 = -\omega_2\left(\frac{L_2\sin(\theta_4-\theta_2)}{L_3\sin\gamma}\right) \qquad (4.30)$$

$$\omega_4 = -\omega_2 \left(\frac{L_2 \sin(\theta_3 - \theta_2)}{L_4 \sin\gamma}\right) \qquad (4.31)$$

Acceleration equations:

$$\alpha_3 = \frac{\alpha_2 L_2 \sin(\theta_2 - \theta_4) + \omega_2^2 L_2 \cos(\theta_2 - \theta_4) - \omega_4^2 L_4 + \omega_3^2 L_3 \cos(\theta_4 - \theta_3)}{L_3 \sin(\theta_4 - \theta_3)} \quad (4.32)$$

$$\alpha_4 = \frac{\alpha_2 L_2 \sin(\theta_2 - \theta_3) + \omega_2^2 L_2 \cos(\theta_2 - \theta_3) - \omega_3^2 L_4 \cos(\theta_4 - \theta_3) + \omega_3^2 L_3}{L_3 \sin(\theta_4 - \theta_3)} \quad (4.33)$$

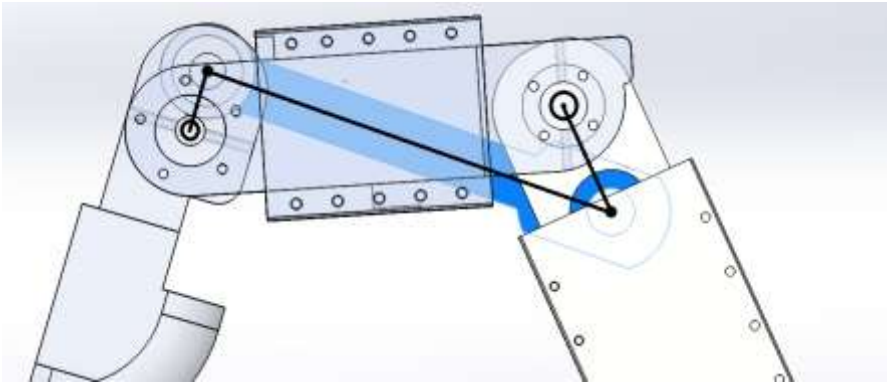

Figure 4.1. Four-bar linkage (non-standard quadrants) 1

Figure 4.1 illustrates that inside the robotic finger also the crank-rocker type of four-bar linkage is used. CD link operates in the opposite quadrant of the standard mechanism, scheme 4.8 shows that the link is assembled below in comparison to scheme 4.6.

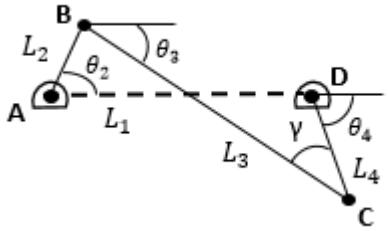

Scheme 4.7. Four-bar linkage (non-standard quadrants) 2

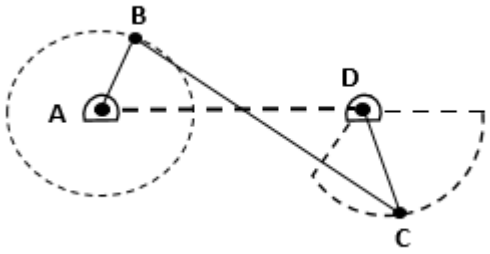

Scheme 4.8. Four-bar linkage (non-standard quadrants) 3

Changes made to the mechanism design should be indicated in the position equations. Hence, equations 4.28 and 4.29 are revised to include functioning of the CD link in a different quadrant:

$$\theta_3 = 2\tan^{-1}\left(\frac{-L_2\sin\theta_2 - L_4\sin\gamma}{L_1 + L_3 - L_2\cos\theta_2 - L_4\cos\gamma}\right) \qquad (4.34)$$

$$\theta_4 = 2\tan^{-1}\left(\frac{L_2\sin\theta_2 + L_3\sin\gamma}{L_2\cos\theta_2 + L_4 - L_1 - L_3\cos\gamma}\right) \qquad (4.35)$$

4.3. Inverse Kinematics Techniques

In this section, brief description of each IK method is given and main advantages and disadvantages are discussed.

4.3.1. Decoupling Technique

Decoupling method is applied for a six DOF manipulator with a spherical wrist. Decoupling method divides the kinematic problem into two independent parts: inverse orientation and inverse position kinematics. This further affects the forward kinematics transformation matrix, splitting it to a translation and rotation matrices product. The translation matrix is then responsible for calculating the position, whereas rotation part describes the orientation of the wrist.[5] Decoupling technique is only applied to manipulators with spherical wrist as in that case the translation matrix only contains the first three joint variables, as the final three joints movement will not affect the position of wrist centre.[6] Therefore, it is possible to equal wrist position vector with the joint variable parameters from transformation matrix to obtain three equations for joint variables. Those can then be solved to find the solutions for first three joint parameters. Once joint position parameters are determined, orientation parameters can be calculated.

The decoupling method greatly simplifies the non-complicated inverse kinematic problem. However, the main disadvantage of this technique is that with the more complex robotic manipulator configuration, complicated trigonometric equations arise and hence may not always be solved. In which case, another approach should be applied for solving the inverse kinematics problem.

4.3.2. Iterative Technique

Iterative technique applies Newton-Raphson method for solving the inverse kinematics problem. With this approach, the joint variables are found by substituting initial guess values for joint parameters into forward kinematics. The guess values are further changed according to modified Newton-Raphson approximation (equation 4.36) and the substitution process is repeated until the difference between q_{n+1} and q_n is less or equal to the required tolerance.

$$q_{n+1} = q_n + J^{-1}\delta T \qquad (4.36)$$

The δT value is the difference between the goal end effector position and the one obtained with the guess values. This value can also be referred to as an error and should be reduced.

The main disadvantage of the iterative technique is that it refers to the forward kinematics in order to solve the inverse problem, which leads to more time and actions required to solve the problem as many iterations can be required to achieve the desired position. However, such method has no application limitations and also eliminates the problem of solving complicated trigonometric equations that arise when decoupling or inverse transformation techniques are applied.

For inverse kinematics, singularities should be found in order to avoid problems. Once Jacobian is obtained, conditions when $|J| = 0$ or $|JJ^T|$ = has to be determined.

4.4. Combined Forward Kinematics

4.4.1. Angles of the Passive Joints

In order to find how passive joints change their values with respect to the input of active joints, it is necessary to obtain their axis positions. Initially, fixed axis is chosen from which rotations will take place. For the coordinates of the passive joints to be defined, they are multiplied by the unit vector. It is important to point out that angular dimensions between axis of the joints remain constant during motion of the mechanism. Thus, constraints $C_H^T C_G$, $C_H^T C_Q$ can be applied and system of equations in vector form is gained. Then, obtained relationship has to be integrated to $C_H^T C_H = 1$, where third row, representing 'z' axis, is studied and general equation of the form $Az_H^2 + Bz_H + C = 0$ is found. After that, solution for z_H is determined and hence passive angles θ_2, θ_3 and θ_4 could be solved by 'z' axis inspection of different routes to C_H and C_Q positions – dependency on the active angles θ_1 and θ_5 is therefore established.[69]

To obtain coordinates of passive connection 'G' in the global coordinate frame, the following multiplication procedure is followed:

$$C_G = \begin{bmatrix} x_G \\ y_G \\ z_G \end{bmatrix} = R(z_1, \theta_1)R(y_1, -\alpha_1)\boldsymbol{u} \quad (4.37)$$

To show direction of the 'z' axis (which is very specific for each joint), unit vector 'u' is introduced, $\mathbf{u} = \begin{bmatrix} 0 \\ 0 \\ 1 \end{bmatrix}$

For the convenience of calculation process presentation, multiplication of two rotation matrices and column unit vector u is shown in two stages below. First, rotation matrices are multiplied to give the following:

$$R(z_1, \theta_1)R(y_1, -\alpha_1) = \begin{bmatrix} c\theta_1 & -s\theta_1 & 0 \\ s\theta_1 & c\theta_1 & 0 \\ 0 & 0 & 1 \end{bmatrix} \begin{bmatrix} c(-25°) & 0 & s(-25°) \\ 0 & 1 & 0 \\ -s(-25°) & 0 & c(-25°) \end{bmatrix} =>$$

$$\begin{bmatrix} c\theta_1 & -s\theta_1 & 0 \\ s\theta_1 & c\theta_1 & 0 \\ 0 & 0 & 1 \end{bmatrix} \begin{bmatrix} c(-25°) & 0 & s(-25°) \\ 0 & 1 & 0 \\ -s(-25°) & 0 & c(-25°) \end{bmatrix} = \begin{bmatrix} c\theta_1 c(-25°) & -s\theta_1 & c\theta_1 s(-25°) \\ s\theta_1 c(-25°) & c\theta_1 & s\theta_1 s(-25°) \\ -s(-25°) & 0 & c(-25°) \end{bmatrix} \quad (4.38)$$

This matrix from equation 4.38 is then multiplied by u to get the final coordinates for passive connection "G",

$$C_G = \begin{bmatrix} c\theta_1 c(-25°) & -s\theta_1 & c\theta_1 s(-25°) \\ s\theta_1 c(-25°) & c\theta_1 & s\theta_1 s(-25°) \\ -s(-25°) & 0 & c(-25°) \end{bmatrix} \begin{bmatrix} 0 \\ 0 \\ 1 \end{bmatrix} = \begin{bmatrix} c\theta_1 s(-25°) \\ s\theta_1 s(-25°) \\ c(-25°) \end{bmatrix} \quad (4.39)$$

Similar procedure is followed to obtain position of passive joint 'H' in the global coordinate frame,

$$\mathrm{C_H} = \begin{bmatrix} x_H \\ y_H \\ z_H \end{bmatrix} = R(z_1, \theta_1) R(y_1, -\alpha_1) R(z_2, \theta_2) R(y_2, -\alpha_2) \boldsymbol{u} \quad (4.40)$$

$$C_H = \begin{bmatrix} c\theta_1 c(-25°) & -s\theta_1 & c\theta_1 s(-25°) \\ s\theta_1 c(-25°) & c\theta_1 & s\theta_1 s(-25°) \\ -s(-25°) & 0 & c(-25°) \end{bmatrix} R(z_2, \theta_2) R(y_2, -\alpha_2) \boldsymbol{u} \quad (4.41)$$

Two new rotation matrices $R(z_2, \theta_2)$ and $R(y_2, -\alpha_2)$ are again calculated separately to give:

$$R(z_2, \theta_2) R(y_2, -\alpha_2) = \begin{bmatrix} c\theta_2 & -s\theta_2 & 0 \\ s\theta_2 & c\theta_2 & 0 \\ 0 & 0 & 1 \end{bmatrix} \begin{bmatrix} c(-40°) & 0 & s(-40°) \\ 0 & 1 & 0 \\ -s(-40°) & 0 & c(-40°) \end{bmatrix} =$$

$$\begin{bmatrix} c\theta_2 c(-40°) & -s\theta_2 & c\theta_2 s(-40°) \\ s\theta_2 c(-40°) & c\theta_2 & s\theta_2 s(-40°) \\ -s(-40°) & 0 & c(-40°) \end{bmatrix} \quad (4.42)$$

It is possible to divide the multiplication of several matrices into smaller fragments as matrix multiplication is associative, and hence (AB)C=A(BC). This property allows to successfully split the equation and make the final multiplication easier. Obtained matrices are then substituted into equation 4.41 and the coordinates for passive joint 'H' are obtained:

$$C_H = \begin{bmatrix} c\theta_1 c(-25°) & -s\theta_1 & c\theta_1 s(-25°) \\ s\theta_1 c(-25°) & c\theta_1 & s\theta_1 s(-25°) \\ -s(-25°) & 0 & c(-25°) \end{bmatrix} \begin{bmatrix} c\theta_2 c(-40°) & -s\theta_2 & c\theta_2 s(-40°) \\ s\theta_2 c(-40°) & c\theta_2 & s\theta_2 s(-40°) \\ -s(-40°) & 0 & c(-40°) \end{bmatrix} \begin{bmatrix} 0 \\ 0 \\ 1 \end{bmatrix} =$$

$$\begin{bmatrix} c\theta_1 c(-25°) c\theta_2 s(-40°) - s\theta_1 s\theta_2 s(-40°) + c\theta_1 s(-25°) c(-40°) \\ s\theta_1 c(-25°) c\theta_2 s(-40°) + c\theta_1 s\theta_2 s(-40°) + s\theta_1 s(-25°) c(-40°) \\ -s(-25°) c\theta_2 s(-40°) + c(-25°) c(-40°) \end{bmatrix} \quad (4.43)$$

Described procedure is repeated to obtain the global coordinates of passive connection 'Q', which is defined by equation 4.44 below:

$$\mathrm{C_Q} = \begin{bmatrix} x_Q \\ y_Q \\ z_Q \end{bmatrix} = R(y_5, \alpha_5) R(z_5, \theta_5) R(y_4, \alpha_4) u \quad (4.44)$$

Given that α_5 is 113° and α_4 is 112°, rotation matrices can be substituted in. As stated earlier, matrix multiplication is associative and therefore can be done in reversed steps to simplify the calculation:

$$\begin{bmatrix} c(113°) & 0 & s(113°) \\ 0 & 1 & 0 \\ -s(113°) & 0 & c(113°) \end{bmatrix}\begin{bmatrix} c\theta_5 & -s\theta_5 & 0 \\ s\theta_5 & c\theta_5 & 0 \\ 0 & 0 & 1 \end{bmatrix}\begin{bmatrix} c(112°) & 0 & s(112°) \\ 0 & 1 & 0 \\ -s(112°) & 0 & c(112°) \end{bmatrix}\begin{bmatrix} 0 \\ 0 \\ 1 \end{bmatrix} =$$

$$\begin{bmatrix} c(113°) & 0 & s(113°) \\ 0 & 1 & 0 \\ -s(113°) & 0 & c(113°) \end{bmatrix}\begin{bmatrix} c\theta_5 & -s\theta_5 & 0 \\ s\theta_5 & c\theta_5 & 0 \\ 0 & 0 & 1 \end{bmatrix}\begin{bmatrix} s(112°) \\ 0 \\ c(112°) \end{bmatrix} =$$

$$\begin{bmatrix} c(113°) & 0 & s(113°) \\ 0 & 1 & 0 \\ -s(113°) & 0 & c(113°) \end{bmatrix}\begin{bmatrix} c\theta_5 s(112°) \\ s\theta_5 s(112°) \\ c(112°) \end{bmatrix} =$$

$$\begin{bmatrix} c(113°)c\theta_5 s(112°) + s(113°)c(112°) \\ s\theta_5 s(112°) \\ -s(113°)c\theta_5 s(112°) + c(113°)c(112°) \end{bmatrix} \quad (4.45)$$

Once the coordinates for passive joints G, H and Q are obtained, geometric constraints must be identified. First, the dot product of the vectors representing position of each passive connection axis should be calculated. Since connection H is a binder for joints G and Q, it is chosen as a reference point for constraint application.

The dot product of C_H^T and C_G was calculated manually, in order to show the calculation process and the use of the main trigonometric identity ($\sin^2 a + \cos^2 a = 1$).

$$C_H^T C_G = \begin{bmatrix} c\theta_1 c(-25°)c\theta_2 s(-40°) - s\theta_1 s\theta_2 s(-40°) + c\theta_1 s(-25°)c(-40°) \\ s\theta_1 c(-25°)c\theta_2 s(-40°) + c\theta_1 s\theta_2 s(-40°) + s\theta_1 s(-25°)c(-40°) \\ -s(-25°)c\theta_2 s(-40°) + c(-25°)c(-40°) \end{bmatrix}^T \cdot \begin{bmatrix} c\theta_1 s(-25°)) \\ s\theta_1 s(-25°) \\ c(-25°) \end{bmatrix} =>$$

$$\boldsymbol{C_H^T C_G} = c^2\theta_1 s(-25°)c(-25°)c\theta_2 s(-40°) - c\theta_1 s(-25°)s\theta_1 s\theta_2 s(-40°) +$$
$$c^2\theta_1 s^2(-25°)c(-40°) + s^2\theta_1 s(-25°)c(-25°)c\theta_2 s(-40°) +$$
$$s\theta_1 s(-25°)c\theta_1 s\theta_2 s(-40°) + s^2\theta_1 s^2(-25°)c(-40°) - c(-25°)s(-25°)c\theta_2 s(-40°) +$$
$$c^2(-25°)c(-40°) = s(-25°)c(-25°)c\theta_2 s(-40°)(c^2\theta_1 + s^2\theta_1) +$$
$$s^2(-25°)c(-40°)(c^2\theta_1 + s^2\theta_1) - c\theta_1 s(-25°)s\theta_1 s\theta_2 s(-40°) +$$
$$s\theta_1 s(-25°)c\theta_1 s\theta_2 s(-40°) - c(-25°)s(-25°)c\theta_2 s(-40°) + c^2(-25°)c(-40°) =$$
$$s(-25°)c(-25°)c\theta_2 s(-40°) + s^2(-25°)c(-40°) - c\theta_1 s(-25°)s\theta_1 s\theta_2 s(-40°) +$$
$$s\theta_1 s(-25°)c\theta_1 s\theta_2 s(-40°) - c(-25°)s(-25°)c\theta_2 s(-40°) + c^2(-25°)c(-40°) =$$
$$c(-40°)\left(s^2(-25°) + c^2(-25°)\right) = \boldsymbol{c(-40°)}$$

Appling another trigonometric identity, which states that cos(-a) = cos(a):

$$C_H^T C_G = \cos 40° = \cos \alpha_2 \quad (4.46)$$

Similar procedure was attempted for C_H^T and C_Q dot product calculation, however, due to absence of the sine and cosine squared after multiplication, the clear simplified solution could not be obtained. Therefore, it was necessary to make essential changes in C_H matrix. According to the mechanism of the palm, it is possible to consider connection 'H' from the other side, i.e. from L perspective. The way in which joint 'H' is described does not affect the mathematical meaning, however, makes the multiplication result dramatically clearer for presentation.

Describing the C_H from the other side, gives the following equation for C_H:

$$C_H = \begin{bmatrix} x_H \\ y_H \\ z_H \end{bmatrix} = R(y_5, \alpha_5)R(z_5, \theta_5)R(y_4, \alpha_4)R(z_4, \theta_4)R(y_3, \alpha_3)u \quad (4.47)$$

Given that α_5 is 113°, α_4 is 112° and α_3 is 70°, rotation matrices can be introduced and stepwise matrix multiplication can take place. For presentation convenience purposes, the $R(y_3, \alpha_3)$ multiplication with unit vector u was omitted and only final matrix ($\begin{bmatrix} s(70°) \\ 0 \\ c(70°) \end{bmatrix}$) was shown in the step-wise calculation. As earlier, the property of associative multiplication is used and hence the calculation is done starting from the end of the equation. The exact process is shown below for reference:

$C_H =$

$$\begin{bmatrix} c(113°) & 0 & s(113°) \\ 0 & 1 & 0 \\ -s(113°) & 0 & c(113°) \end{bmatrix}\begin{bmatrix} c\theta_5 & -s\theta_5 & 0 \\ s\theta_5 & c\theta_5 & 0 \\ 0 & 0 & 1 \end{bmatrix}\begin{bmatrix} c(112°) & 0 & s(112°) \\ 0 & 1 & 0 \\ -s(112°) & 0 & c(112°) \end{bmatrix}\begin{bmatrix} c\theta_4 & -s\theta_4 & 0 \\ s\theta_4 & c\theta_4 & 0 \\ 0 & 0 & 1 \end{bmatrix}\begin{bmatrix} s(70°) \\ 0 \\ c(70°) \end{bmatrix} =$$

$$= \begin{bmatrix} c(113°) & 0 & s(113°) \\ 0 & 1 & 0 \\ -s(113°) & 0 & c(113°) \end{bmatrix}\begin{bmatrix} c\theta_5 & -s\theta_5 & 0 \\ s\theta_5 & c\theta_5 & 0 \\ 0 & 0 & 1 \end{bmatrix}\begin{bmatrix} c(112°) & 0 & s(112°) \\ 0 & 1 & 0 \\ -s(112°) & 0 & c(112°) \end{bmatrix}\begin{bmatrix} c\theta_4 s(70°) \\ s\theta_4 s(70°) \\ c(70°) \end{bmatrix} =$$

$$= \begin{bmatrix} c(113°) & 0 & s(113°) \\ 0 & 1 & 0 \\ -s(113°) & 0 & c(113°) \end{bmatrix}\begin{bmatrix} c\theta_5 & -s\theta_5 & 0 \\ s\theta_5 & c\theta_5 & 0 \\ 0 & 0 & 1 \end{bmatrix}\begin{bmatrix} c(112°)c\theta_4 s(70°) + s(112°)c(70°) \\ s\theta_4 s(70°) \\ -s(112°)c\theta_4 s(70°) + c(112°)c(70°) \end{bmatrix} =$$

$$= \begin{bmatrix} c(113°) & 0 & s(113°) \\ 0 & 1 & 0 \\ -s(113°) & 0 & c(113°) \end{bmatrix}\begin{bmatrix} c\theta_5 c(112°)c\theta_4 s(70°) + c\theta_5 s(112°)c(70°) - s\theta_5 s\theta_4 s(70°) \\ s\theta_5 c(112°)c\theta_4 s(70°) + s\theta_5 s(112°)c(70°) + c\theta_5 s\theta_4 s(70°) \\ -s(112°)c\theta_4 s(70°) + c(112°)c(70°) \end{bmatrix}$$

Therefore, C_H position coordinates from L perspective is obtained:

$$\begin{bmatrix} c(113°)c\theta_5c(112°)c\theta_4s(70°) + c(113°)c\theta_5s(112°)c(70°) - c(113°)s\theta_5s\theta_4s(70°) - s(113°)s(112°)c\theta_4s(70°) + s(113°)c(112°)c(70°) \\ s\theta_5c(112°)c\theta_4s(70°) + s\theta_5s(112°)c(70°) + c\theta_5s\theta_4s(70°) \\ -s(113°)c\theta_5c(112°)c\theta_4s(70°) - s(113°)c\theta_5s(112°)c(70°) + s(113°)s\theta_5s\theta_4s(70°) - c(113°)s(112°)c\theta_4s(70°) + c(113°)c(112°)c(70°) \end{bmatrix}$$

(4.48)

Once the new set of coordinates for connection H is obtained, it's transpose can be multiplied with C_Q shown in equation 4.45. For the clear presentation of results, the factors C_H^T and C_Q were omitted. The final fully simplified expression for dot product of these two joints is given below:

$$C_H^T C_Q = \cos 70° = \cos \alpha_3 \quad (4.49)$$

Following the same procedure for C_H^T and C_H with any of C_H matrices from either equation 4.43 or 4.48, the product of transpose and actual matrix gives 1. Therefore:

$$C_H^T C_H = 1 \qquad (4.50)$$

Once all the answers are obtained, constraints could be set in a general form:

$$\begin{bmatrix} x_G & y_G & z_G \\ x_Q & y_Q & z_Q \end{bmatrix} \begin{bmatrix} x_H \\ y_H \\ z_H \end{bmatrix} = \begin{bmatrix} c\alpha_2 \\ c\alpha_3 \end{bmatrix} \qquad (4.51)$$

Multiplying the given matrices and rearranging the equation 4.51 in order to make it suitable for further solution:

$$\begin{bmatrix} x_G x_H + y_G y_H + z_G z_H \\ x_Q x_H + y_Q y_H + z_Q z_H \end{bmatrix} = \begin{bmatrix} c\alpha_2 \\ c\alpha_3 \end{bmatrix}$$

$$\begin{bmatrix} x_G x_H + y_G y_H \\ x_Q x_H + y_Q y_H \end{bmatrix} = \begin{bmatrix} c\alpha_2 - z_G z_H \\ c\alpha_3 - z_Q z_H \end{bmatrix} \qquad (4.52)$$

Equation 4.52 has the required form to solve the above system of linear equations. Cramer's rule can be used efficiently in determination of single variable without the need of solving the whole system. According to Cramer's rule:

$$x = \frac{D_x}{D}; y = \frac{D_y}{D}; z = \frac{D_z}{D} \qquad (4.53)$$

Where D is the coefficient matrix's determinant and D_x, D_y and D_z is the D matrix with answer column in place of x, y and z respectively.

In terms of coefficients for X_H and Y_H: $D = \begin{vmatrix} x_G & y_G \\ x_Q & y_Q \end{vmatrix}$ and therefore:

$$D = x_G y_Q - x_Q y_G \qquad (4.54)$$

Inserting answer column in x and y columns to find D_x and D_y respectively:

$$D_x = \begin{vmatrix} c\alpha_2 - z_G z_H & y_G \\ c\alpha_3 - z_Q z_H & y_Q \end{vmatrix} = c\alpha_2 y_Q - z_G z_H y_Q - c\alpha_3 y_G + z_Q z_H y_G$$

$$D_y = \begin{vmatrix} x_G & c\alpha_2 - z_G z_H \\ x_Q & c\alpha_3 - z_Q z_H \end{vmatrix} = c\alpha_3 x_G - z_Q z_H x_G - c\alpha_2 x_Q + z_G z_H x_Q$$

Then X and Y are given as:

$$x_H = \frac{D_x}{D} = \frac{c\alpha_2 y_Q - z_G z_H y_Q - c\alpha_3 y_G + z_Q z_H y_G}{x_G y_Q - x_Q y_G} = \frac{c\alpha_2 y_Q - c\alpha_3 y_G}{x_G y_Q - x_Q y_G} + \frac{(z_Q y_G - z_G y_Q)}{x_G y_Q - x_Q y_G} z_H$$

$$y_H = \frac{D_y}{D} = \frac{c\alpha_3 x_G - z_Q z_H x_G - c\alpha_2 x_Q + z_G z_H x_Q}{x_G y_Q - x_Q y_G} = \frac{c\alpha_3 x_G - c\alpha_2 x_Q}{x_G y_Q - x_Q y_G} + \frac{(z_G x_Q - z_Q x_G)}{x_G y_Q - x_Q y_G} z_H$$

This can be written in terms of Z_H as:

$$x_H = W + I z_H \qquad (4.55)$$

$$y_H = V + N z_H \qquad (4.56)$$

Where, $W = \frac{c\alpha_2 y_Q - c\alpha_3 y_G}{x_G y_Q - x_Q y_G}$; $I = \frac{(z_Q y_G - z_G y_Q)}{x_G y_Q - x_Q y_G}$; $V = \frac{c\alpha_3 x_G - c\alpha_2 x_Q}{x_G y_Q - x_Q y_G}$ and $N = \frac{(z_G x_Q - z_Q x_G)}{x_G y_Q - x_Q y_G}$.

Substituting Equations 4.55 and 4.56 into equation 4.50, gives:

$$[x_H \quad y_H \quad z_H] \begin{bmatrix} x_H \\ y_H \\ z_H \end{bmatrix} = 1 \text{ (Eq. 4.50 general form)}$$

$$[W + I z_H \quad V + N z_H \quad z_H] \begin{bmatrix} W + I z_H \\ V + N z_H \\ z_H \end{bmatrix} = (W + I z_H)^2 + (V + N z_H)^2 + z_H^2 = 1$$

$$= W^2 + 2WI z_H + I^2 z_H^2 + V^2 + 2VN z_H + N^2 z_H^2 + z_H^2 - 1 = 0$$

Above can be written as a generalized quadratic equation form for z_H:

$$A z_H^2 + B z_H + C = 0 \qquad (4.57)$$

Where, $A = I^2 + N^2 + 1$; $B = 2WI + 2VN$ and $C = W^2 + V^2 - 1$.

Equation 4.57 can now be solved for z_H to give:

$$z_H = \frac{-B \pm \sqrt{B^2 - 4AC}}{2A} \qquad (4.58)$$

Now, when z_H value is determined, it is possible to obtain the unknown angles $(\theta_2, \theta_3, \theta_4)$.

In order to define θ_2, equation 4.58 is compared with Z component of equation 4.43:

$$z_H = -s(-25°)c\theta_2 s(-40°) + c(-25°)c(-40°)$$

$$z_H - c(-25°)c(-40°) = -s(-25°)c\theta_2 s(-40°)$$

$$\frac{c(-25°)c(-40°)}{s(-25°)s(-40°)} - \frac{z_H}{s(-25°)s(-40°)} = c\theta_2$$

$$c\theta_2 = \cot(-25°)\cot(-40°) - \frac{z_H}{s(-25°)s(-40°)}$$

$$\theta_2 = \cos^{-1}\left(\cot(-25°)\cot(-40°) - \frac{z_H}{s(-25°)s(-40°)}\right) \qquad (4.59)$$

In order to define θ_4, equation 4.58 is compared to Z component of equation 4.48.

$$\begin{aligned} z_H = {} & -s(113°)c\theta_5 c(112°)c\theta_4 s(70°) - s(113°)c\theta_5 s(112°)c(70°) \\ & + s(113°)s\theta_5 s\theta_4 s(70°) - c(113°)s(112°)c\theta_4 s(70°) \\ & + c(113°)c(112°)c(70°) \end{aligned}$$

$$\begin{aligned} & s(113°)c\theta_5 c(112°)c\theta_4 s(70°) + c(113°)s(112°)c\theta_4 s(70°) - s(113°)s\theta_5 s\theta_4 s(70°) \\ & = c(113°)c(112°)c(70°) - s(113°)c\theta_5 s(112°)c(70°) - z_H \end{aligned}$$

This then can be written as:

$$Ac\theta_4 + Bs\theta_4 = C \qquad (4.60)$$

Where, $A = s(113°)c\theta_5 c(112°)s(70°) + c(113°)s(112°)s(70°)$; $B = -s(113°)s\theta_5 s(70°)$ and $C = c(113°)c(112°)c(70°) - s(113°)c\theta_5 s(112°)c(70°) - z_H$

Once the general form of trigonometric equation is obtained, θ_4 can be calculated.

$$Ac\theta_4 + Bs\theta_4 = C$$

$$Ac\theta_4 = C - Bs\theta_4$$

Applying that $sin^2\alpha + cos^2\alpha = 1$ and therefore, $sin^2 = 1 - cos^2$, *which gives* $sin\alpha\ \sqrt{1 - cos^2\alpha}$:

$$Ac\theta_4 - C = -B\sqrt{1 - c^2\theta_4}$$

Taking square of the equation above and rearranging:

$$(Ac\theta_4 - C)^2 = (-B\sqrt{1 - c^2\theta_4})^2$$

$$A^2c^2\theta_4 - 2ACc\theta_4 + C^2 = B^2(1 - c^2\theta_4)$$

$$A^2c^2\theta_4 - 2ACc\theta_4 + C^2 = B^2 - B^2c^2\theta_4$$

$$A^2c^2\theta_4 + B^2c^2\theta_4 - 2ACc\theta_4 = B^2 - C^2$$

$$(A^2 + B^2)c^2\theta_4 - (2AC)c\theta_4 + (C^2 - B^2) = 0 \quad (4.61)$$

The equation is now in usual quadratic equation form with coefficients in green. Combining equation 4.61 with general quadratic equation solutions ($x = \frac{-b \mp \sqrt{b^2-4ac}}{2a}$):

$$c\theta_4 = \frac{2AC \mp \sqrt{(-2AC)^2 - 4(A^2 + B^2)(C^2 - B^2)}}{2(A^2 + B^2)}$$

$$c\theta_4 = \frac{2AC \mp \sqrt{4A^2C^2 - 4A^2C^2 + 4A^2B^2 - 4B^2C^2 + 4B^4}}{2(A^2 + B^2)}$$

$$c\theta_4 = \frac{2AC \mp \sqrt{4(A^2B^2 - B^2C^2 + B^4)}}{2(A^2 + B^2)}$$

$$c\theta_4 = \frac{2AC \mp \sqrt{4B^2(A^2 - C^2 + B^2)}}{2(A^2 + B^2)}$$

$$c\theta_4 = \frac{2AC \mp 2B\sqrt{(A^2 - C^2 + B^2)}}{2(A^2 + B^2)}$$

$$c\theta_4 = \frac{AC \mp B\sqrt{(A^2 - C^2 + B^2)}}{(A^2 + B^2)}$$

Now, θ_4 can be found taking inverse of cosine:

$$\theta_4 = \cos^{-1}\left(\frac{AC \mp B\sqrt{(A^2-C^2+B^2)}}{(A^2+B^2)}\right) \quad (4.62)$$

In order to obtain the equations for θ_3, it is necessary to describe position coordinates of passive joint 'Q' from L-perspective:

$$C_Q = \begin{bmatrix} x_Q \\ y_Q \\ z_Q \end{bmatrix} = R(z_1, \theta_1)R(y_1, -\alpha_1)R(z_2, \theta_2)R(y_2, -\alpha_2)R(z_3, \theta_3)R(y_3, -\alpha_3)u \quad (4.63)$$

Following the same procedure as earlier in determining C_Q, named rotation matrices are introduces and multiplied to give the final result to last two factors:

$$\begin{bmatrix} c\theta_1 c(-25°) & -s\theta_1 & c\theta_1 s(-25°) \\ s\theta_1 c(-25°) & c\theta_1 & s\theta_1 s(-25°) \\ -s(-25°) & 0 & c(-25°) \end{bmatrix} \begin{bmatrix} c\theta_2 c(-40°)c\theta_3 s(-70°) + c\theta_2 s(-40°)c(-70°) - s\theta_2 s\theta_3 s(-70°) \\ s\theta_2 c(-40°)c\theta_3 s(-70°) + s\theta_2 s(-40°)c(-70°) + c\theta_2 s\theta_3 s(-70°) \\ -s(-40°)c\theta_3 s(-70°) + c(-40°)c(-70°) \end{bmatrix}$$

(4.64)

As it is not possible to clearly show the matrix in full due to space limitations, the final coefficients of the C_Q matrix are given below:

$$\begin{aligned} x_Q = {} & c\theta_1 c(-25°)c\theta_2 c(-40°)c\theta_3 s(-70°) + c\theta_1 c(-25°)c\theta_2 s(-40°)c(-70°) \\ & - c\theta_1 c(-25°)s\theta_2 s\theta_3 s(-70°) - s\theta_1 s\theta_2 c(-40°)c\theta_3 s(-70°) \\ & - s\theta_1 s\theta_2 s(-40°)c(-70°) - s\theta_1 c\theta_2 s\theta_3 s(-70°) \\ & - c\theta_1 s(-25°)s(-40°)c\theta_3 s(-70°) + c\theta_1 s(-25°)c(-40°)c(-70°) \end{aligned}$$

$$\begin{aligned} y_Q = {} & s\theta_1 c(-25°)c\theta_2 c(-40°)c\theta_3 s(-70°) + s\theta_1 c(-25°)c\theta_2 s(-40°)c(-70°) \\ & - s\theta_1 c(-25°)s\theta_2 s\theta_3 s(-70°) + c\theta_1 s\theta_2 c(-40°)c\theta_3 s(-70°) \\ & + c\theta_1 s\theta_2 s(-40°)c(-70°) + c\theta_1 c\theta_2 s\theta_3 s(-70°) \\ & - s\theta_1 s(-25°)s(-40°)c\theta_3 s(-70°) + s\theta_1 s(-25°)c(-40°)c(-70°) \end{aligned}$$

$$\begin{aligned} z_Q = {} & -s(-25°)c\theta_2 c(-40°)c\theta_3 s(-70°) - s(-25°)c\theta_2 s(-40°)c(-70°) + \\ & s(-25°)s\theta_2 s\theta_3 s(-70°) - c(-25°)s(-40°)c\theta_3 s(-70°) + c(-25°)c(-40°)c(-70°) \end{aligned}$$

Since mathematically the original C_Q matrix (from R-perspective) and C_Q matrix from L-perspective (equation 4.52) are similar, the following equality can be set:

$$R(z_1, \theta_1)R(y_1, -\alpha_1)R(z_2, \theta_2)R(y_2, -\alpha_2)R(z_3, \theta_3)R(y_3, -\alpha_3)u = R(y_5, \alpha_5)R(z_5, \theta_5)R(y_4, \alpha_4)u \quad (4.65)$$

According to equation 4.53, coefficients of matrices from equations 4.45 and 4.64 can be compared.

From the Z_Q perspective:

$$-s(-25°)c\theta_2 c(-40°)c\theta_3 s(-70°) - s(-25°)c\theta_2 s(-40°)c(-70°) + s(-25°)s\theta_2 s\theta_3 s(-70°) - c(-25°)s(-40°)c\theta_3 s(-70°) + c(-25°)c(-40°)c(-70°) = -s(113°)c\theta_5 s(112°) + c(113°)c(112°) \Rightarrow$$

$$-s(-25°)c\theta_2 s(-40°)c(-70°) + c(-25°)c(-40°)c(-70°) + s(113°)c\theta_5 s(112°) - c(113°)c(112°) = s(-25°)c\theta_2 c(-40°)c\theta_3 s(-70°) + c(-25°)s(-40°)c\theta_3 s(-70°) - s(-25°)s\theta_2 s\theta_3 s(-70°) \Rightarrow$$

$c\theta_3\big(s(-25°)c\theta_2 c(-40°)s(-70°) + c(-25°)s(-40°)s(-70°)\big) +$
$s\theta_3\big(-s(-25°)s\theta_2 s(-70°)\big) = c(-25°)c(-40°)c(-70°) - c(113°)c(112°) +$
$s(113°)c\theta_5 s(112°) - s(-25°)c\theta_2 s(-40°)c(-70°)$

This gives:

$$A'c\theta_3 + B's\theta_3 = C' \qquad (4.66)$$

$A' = s(-25°)c\theta_2 c(-40°)s(-70°) + c(-25°)s(-40°)s(-70°)$; $B' =$
$-s(-25°)s\theta_2 s(-70°)$; $C' = c(-25°)c(-40°)c(-70°) - c(113°)c(112°) +$
$s(113°)c\theta_5 s(112°) - \ s(-25°)c\theta_2 s(-40°)c(-70°)$

As equation 4.66 is identical to equation 4.60, it's solution must be exactly the same once appropriate coefficients are inserted and notation is changed. This means that:

$$c\theta_3 = \frac{A'C' \mp B'\sqrt{(A'^2 - C'^2 + B'^2)}}{(A'^2 + B'^2)} \qquad (4.67)$$

Now, θ_3 can be found taking inverse of cosine:

$$\theta_3 = arccos\left(\frac{A'C' \mp B'\sqrt{(A'^2 - C'^2 + B'^2)}}{(A'^2 + B'^2)}\right) \qquad (4.68)$$

4.4.2. Further Kinematics. Transformations to the Fingertips.

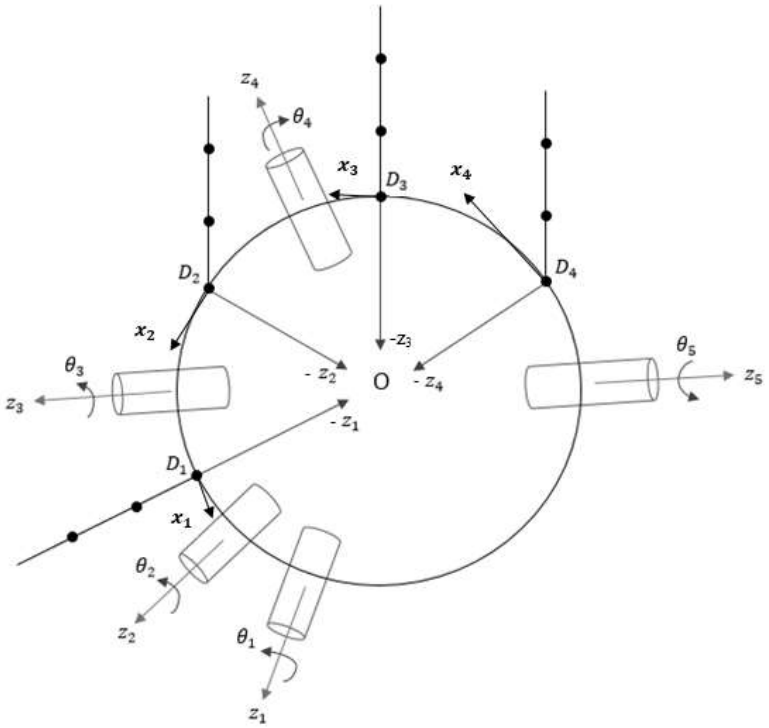

Scheme 4.9. Combined Kinematics

y_{D_i} $(i = 3, 4)$ is directed along $z_{D_i} \times z_4$. y_{D_2} is directed along $z_{D_2} \times z_3$. y_{D_1} is directed along $z_{D_1} \times z_2$.

In terms of fingers, each finger's local coordinate ($E_i$with x_i, y_i and z_i) frame is set at the revolute joint located in the basement of the finger. x_i axis is directed along the $E_i D_i$, but x_i is pointing to the same direction as the lower joint of each finger.

For $i = 2, 3, 4$, angle between $z_{D_i}$and x_i is Δ_i and distance between D_i and E_i is S_i. The thumb $(i = 1)$ has Δ_1 for angle between OD_1 and pulley axis is W. S_1 stands for distance between D_1 and E_1. Angle between z axis of these points is given as Ψ.

Considering given geometric positioning and dependence, it is now possible to arrange a general relationship in terms of global coordinate frame located in the centre of the palm.

For the thumb (i=1), it is necessary to consider two joints, including actuated joint. First, rotation of the 'z_1' axis occurs and then its displacement around 'y' axis leads to the second connection. According to the right hand rule, displacement will be classified as negative. After that, rotation of ('z_2' axis) the second connection occurs. Next displacement should

lead to the attachment point of the finger, 'φ_1' is introduced as the angle between the second connection and the attachment point. Therefore,

$$R(z0_1, \theta_1)R(y_1, -\alpha_1)R(z_2, \theta_2)R(y_2, -\varphi_1) \qquad (4.69)$$

For the index finger (i=2), previous order is repeated, but displacement from the second joint is now translated to the third joint, not thumb. After rotation of the third connection is considered, translation to the index finger occurs. Therefore,

$$R(z_1, \theta_1)R(y_1, -\alpha_1)R(z_2, \theta_2)R(y_2, -\alpha_2)\ R(z_3, \theta_3)\ R(y_3, -\varphi_2') \quad (4.70)$$

where: φ_2' – angle between the third joint and attachment point of the index finger.

From the other motor prospective, only two joints (not 3) should be considered, i.e. four and five (and then final displacement to the attachment point from connection four is done). This order is shorter by one rotation matrix. Since the second actuated joint is located in different direction, translation from the starting point is followed by rotation of the actuated joint. Order of the sequence is changed. In addition, displacement angles around 'y' axis are now positive. Therefore,

$$R(y_5, \alpha_5)R(z_5, \theta_5)R(y_4, \alpha_4)\ R(z_4, \theta_4)\ R(y_3, \varphi_2) \qquad (4.71)$$

For the fingers 3 and 4 (i=3 and 4), after displacement to the fifth connection is shown and rotation of that connection taken into account, final displacement for each finger separately could be done:

$$R(y_5, \alpha_5)R(z_5, \theta_5)R(y_4, \varphi_i) \qquad (4.72)$$

The following 'condition bracket' shows sequences of reaching attachment point of each finger through rotation matrices:

$$R_{OD_i} = \begin{cases} R(z_1, \theta_1)R(y_1, -\alpha_1)R(z_2, \theta_2)R(y_2, -\varphi_1) & if\ i = 1 \\ R(y_5, \alpha_5)R(z_5, \theta_5)R(y_4, \alpha_4)\ R(z_4, \theta_4)R(y_3, \varphi_2) & if\ i = 2 \\ R(y_5, \alpha_5)R(z_5, \theta_5)R(y_4, \varphi_i) & if\ i = 3\ and\ 4 \end{cases} \qquad (4.73)$$

To represent attachment point in global coordinates, transformation matrix is constructed:

$$T_{OD_i} = \begin{bmatrix} R_{OD_i} & R_{OD_i}\varepsilon' \\ 0\ \ 0\ \ 0 & 1 \end{bmatrix}, \text{(i = 1,2,3,4)}$$

where: $\varepsilon' = [0, 0, L]^T$ and $R_{OD_i}\varepsilon'$ gives position vector of point D_i in the global coordinates. The 'L' represents the radius to the attachment point. It is not equal to the radius of the virtual

sphere, because attachment points are not allocated in the symmetrical manner. Some points are located closer to the centre of the palm, some are shifted away and are greater than the radius of the virtual sphere.

In order to translate local coordinate frame of the finger's lower joint to the global coordinate frame, the following transformation matrix is formed:

$$T_{OE_i} = T_{OD_i} T_{DE_i} = \begin{bmatrix} R_{OE_i} & P_{OE_i} \\ 0 \quad 0 \quad 0 & 1 \end{bmatrix} \qquad (4.74)$$

Then, in order to reach each fingertip and make coordinates global:

$$T_{O\_fingertip} = T_{OE_i} T_{E_i\_fingertip} \qquad (4.75)$$

Therefore, overall orientations and translations for each finger are as follows:

4.4.2.1. For the thumb (theta 2 can have two variations)

Round brackets are used in order to indicate that the several matrices represent one particular transformation. In the following order:

$${}^0_6T = {}^0_1T\,{}^1_2T\,{}^2_3T\,{}^3_4T\,{}^4_5T\,{}^5_6T = \begin{bmatrix} cos\theta_1 & -sin\theta_1 & 0 & 0 \\ sin\theta_1 & cos\theta_1 & 0 & 0 \\ 0 & 0 & 1 & 0 \\ 0 & 0 & 0 & 1 \end{bmatrix} * A_1(B_1C_1)(D_1E_1)F_1G_1 \qquad (4.76)$$

Where: $A_1 = \begin{bmatrix} \cos(-25) & 0 & \sin(-25) & 0 \\ 0 & 1 & 0 & 0 \\ -\sin(-25) & 0 & \cos(-25) & 0 \\ 0 & 0 & 0 & 1 \end{bmatrix} \begin{bmatrix} cos\theta_2 & -sin\theta_2 & 0 & 0 \\ sin\theta_2 & cos\theta_2 & 0 & 0 \\ 0 & 0 & 1 & 0 \\ 0 & 0 & 0 & 1 \end{bmatrix}$

$$B_1 = \begin{bmatrix} \cos(-17) & 0 & \sin(-17) & 0 \\ 0 & 1 & 0 & 0 \\ -\sin(-17) & 0 & \cos(-17) & 0 \\ 0 & 0 & 0 & 1 \end{bmatrix} \begin{bmatrix} 1 & 0 & 0 & 0 \\ 0 & 1 & 0 & 0 \\ 0 & 0 & 1 & 45 \\ 0 & 0 & 0 & 1 \end{bmatrix} \begin{bmatrix} \cos(34) & 0 & \sin(34) & 0 \\ 0 & 1 & 0 & 0 \\ -\sin(34) & 0 & \cos(34) & 0 \\ 0 & 0 & 0 & 1 \end{bmatrix}$$

$$C_1 = \begin{bmatrix} \cos(0{,}0019\theta^2{}_6 + 0{,}1256\theta_6 - 0{,}7287) & -\sin(0{,}0019\theta^2{}_6 + 0{,}1256\theta_6 - 0{,}7287) & 0 & 0 \\ \sin(0{,}0019\theta^2{}_6 + 0{,}1256\theta_6 - 0{,}7287) & cos(0{,}0019\theta^2{}_6 + 0{,}1256\theta_6 - 0{,}7287) & 0 & 0 \\ 0 & 0 & 1 & 0 \\ 0 & 0 & 0 & 1 \end{bmatrix}$$

$$D_1 = \begin{bmatrix} 1 & 0 & 0 & -59.05 \\ 0 & 1 & 0 & 0 \\ 0 & 0 & 1 & 0 \\ 0 & 0 & 0 & 1 \end{bmatrix} \begin{bmatrix} 1 & 0 & 0 & 0 \\ 0 & \cos(-72) & -\sin(-72) & 0 \\ 0 & \sin(-72) & \cos(-72) & 0 \\ 0 & 0 & 0 & 1 \end{bmatrix}$$

$$E_1 = \begin{bmatrix} \cos(-0{,}0063\theta^2{}_7 + 1{,}8006\theta_7 - 0{,}7794) & -\sin(-0{,}0063\theta^2{}_7 + 1{,}8006\theta_7 - 0{,}7794) & 0 & 0 \\ \sin(-0{,}0063\theta^2{}_7 + 1{,}8006\theta_7 - 0{,}7794) & \cos(-0{,}0063\theta^2{}_7 + 1{,}8006\theta_7 - 0{,}7794) & 0 & 0 \\ 0 & 0 & 1 & 0 \\ 0 & 0 & 0 & 1 \end{bmatrix}$$

$$F_1 = \begin{bmatrix} \cos(0{,}0034{\theta^2}_7 + 1{,}3417\theta_7 + 0{,}5973) & -\sin(0{,}0034{\theta^2}_7 + 1{,}3417\theta_7 + 0{,}5973) & 0 & -31.50 \\ \sin(0{,}0034{\theta^2}_7 + 1{,}3417\theta_7 + 0{,}5973) & \cos(0{,}0034{\theta^2}_7 + 1{,}3417\theta_7 + 0{,}5973) & 0 & 0 \\ 0 & 0 & 1 & 0 \\ 0 & 0 & 0 & 1 \end{bmatrix}$$

$$G_1 = \begin{bmatrix} 1 & 0 & 0 & -27.45 \\ 0 & 1 & 0 & 0 \\ 0 & 0 & 1 & 0 \\ 0 & 0 & 0 & 1 \end{bmatrix}$$

4.4.2.2. For the index finger (theta 4 can have four variations)

$$ {}^0_6T = {}^0_1T\,{}^1_2T\,{}^2_3T\,{}^3_4T\,{}^4_5T\,{}^5_6T = A_2B_2(C_2D_2)E_2F_2G_2 \qquad (4.77)$$

Where: $A_2 = \begin{bmatrix} \cos(113) & 0 & \sin(113) & 0 \\ 0 & 1 & 0 & 0 \\ -\sin(113) & 0 & \cos(113) & 0 \\ 0 & 0 & 0 & 1 \end{bmatrix} \begin{bmatrix} cos\theta_5 & -sin\theta_5 & 0 & 0 \\ sin\theta_5 & cos\theta_5 & 0 & 0 \\ 0 & 0 & 1 & 0 \\ 0 & 0 & 0 & 1 \end{bmatrix}$

$$B_2 = \begin{bmatrix} \cos(112) & 0 & \sin(112) & 0 \\ 0 & 1 & 0 & 0 \\ -\sin(112) & 0 & \cos(112) & 0 \\ 0 & 0 & 0 & 1 \end{bmatrix} \begin{bmatrix} cos\theta_4 & -sin\theta_4 & 0 & 0 \\ sin\theta_4 & cos\theta_4 & 0 & 0 \\ 0 & 0 & 1 & 0 \\ 0 & 0 & 0 & 1 \end{bmatrix}$$

$$C_2 = \begin{bmatrix} \cos(46) & 0 & \sin(46) & 0 \\ 0 & 1 & 0 & 0 \\ -\sin(46) & 0 & \cos(46) & 0 \\ 0 & 0 & 0 & 1 \end{bmatrix} \begin{bmatrix} 1 & 0 & 0 & 0 \\ 0 & 1 & 0 & 0 \\ 0 & 0 & 1 & 31.75 \\ 0 & 0 & 0 & 1 \end{bmatrix} \begin{bmatrix} \cos(-148.67 - 180) & 0 & \sin(-148.67 - 180) & 0 \\ 0 & 1 & 0 & 0 \\ -\sin(-148.67 - 180) & 0 & \cos(-148.67 - 180) & 0 \\ 0 & 0 & 0 & 1 \end{bmatrix}$$

$$D_2 = \begin{bmatrix} 1 & 0 & 0 & -70 \\ 0 & 1 & 0 & 0 \\ 0 & 0 & 1 & 0 \\ 0 & 0 & 0 & 1 \end{bmatrix} \begin{bmatrix} cos\theta_8 & -sin\theta_8 & 0 & 0 \\ sin\theta_8 & cos\theta_8 & 0 & 0 \\ 0 & 0 & 1 & 0 \\ 0 & 0 & 0 & 1 \end{bmatrix}$$

$$E_2 = \begin{bmatrix} cos(-0{,}0063{\theta^2}_9 + 1{,}8006\theta_9 - 0{,}7794) & -sin(-0{,}0063{\theta^2}_9 + 1{,}8006\theta_9 - 0{,}7794) & 0 & -47.45 \\ sin(-0{,}0063{\theta^2}_9 + 1{,}8006\theta_9 - 0{,}7794) & cos(-0{,}0063{\theta^2}_9 + 1{,}8006\theta_9 - 0{,}7794) & 0 & 0 \\ 0 & 0 & 1 & 0 \\ 0 & 0 & 0 & 1 \end{bmatrix}$$

$$F_2 \begin{bmatrix} cos(0{,}0034{\theta^2}_9 + 1{,}3417\theta_9 + 0{,}5973) & -sin(0{,}0034{\theta^2}_9 + 1{,}3417\theta_9 + 0{,}5973) & 0 & -31.50 \\ \sin(0{,}0034{\theta^2}_9 + 1{,}3417\theta_9 + 0{,}5973) & \cos(0{,}0034{\theta^2}_9 + 1{,}3417\theta_9 + 0{,}5973) & 0 & 0 \\ 0 & 0 & 1 & 0 \\ 0 & 0 & 0 & 1 \end{bmatrix}$$

$$G_2 = \begin{bmatrix} 1 & 0 & 0 & -27.45 \\ 0 & 1 & 0 & 0 \\ 0 & 0 & 1 & 0 \\ 0 & 0 & 0 & 1 \end{bmatrix}$$

4.4.2.3. For the middle finger

$$ {}^{0}_{5}T = {}^{0}_{1}T\,{}^{1}_{2}T\,{}^{2}_{3}T\,{}^{3}_{4}T\,{}^{4}_{5}T = A_3(B_3C_3)D_3E_3F_3 \qquad (4.78) $$

Where: $A_3 = \begin{bmatrix} \cos(113) & 0 & \sin(113) & 0 \\ 0 & 1 & 0 & 0 \\ -\sin(113) & 0 & \cos(113) & 0 \\ 0 & 0 & 0 & 1 \end{bmatrix} \begin{bmatrix} cos\theta_5 & -sin\theta_5 & 0 & 0 \\ sin\theta_5 & cos\theta_5 & 0 & 0 \\ 0 & 0 & 1 & 0 \\ 0 & 0 & 0 & 1 \end{bmatrix}$

$B_3 = \begin{bmatrix} \cos(70) & 0 & \sin(70) & 0 \\ 0 & 1 & 0 & 0 \\ -\sin(70) & 0 & \cos(70) & 0 \\ 0 & 0 & 0 & 1 \end{bmatrix} \begin{bmatrix} 1 & 0 & 0 & 0 \\ 0 & 1 & 0 & 0 \\ 0 & 0 & 1 & 20.5 \\ 0 & 0 & 0 & 1 \end{bmatrix} \begin{bmatrix} \cos(-60.67-180) & 0 & \sin(-60.67-180) & 0 \\ 0 & 1 & 0 & 0 \\ -\sin(-60.67-180) & 0 & \cos(-60.67-180) & 0 \\ 0 & 0 & 0 & 1 \end{bmatrix}$

$C_3 = \begin{bmatrix} 1 & 0 & 0 & -70 \\ 0 & 1 & 0 & 0 \\ 0 & 0 & 1 & 0 \\ 0 & 0 & 0 & 1 \end{bmatrix} \begin{bmatrix} cos\theta_{10} & -sin\theta_{10} & 0 & 0 \\ sin\theta_{10} & cos\theta_{10} & 0 & 0 \\ 0 & 0 & 1 & 0 \\ 0 & 0 & 0 & 1 \end{bmatrix}$

$D_3 = \begin{bmatrix} cos(-0{,}0063{\theta^2}_{11} + 1{,}8006\theta_{11} - 0{,}7794) & -sin(-0{,}0063{\theta^2}_{11} + 1{,}8006\theta_{11} - 0{,}7794) & 0 & -47.45 \\ sin(-0{,}0063{\theta^2}_{11} + 1{,}8006\theta_{11} - 0{,}7794) & cos(-0{,}0063{\theta^2}_{11} + 1{,}8006\theta_{11} - 0{,}7794) & 0 & 0 \\ 0 & 0 & 1 & 0 \\ 0 & 0 & 0 & 1 \end{bmatrix}$

$E_3 = \begin{bmatrix} cos(0{,}0034{\theta^2}_{11} + 1{,}3417\theta_{11} + 0{,}5973) & -sin(0{,}0034{\theta^2}_{11} + 1{,}3417\theta_{11} + 0{,}5973) & 0 & -31.50 \\ \sin(0{,}0034{\theta^2}_{11} + 1{,}3417\theta_{11} + 0{,}5973) & \cos(0{,}0034{\theta^2}_{11} + 1{,}3417\theta_{11} + 0{,}5973) & 0 & 0 \\ 0 & 0 & 1 & 0 \\ 0 & 0 & 0 & 1 \end{bmatrix}$

$F_3 = \begin{bmatrix} 1 & 0 & 0 & -27.45 \\ 0 & 1 & 0 & 0 \\ 0 & 0 & 1 & 0 \\ 0 & 0 & 0 & 1 \end{bmatrix}$

4.4.2.4. For the ring finger

$$ {}^{0}_{5}T = {}^{0}_{1}T\,{}^{1}_{2}T\,{}^{2}_{3}T\,{}^{3}_{4}T\,{}^{4}_{5}T = A_4(B_4C_4)D_4E_4F_4 \qquad (4.79) $$

Where: $A_4 = \begin{bmatrix} \cos(113) & 0 & \sin(113) & 0 \\ 0 & 1 & 0 & 0 \\ -\sin(113) & 0 & \cos(113) & 0 \\ 0 & 0 & 0 & 1 \end{bmatrix} \begin{bmatrix} cos\theta_5 & -sin\theta_5 & 0 & 0 \\ sin\theta_5 & cos\theta_5 & 0 & 0 \\ 0 & 0 & 1 & 0 \\ 0 & 0 & 0 & 1 \end{bmatrix}$

$B_4 = \begin{bmatrix} \cos(20) & 0 & \sin(20) & 0 \\ 0 & 1 & 0 & 0 \\ -\sin(20) & 0 & \cos(20) & 0 \\ 0 & 0 & 0 & 1 \end{bmatrix} \begin{bmatrix} 1 & 0 & 0 & 0 \\ 0 & 1 & 0 & 0 \\ 0 & 0 & 1 & 38.5 \\ 0 & 0 & 0 & 1 \end{bmatrix} \begin{bmatrix} \cos(-190.67) & 0 & \sin(-190.67) & 0 \\ 0 & 1 & 0 & 0 \\ -\sin(-190.67) & 0 & \cos(-190.67) & 0 \\ 0 & 0 & 0 & 1 \end{bmatrix}$

$C_4 = \begin{bmatrix} 1 & 0 & 0 & -70 \\ 0 & 1 & 0 & 0 \\ 0 & 0 & 1 & 0 \\ 0 & 0 & 0 & 1 \end{bmatrix} \begin{bmatrix} cos\theta_{12} & -sin\theta_{12} & 0 & 0 \\ sin\theta_{12} & cos\theta_{12} & 0 & 0 \\ 0 & 0 & 1 & 0 \\ 0 & 0 & 0 & 1 \end{bmatrix}$

$$D_4 = \begin{bmatrix} cos(-0{,}0063\theta^2{}_{13} + 1{,}8006\theta_{13} - 0{,}7794) & -sin(-0{,}0063\theta^2{}_{13} + 1{,}8006\theta_{13} - 0{,}7794) & 0 & -47.45 \\ sin(-0{,}0063\theta^2{}_{13} + 1{,}8006\theta_{13} - 0{,}7794) & cos(-0{,}0063\theta^2{}_{13} + 1{,}8006\theta_{13} - 0{,}7794) & 0 & 0 \\ 0 & 0 & 1 & 0 \\ 0 & 0 & 0 & 1 \end{bmatrix}$$

$$E_4 = \begin{bmatrix} \cos(0{,}0034\theta^2{}_{13} + 1{,}3417\theta_{13} + 0{,}5973) & -\sin(0{,}0034\theta^2{}_{13} + 1{,}3417\theta_{13} + 0{,}5973) & 0 & -31.50 \\ \sin(0{,}0034\theta^2{}_{13} + 1{,}3417\theta_{13} + 0{,}5973) & \cos(0{,}0034\theta^2{}_{13} + 1{,}3417\theta_{13} + 0{,}5973) & 0 & 0 \\ 0 & 0 & 1 & 0 \\ 0 & 0 & 0 & 1 \end{bmatrix}$$

$$F_4 = \begin{bmatrix} 1 & 0 & 0 & -27.45 \\ 0 & 1 & 0 & 0 \\ 0 & 0 & 1 & 0 \\ 0 & 0 & 0 & 1 \end{bmatrix}$$

4.5. Velocities and Accelerations

4.5.1. Velocities and Accelerations of the Passive Joints in the Palm

When positions of the passive joints were determined, their differentiation was done. Unfortunately, first and second differentiation for velocities and accelerations yields too complex outcome that is hard to process for the simulation software. Hence, different way for velocity and acceleration determination should be used.

Using equation 4.13, it is possible to produce loop equations of the palm for velocities and accelerations in terms of screw theory.

Since screws are crossing the origin, their moment part is 0. Therefore, screws of joints M, G, H, Q and L are formed with reference to the frame O-xyz that is set to be global. Notation of joints' axis positions (unit axis) remains the same as in the previous section (position analysis). For each joint, screws are:

$$\$_{\boldsymbol{M}} = \left(\mathrm{C}_{\boldsymbol{M}}^{\boldsymbol{T}}; \mathbf{0\ 0\ 0}\right), \$_{\boldsymbol{G}} = \left(\boldsymbol{C}_{\boldsymbol{G}}^{\boldsymbol{T}}; \mathbf{0\ 0\ 0}\right), \$_{\boldsymbol{H}} = \left(\boldsymbol{C}_{\boldsymbol{H}}^{\boldsymbol{T}}; \mathbf{0\ 0\ 0}\right), \$_{\boldsymbol{Q}} = \left(\boldsymbol{C}_{\boldsymbol{Q}}^{\boldsymbol{T}}; \mathbf{0\ 0\ 0}\right), \$_{\boldsymbol{L}} = \left(\boldsymbol{C}_{\boldsymbol{L}}^{\boldsymbol{T}}; \mathbf{0\ 0\ 0}\right) \quad (4.80)$$

where $\$_{\boldsymbol{M}}$'s first part is joint's axis considered as reference and:

$$\boldsymbol{C_M} = \begin{bmatrix} \mathbf{0} \\ \mathbf{0} \\ \mathbf{1} \end{bmatrix}, \boldsymbol{C_L} = \boldsymbol{R}(\boldsymbol{y_5}, \boldsymbol{\alpha_5}). \begin{bmatrix} \mathbf{0} \\ \mathbf{0} \\ \mathbf{1} \end{bmatrix} \quad (4.81)$$

Systems of twists for a closed loop serial mechanism, using 4.82:

$$\$_{\boldsymbol{M}}\dot{\boldsymbol{\theta}}_{\mathbf{1}} + \$_{\boldsymbol{G}}\dot{\boldsymbol{\theta}}_{\mathbf{2}} + \$_{\boldsymbol{H}}\dot{\boldsymbol{\theta}}_{\mathbf{3}} + \$_{\boldsymbol{Q}}\dot{\boldsymbol{\theta}}_{\mathbf{4}} + \$_{\boldsymbol{L}}\dot{\boldsymbol{\theta}}_{\mathbf{5}} = \mathbf{0} \quad (4.82)$$

Considering that twist of link 3 can be expressed by 2 different routes, taking twists about link 3,

$$\$_{\boldsymbol{M}}\dot{\boldsymbol{\theta}}_{\mathbf{1}} + \$_{\boldsymbol{L}}\dot{\boldsymbol{\theta}}_{\mathbf{5}} = \$_{\boldsymbol{G}}\dot{\boldsymbol{\theta}}_{\mathbf{2}} + \$_{\boldsymbol{H}}\dot{\boldsymbol{\theta}}_{\mathbf{3}} + \$_{\boldsymbol{Q}}\dot{\boldsymbol{\theta}}_{\mathbf{4}}$$

$$[\$_M \quad \$_L]\begin{bmatrix}\dot{\boldsymbol{\theta}}_1\\ \dot{\boldsymbol{\theta}}_5\end{bmatrix} = [\$_G \quad \$_H \quad \$_Q]\begin{bmatrix}\dot{\boldsymbol{\theta}}_2\\ \dot{\boldsymbol{\theta}}_3\\ \dot{\boldsymbol{\theta}}_4\end{bmatrix}$$

$$[\$_G \quad \$_H \quad \$_Q]^{-1}[\$_M \quad \$_L]\begin{bmatrix}\dot{\boldsymbol{\theta}}_1\\ \dot{\boldsymbol{\theta}}_5\end{bmatrix} = \begin{bmatrix}\dot{\boldsymbol{\theta}}_2\\ \dot{\boldsymbol{\theta}}_3\\ \dot{\boldsymbol{\theta}}_4\end{bmatrix} \qquad (4.83)$$

Moment parts of screws are 0, therefore equation above takes the following form,

$$\begin{bmatrix}\begin{bmatrix}c\theta_1 s(-25°)\\ s\theta_1 s(-25°)\\ c(-25°)\end{bmatrix} & \mathrm{C}_H & \begin{bmatrix}c(113°)c\theta_5 s(112°)+s(113°)c(112°)\\ s\theta_5 s(112°)\\ -s(113°)c\theta_5 s(112°)+c(113°)c(112°)\end{bmatrix}\end{bmatrix}^{-1}.\begin{bmatrix}\begin{bmatrix}0\\0\\1\end{bmatrix} & \begin{bmatrix}s\alpha_5\\0\\c\alpha_5\end{bmatrix}\end{bmatrix}.\begin{bmatrix}\dot{\theta}_1\\ \dot{\theta}_5\end{bmatrix} = \begin{bmatrix}\dot{\theta}_2\\ \dot{\theta}_3\\ \dot{\theta}_4\end{bmatrix}$$

Systems of screws carrying accelerations for a closed loop serial mechanism, using:

$$\$_M\ddot{\boldsymbol{\theta}}_1 + \$_G\ddot{\boldsymbol{\theta}}_2 + \$_H\ddot{\boldsymbol{\theta}}_3 + \$_Q\ddot{\boldsymbol{\theta}}_4 + \$_L\ddot{\boldsymbol{\theta}}_5 + \boldsymbol{L_6} = \mathbf{0}$$

$$\boldsymbol{L_6} = \left[\dot{\boldsymbol{\theta}}_1\$_1 \quad \dot{\boldsymbol{\theta}}_2\$_2 + \dot{\boldsymbol{\theta}}_3\$_3 + \dot{\boldsymbol{\theta}}_4\$_4 + \dot{\boldsymbol{\theta}}_5\$_5\right] + \left[\dot{\boldsymbol{\theta}}_2\$_2 \quad \dot{\boldsymbol{\theta}}_3\$_3 + \dot{\boldsymbol{\theta}}_4\$_4 + \dot{\boldsymbol{\theta}}_5\$_5\right] + \left[\dot{\boldsymbol{\theta}}_3\$_3 \quad \dot{\boldsymbol{\theta}}_4\$_4 + \dot{\boldsymbol{\theta}}_5\$_5\right] + [\dot{\boldsymbol{\theta}}_4\$_4 + \dot{\boldsymbol{\theta}}_5\$_5] \qquad (4.84)$$

After inspecting equation 4.84, it is possible to see that,

$$\$_G\dot{\boldsymbol{\theta}}_2 + \$_H\dot{\boldsymbol{\theta}}_3 + \$_Q\dot{\boldsymbol{\theta}}_4 + \$_L\dot{\boldsymbol{\theta}}_5 = -\$_M\dot{\boldsymbol{\theta}}_1$$

Therefore, $[\boldsymbol{\omega_1}\$_1 \quad \boldsymbol{\omega_2}\$_2 + \boldsymbol{\omega_3}\$_3 + \boldsymbol{\omega_4}\$_4 + \boldsymbol{\omega_5}\$_5] = [\boldsymbol{\omega_1}\$_1 \quad -\boldsymbol{\omega_1}\$_1] = \mathbf{0}$

$$\boldsymbol{L_6} = \left[\dot{\boldsymbol{\theta}}_2\$_2 \quad \dot{\boldsymbol{\theta}}_3\$_3 + \dot{\boldsymbol{\theta}}_4\$_4 + \dot{\boldsymbol{\theta}}_5\$_5\right] + \left[\dot{\boldsymbol{\theta}}_3\$_3 \quad \dot{\boldsymbol{\theta}}_4\$_4 + \dot{\boldsymbol{\theta}}_5\$_5\right] + [\dot{\boldsymbol{\theta}}_4\$_4 + \dot{\boldsymbol{\theta}}_5\$_5]$$

In order to obtain accelerations of passive joints, acceleration of link 3 is expressed through two different routes:

$$\$_M\ddot{\boldsymbol{\theta}}_1 + \$_L\ddot{\boldsymbol{\theta}}_5 + \boldsymbol{L_{r1}} = \$_G\ddot{\boldsymbol{\theta}}_2 + \$_H\ddot{\boldsymbol{\theta}}_3 + \$_Q\ddot{\boldsymbol{\theta}}_4 + \boldsymbol{L_{r2}} \qquad (4.85)$$

where $\boldsymbol{L_{r1}} = [\$_M\dot{\boldsymbol{\theta}}_5 \quad \$_L\dot{\boldsymbol{\theta}}_1]$, $\boldsymbol{L_{r2}} = \left[\$_G\dot{\boldsymbol{\theta}}_2 \quad \$_H\dot{\boldsymbol{\theta}}_3 + \$_Q\dot{\boldsymbol{\theta}}_4\right] + [\$_H\dot{\boldsymbol{\theta}}_3 \quad \$_Q\dot{\boldsymbol{\theta}}_4]$

Then, accelerations are taken out and accelerations of passive joints are expressed in terms of active joints,

$$[\$_M \quad \$_L]\begin{bmatrix}\ddot{\boldsymbol{\theta}}_1\\ \ddot{\boldsymbol{\theta}}_5\end{bmatrix} + \boldsymbol{L_{r1}} = [\$_G \quad \$_H \quad \$_Q]\begin{bmatrix}\ddot{\boldsymbol{\theta}}_2\\ \ddot{\boldsymbol{\theta}}_3\\ \ddot{\boldsymbol{\theta}}_4\end{bmatrix} + \boldsymbol{L_{r2}}$$

$$[\$_M \quad \$_L]\begin{bmatrix}\ddot{\boldsymbol{\theta}}_1\\ \ddot{\boldsymbol{\theta}}_5\end{bmatrix} + [\$_M\dot{\boldsymbol{\theta}}_5 \quad \$_L\dot{\boldsymbol{\theta}}_1] = [\$_G \quad \$_H \quad \$_Q]\begin{bmatrix}\ddot{\boldsymbol{\theta}}_2\\ \ddot{\boldsymbol{\theta}}_3\\ \ddot{\boldsymbol{\theta}}_4\end{bmatrix} + [\$_G\dot{\boldsymbol{\theta}}_2 \quad \$_H\dot{\boldsymbol{\theta}}_3 + \$_Q\dot{\boldsymbol{\theta}}_4] + [\$_H\dot{\boldsymbol{\theta}}_3 \quad \$_Q\dot{\boldsymbol{\theta}}_4]$$

Lie product of screws:

$$[\$_M \quad \$_L]\begin{bmatrix}\ddot{\boldsymbol{\theta}}_1\\ \ddot{\boldsymbol{\theta}}_5\end{bmatrix} + \begin{bmatrix}\$_M\dot{\boldsymbol{\theta}}_5 \times \$_L\dot{\boldsymbol{\theta}}_1\\ \mathbf{0}\end{bmatrix} = [\$_G \quad \$_H \quad \$_Q]\begin{bmatrix}\ddot{\boldsymbol{\theta}}_2\\ \ddot{\boldsymbol{\theta}}_3\\ \ddot{\boldsymbol{\theta}}_4\end{bmatrix} + \begin{bmatrix}\$_G\dot{\boldsymbol{\theta}}_2 \times (\$_H\dot{\boldsymbol{\theta}}_3 + \$_Q\dot{\boldsymbol{\theta}}_4)\\ \mathbf{0}\end{bmatrix} + \begin{bmatrix}\$_H\dot{\boldsymbol{\theta}}_3 \times \$_Q\dot{\boldsymbol{\theta}}_4\\ \mathbf{0}\end{bmatrix} \quad (2.72)$$

As moment parts are zero, equation is reformed to give 4.86:

$$[\boldsymbol{C_G} \quad \boldsymbol{C_H} \quad \boldsymbol{C_Q}]^{-1}\left([\boldsymbol{C_M} \quad \boldsymbol{C_L}]\begin{bmatrix}\ddot{\boldsymbol{\theta}}_1\\ \ddot{\boldsymbol{\theta}}_5\end{bmatrix} + [\boldsymbol{C_M}\dot{\boldsymbol{\theta}}_5 \times \boldsymbol{C_L}\dot{\boldsymbol{\theta}}_1] - [\boldsymbol{C_G}\dot{\boldsymbol{\theta}}_2 \times (\boldsymbol{C_H}\dot{\boldsymbol{\theta}}_3 + \boldsymbol{C_Q}\dot{\boldsymbol{\theta}}_4)] - [\boldsymbol{C_H}\dot{\boldsymbol{\theta}}_3 \times \boldsymbol{C_Q}\dot{\boldsymbol{\theta}}_4]\right) = \begin{bmatrix}\ddot{\boldsymbol{\theta}}_2\\ \ddot{\boldsymbol{\theta}}_3\\ \ddot{\boldsymbol{\theta}}_4\end{bmatrix} \quad (4.86)$$

4.5.2. Thumb Velocities and Accelerations

For the numerical results regarding transmission ratios for angles, velocities and accelerations, they are present in the end of this chapter.

Using velocity and acceleration formulae, the following equations for thumb are constructed.

$$^1\omega_1 = {}^1_0R\,{}^0\omega_0 + \dot{\theta}_1\,{}^1Z_1 = [0 \quad 0 \quad \dot{\theta}_1]^T \quad (4.87)$$

Angular velocity, $\dot{\theta}_1$, is known since it is caused by the DC motor.

$$^1\dot{\omega}_1 = {}^1_0R\,{}^0\dot{\omega}_0 + {}^1_0R\,{}^0\omega_0 \times \dot{\theta}_1\,{}^1Z_1 + \ddot{\theta}_1\,{}^1Z_1 = \ddot{\theta}_1\,{}^1Z_1 \quad (4.88)$$

$^1V_1 \; and \; {}^1\dot{v}_1 = \begin{bmatrix}0\\0\\0\end{bmatrix}$, because the joint is stationary.

$$^2\omega_2 = {}^2_1R\,{}^1\omega_1 + \dot{\theta}_2 * {}^2Z_2 = \left(R(y_1,-\alpha_1)R(z_2,\theta_2)\right)^T.\,{}^1\omega_1 + [0 \quad 0 \quad \dot{\theta}_2]^T =$$

$$\left(\begin{bmatrix}cos\alpha_1 & 0 & -sin\alpha_1\\ 0 & 1 & 0\\ sin\alpha_1 & 0 & cos\alpha_1\end{bmatrix}\begin{bmatrix}cos\theta_2 & -sin\theta_2 & 0\\ sin\theta_2 & cos\theta_2 & 0\\ 0 & 0 & 1\end{bmatrix}\right)^T\begin{bmatrix}0\\0\\\dot{\theta}_1\end{bmatrix} + \begin{bmatrix}0\\0\\\dot{\theta}_2\end{bmatrix} =$$

$$\left(\begin{bmatrix}cos\alpha_1cos\theta_2 & -cos\alpha_1sin\theta_2 & -sin\alpha_1\\ sin\theta_2 & cos\theta_2 & 0\\ sin\alpha_1cos\theta_2 & -sin\alpha_1sin\theta_2 & cos\alpha_1\end{bmatrix}\right)^T\begin{bmatrix}0\\0\\\dot{\theta}_1\end{bmatrix} + \begin{bmatrix}0\\0\\\dot{\theta}_2\end{bmatrix} =$$

$$\begin{bmatrix}cos\alpha_1cos\theta_2 & sin\theta_2 & sin\alpha_1cos\theta_2\\ -cos\alpha_1sin\theta_2 & cos\theta_2 & -sin\alpha_1sin\theta_2\\ -sin\alpha_1 & 0 & cos\alpha_1\end{bmatrix}\begin{bmatrix}0\\0\\\dot{\theta}_1\end{bmatrix} + \begin{bmatrix}0\\0\\\dot{\theta}_2\end{bmatrix} = \begin{bmatrix}sin\alpha_1cos\theta_2\dot{\theta}_1\\ -sin\alpha_1sin\theta_2\dot{\theta}_1\\ cos\alpha_1\dot{\theta}_1 + \dot{\theta}_2\end{bmatrix} \quad (4.89)$$

$$^{2}\dot{\omega}_2 = {}^{2}_{1}R\,{}^{1}\dot{\omega}_1 + {}^{2}_{1}R\,{}^{1}\omega_1 \times \dot{\theta}_2\,{}^{2}Z_2 + \ddot{\theta}_2\,{}^{2}Z_2 = \begin{bmatrix} cos\alpha_1 cos\theta_2 & sin\theta_2 & sin\alpha_1 cos\theta_2 \\ -cos\alpha_1 sin\theta_2 & cos\theta_2 & -sin\alpha_1 sin\theta_2 \\ -sin\alpha_1 & 0 & cos\alpha_1 \end{bmatrix} \begin{bmatrix} 0 \\ 0 \\ \ddot{\theta}_1 \end{bmatrix} +$$

$$\left(\begin{bmatrix} cos\alpha_1 cos\theta_2 & sin\theta_2 & sin\alpha_1 cos\theta_2 \\ -cos\alpha_1 sin\theta_2 & cos\theta_2 & -sin\alpha_1 sin\theta_2 \\ -sin\alpha_1 & 0 & cos\alpha_1 \end{bmatrix} \begin{bmatrix} 0 \\ 0 \\ \dot{\theta}_1 \end{bmatrix} \right) \times \begin{bmatrix} 0 \\ 0 \\ \dot{\theta}_2 \end{bmatrix} + \begin{bmatrix} 0 \\ 0 \\ \ddot{\theta}_2 \end{bmatrix} \qquad (4.90)$$

$$^{2}V_2 = {}^{2}_{1}R({}^{1}v_1 + {}^{1}\omega_1 \times {}^{1}P_2) = \left(R(y_1, -\alpha_1)R(z_2, \theta_2)\right)^{T} \left(\begin{bmatrix} 0 \\ 0 \\ \dot{\theta}_1 \end{bmatrix} \times \left(R(y_1, -\alpha_1)R(z_2, \theta_2) \begin{bmatrix} a_1 \\ 0 \\ a_2 \end{bmatrix} \right) \right) \qquad (4.91)$$

where $\boldsymbol{a_1}$ and $\boldsymbol{a_2}$ is distance from O to the joint.

$$^{2}\dot{v}_2 = {}^{2}_{1}R({}^{1}\dot{\omega}_1 \times {}^{1}P_2 + {}^{1}\omega_1 \times ({}^{1}\omega_1 \times {}^{1}P_2) + {}^{1}\dot{v}_1) =$$

$$\begin{bmatrix} cos\alpha_1 cos\theta_2 & sin\theta_2 & sin\alpha_1 cos\theta_2 \\ -cos\alpha_1 sin\theta_2 & cos\theta_2 & -sin\alpha_1 sin\theta_2 \\ -sin\alpha_1 & 0 & cos\alpha_1 \end{bmatrix} * \left({}^{1}\dot{\omega}_1 \times {}^{1}P_2 + \begin{bmatrix} 0 \\ 0 \\ \dot{\theta}_1 \end{bmatrix} \times ({}^{1}\omega_1 \times {}^{1}P_2) + 0 \right) \qquad (4.92)$$

The rest of equations are presented in general form for convenience of presentation:

$$^{3}\omega_3 = {}^{3}_{2}R\,^{2}\omega_2 + \dot{\theta}_6 * ratio_1 * {}^{6}Z_6 \quad (4.93)$$

$$^{3}\dot{\omega}_3 = {}^{3}_{2}R\,^{2}\dot{\omega}_2 + {}^{3}_{2}R\,^{2}\omega_2 \times (dependant\_\dot{\theta}_6) * {}^{6}Z_6 + dependant\_\ddot{\theta}_6 * {}^{6}Z_6 \quad (4.94)$$

$$^{3}V_3 = {}^{3}_{2}R(^{2}v_2 + {}^{2}\omega_2 \times {}^{2}P_3) \quad (4.95)$$

$$^{3}\dot{v}_3 = {}^{3}_{2}R(^{2}\dot{\omega}_2 \times {}^{2}P_3 + {}^{2}\omega_2 \times (^{2}\omega_2 \times {}^{2}P_3) + {}^{2}\dot{v}_2) \quad (4.96)$$

$$^{4}\omega_4 = {}^{4}_{3}R\,^{3}\omega_3 + \dot{\theta}_7 * {}^{7}Z_7 \quad (4.97)$$

$$^{4}\dot{\omega}_4 = {}^{4}_{3}R\,^{3}\dot{\omega}_3 + {}^{4}_{3}R\,^{3}\omega_3 \times \dot{\theta}_7\,{}^{7}Z_7 + \ddot{\theta}_7\,{}^{7}Z_7 \quad (4.98)$$

$$^{4}V_4 = {}^{4}_{3}R(^{3}v_3 + {}^{3}\omega_3 \times {}^{3}P_4) \quad (4.99)$$

$$^{4}\dot{v}_4 = {}^{4}_{3}R(^{3}\dot{\omega}_3 \times {}^{3}P_4 + {}^{3}\omega_3 \times (^{3}\omega_3 \times {}^{3}P_4) + {}^{3}\dot{v}_3) \quad (4.100)$$

$$^{5}\omega_5 = {}^{5}_{4}R\,^{4}\omega_4 + \dot{\theta}_7 * ratio_2 * {}^{8}Z_8 \quad (4.101)$$

$$^{5}\dot{\omega}_5 = {}^{5}_{4}R\,^{4}\dot{\omega}_4 + {}^{5}_{4}R\,^{4}\omega_4 \times dependant\_\dot{\theta}_7 * {}^{8}Z_8 + dependant\_\ddot{\theta}_7 * ratio_2 * {}^{8}Z_8 \quad (4.102)$$

$$^{5}V_5 = {}^{5}_{4}R(^{4}v_4 + {}^{4}\omega_4 \times {}^{4}P_5) \quad (4.103)$$

$$^{5}\dot{v}_5 = {}^{5}_{4}R(^{4}\dot{\omega}_4 \times {}^{4}P_5 + {}^{4}\omega_4 \times (^{4}\omega_4 \times {}^{4}P_5) + {}^{4}\dot{v}_4) \quad (4.104)$$

$$^{6}\omega_6 = {}^{5}\omega_5 \quad (4.105)$$

$$^{6}\dot{\omega}_6 = {}^{5}\dot{\omega}_5 \quad (4.106)$$

$$^{6}V_6 = {}^{6}_{5}R(^{5}v_5 + {}^{5}\omega_5 \times {}^{5}P_6) \quad (4.107)$$

$$^{6}\dot{v}_6 = {}^{6}_{5}R(^{5}\omega_5 \times {}^{5}P_6 + {}^{5}\omega_5 \times (^{5}\omega_5 \times {}^{5}P_6) + {}^{5}\dot{v}_5) \quad (4.108)$$

Please note that equations 4.93 and 4.94, as well as equations 4.101 and 4.102, have ratios and vel/accel dependences that are related to the four-bar linkage presence – outer and inner respectively. These values can be obtained using equations 4.26 – 4.35 or using SimMechanics simulation of the mechanism CAD model.

Analogically, using mentioned equations, it is possible to find velocities and accelerations of other fingertips. Jacobian of the finger is defined. For obtaining required local angles, velocities and accelerations from given vectors, inverse Jacobian technique is used.

$$\begin{bmatrix} {}^{6}v_6 \\ {}^{6}\omega_6 \end{bmatrix} = {}^{6}J(\theta)\dot{\theta} = \begin{bmatrix} b_{11} & b_{12} & b_{13} & b_{14} \\ b_{21} & b_{22} & b_{23} & b_{24} \\ b_{31} & b_{32} & b_{33} & b_{34} \\ b_{41} & b_{42} & b_{43} & b_{44} \\ b_{51} & b_{52} & b_{53} & b_{54} \\ b_{61} & b_{62} & b_{63} & b_{64} \end{bmatrix} \begin{bmatrix} \dot{\theta}_1 \\ \dot{\theta}_2 \\ \dot{\theta}_6 \\ \dot{\theta}_7 \end{bmatrix} \tag{4.109}$$

$$\begin{bmatrix} \dot{\theta}_1 \\ \dot{\theta}_2 \\ \dot{\theta}_6 \\ \dot{\theta}_7 \end{bmatrix} = {}^{6}J^{-1}(\theta) \begin{bmatrix} {}^{6}v_6 \\ {}^{6}\omega_6 \end{bmatrix} = \begin{bmatrix} b_{11} & b_{12} & b_{13} & b_{14} \\ b_{21} & b_{22} & b_{23} & b_{24} \\ b_{31} & b_{32} & b_{33} & b_{34} \\ b_{41} & b_{42} & b_{43} & b_{44} \\ b_{51} & b_{52} & b_{53} & b_{54} \\ b_{61} & b_{62} & b_{63} & b_{64} \end{bmatrix}^{-1} \begin{bmatrix} {}^{6}v_6 \\ {}^{6}\omega_6 \end{bmatrix} \tag{4.110}$$

$$\begin{bmatrix} {}^{6}\dot{v}_6 \\ {}^{6}\dot{\omega}_6 \end{bmatrix} = {}^{6}J(\theta)\ddot{\theta} + {}^{6}\dot{J}(\theta)\dot{\theta} = \begin{bmatrix} c_{11} & c_{12} & c_{13} & c_{14} \\ c_{21} & c_{22} & c_{23} & c_{24} \\ c_{31} & c_{32} & c_{33} & c_{34} \\ c_{41} & c_{42} & c_{43} & c_{44} \\ c_{51} & c_{52} & c_{53} & c_{54} \\ c_{61} & c_{62} & c_{63} & c_{64} \end{bmatrix} \begin{bmatrix} \ddot{\theta}_1 \\ \ddot{\theta}_2 \\ \ddot{\theta}_6 \\ \ddot{\theta}_7 \end{bmatrix} + \begin{bmatrix} \dot{b}_{11} & \dot{b}_{12} & \dot{b}_{13} & \dot{b}_{14} \\ \dot{b}_{21} & \dot{b}_{22} & \dot{b}_{23} & \dot{b}_{24} \\ \dot{b}_{31} & \dot{b}_{32} & \dot{b}_{33} & \dot{b}_{34} \\ \dot{b}_{41} & \dot{b}_{42} & \dot{b}_{43} & \dot{b}_{44} \\ \dot{b}_{51} & \dot{b}_{52} & \dot{b}_{53} & \dot{b}_{54} \\ \dot{b}_{61} & \dot{b}_{62} & \dot{b}_{63} & \dot{b}_{64} \end{bmatrix} \begin{bmatrix} \dot{\theta}_1 \\ \dot{\theta}_2 \\ \dot{\theta}_6 \\ \dot{\theta}_7 \end{bmatrix} \tag{4.111}$$

$$\begin{bmatrix} \ddot{\theta}_1 \\ \ddot{\theta}_2 \\ \ddot{\theta}_6 \\ \ddot{\theta}_7 \end{bmatrix} = {}^{6}J^{-1}(\theta)\left(\begin{bmatrix} {}^{6}\dot{v}_6 \\ {}^{6}\dot{\omega}_6 \end{bmatrix} - {}^{6}\dot{J}(\theta)\dot{\theta}\right) =$$

$$= \begin{bmatrix} c_{11} & c_{12} & c_{13} & c_{14} \\ c_{21} & c_{22} & c_{23} & c_{24} \\ c_{31} & c_{32} & c_{33} & c_{34} \\ c_{41} & c_{42} & c_{43} & c_{44} \\ c_{51} & c_{52} & c_{53} & c_{54} \\ c_{61} & c_{62} & c_{63} & c_{64} \end{bmatrix}^{-1} \left(\begin{bmatrix} {}^{6}\dot{v}_6 \\ {}^{6}\dot{\omega}_6 \end{bmatrix} - \begin{bmatrix} \dot{b}_{11} & \dot{b}_{12} & \dot{b}_{13} & \dot{b}_{14} \\ \dot{b}_{21} & \dot{b}_{22} & \dot{b}_{23} & \dot{b}_{24} \\ \dot{b}_{31} & \dot{b}_{32} & \dot{b}_{33} & \dot{b}_{34} \\ \dot{b}_{41} & \dot{b}_{42} & \dot{b}_{43} & \dot{b}_{44} \\ \dot{b}_{51} & \dot{b}_{52} & \dot{b}_{53} & \dot{b}_{54} \\ \dot{b}_{61} & \dot{b}_{62} & \dot{b}_{63} & \dot{b}_{64} \end{bmatrix} \begin{bmatrix} \dot{\theta}_1 \\ \dot{\theta}_2 \\ \dot{\theta}_6 \\ \dot{\theta}_7 \end{bmatrix} \right) \tag{4.112}$$

4.6. Simulation Results

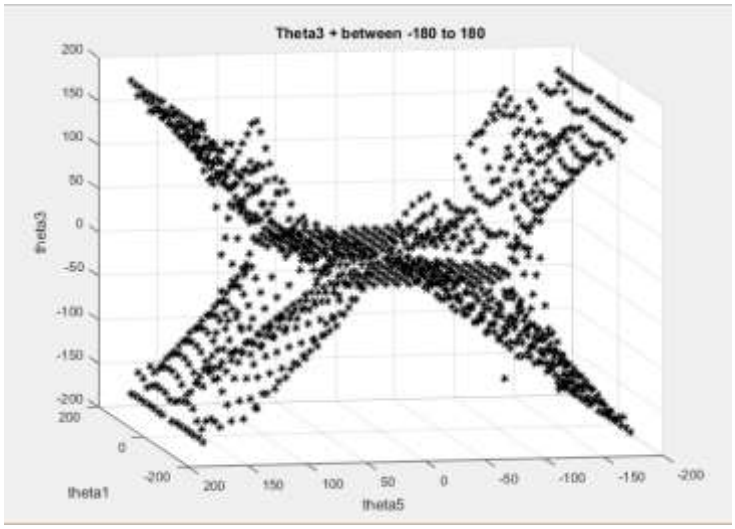

Figure 4.2. Workspace of theta 3 joint (palm) in degrees.

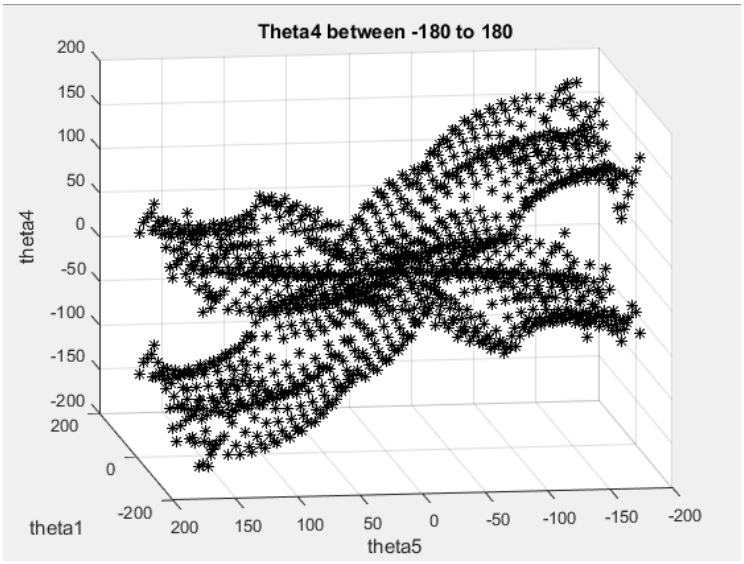

Figure 4.3. Workspace of theta 4 joint (palm) in degrees.

Once the kinematics of the palm's structure was studied, the principal joints are assessed. Figures 4.2 and 4.3 show how theta 3 and theta 4 joint angles are dependent on the actuated by DC motors joint angles theta 1 and theta 5. Configuration of the joints can be retrieved from the figure 3.2.

Figure 4.2 indicates that the theta 3 has impressive amount of various configurations. It is also possible to recognize the position areas (common for both figures) – the upper part of the plot is related to 0 degrees −> 180 degrees, whereas the bottom part is related to 180 degrees −> 360 degrees. On the other hand, figure 4.3 shows that the theta 4 joint has limited position variation.

It is very important to mention that flexibility of the theta 3 joint is beneficial for the thumb module to achieve greater number of grasping patterns. However, limitations of the theta 4 joint save index finger from unwanted interaction/overlap with other fingers and excessive motion that is hard to control.

Further figures 4.4. to 4.8. are based on SimMechanics (module of the MatLab) simulation. The same results can be obtained by application of equations 4.26 to 4.35.

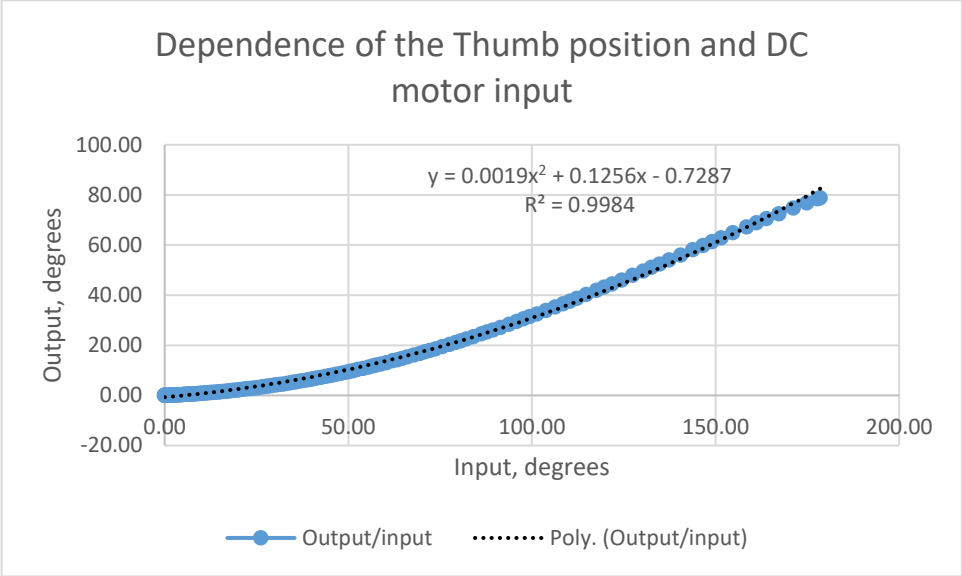

Figure 4.4. Dependence of the Thumb position and DC motor input.

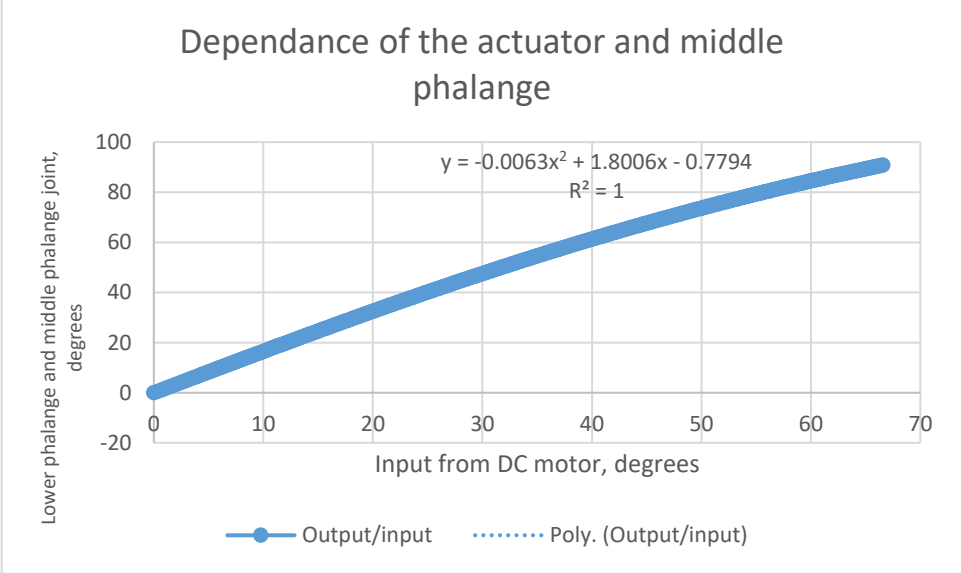

Figure 4.5. Dependence of the actuator and middle phalange.

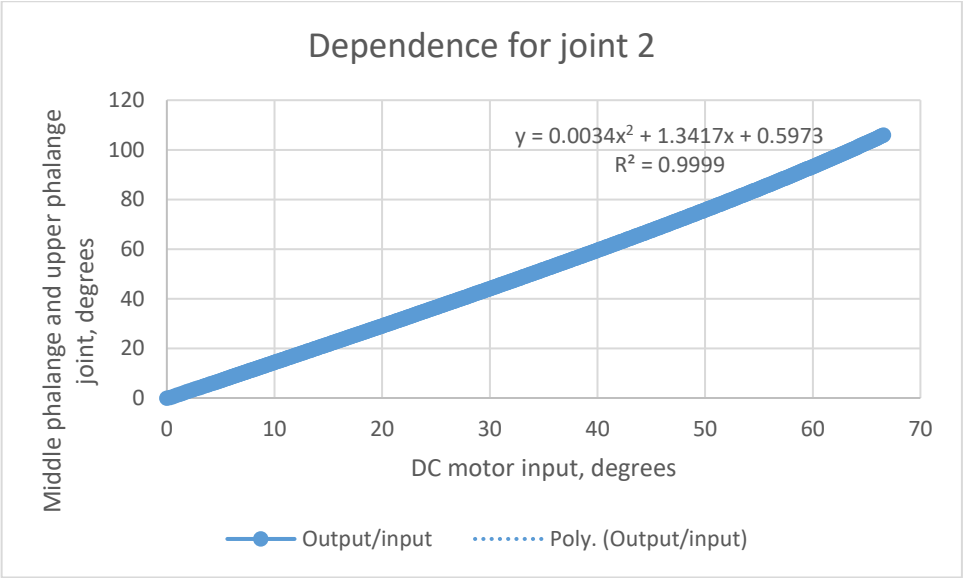

Figure 4.6. Dependence of the middle phalange and upper phalange joint.

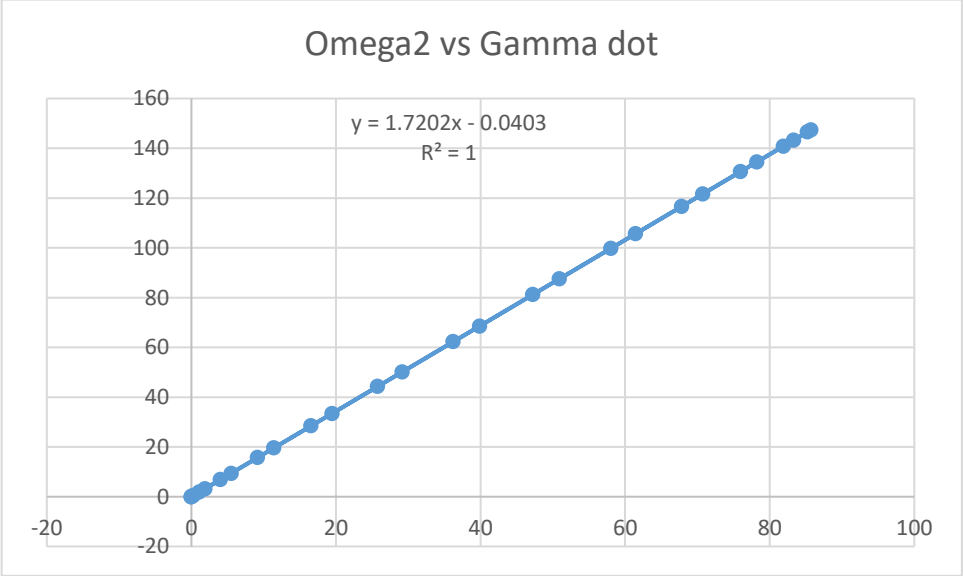

Figure 4.7. Omega and Gamma dot relationship.

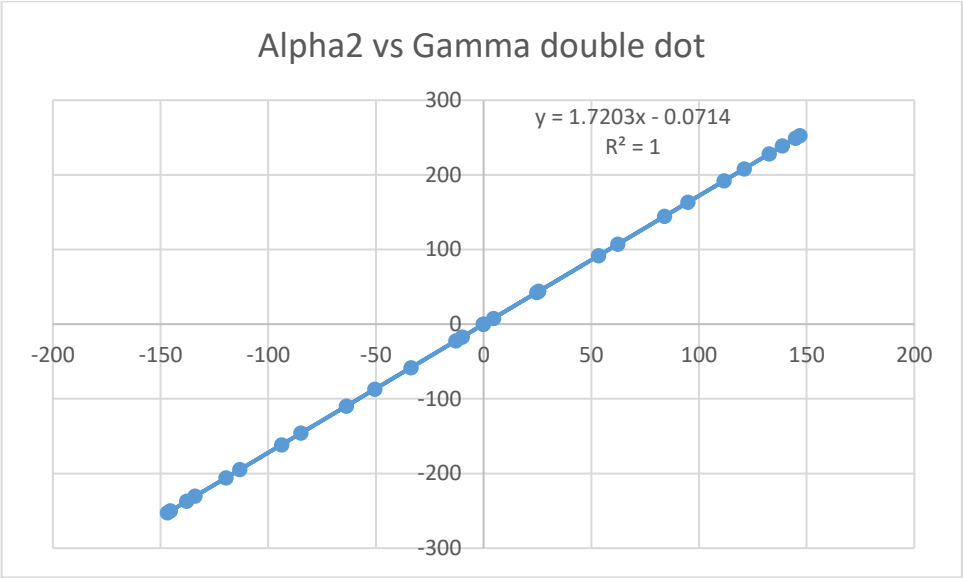

Figure 4.8. Relationship of Alpha2 and Gamma double dot

Figures 4.7 and 4.8 highlight important relationship establishment that is vital for the analysis of the four-bar mechanism inside the fingers. Since the actuated link on the scheme 4.8 is BC and gamma is an input angle, obtained relationships solve the problem of calculating velocities and accelerations for the specified motion.

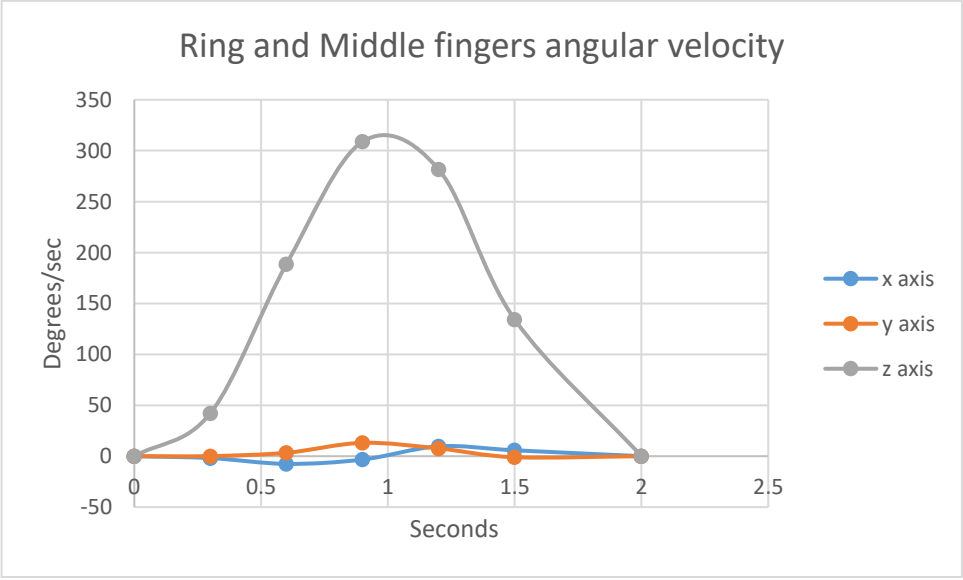

Figure 4.9. Ring and Middle fingers angular velocity

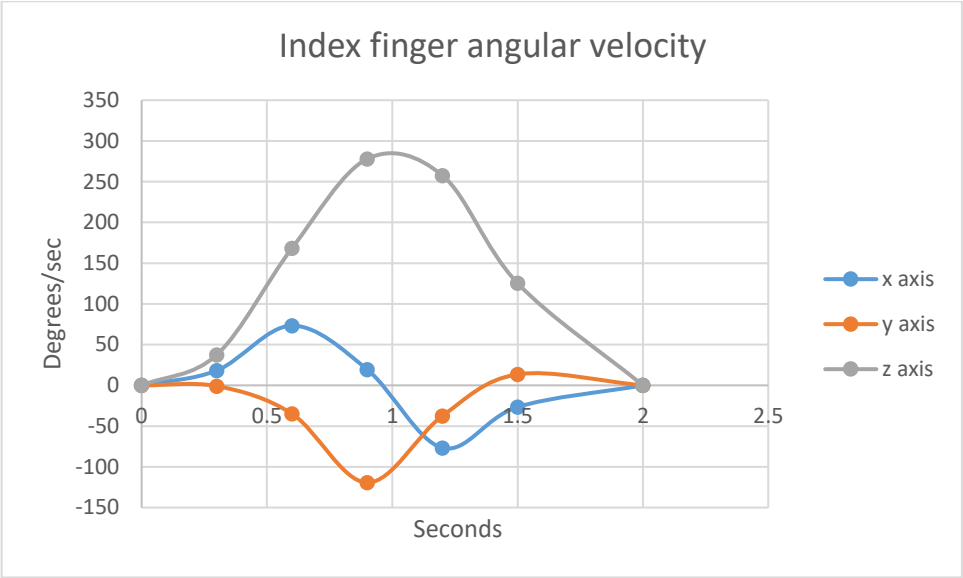

Figure 4.10. Index finger angular velocity

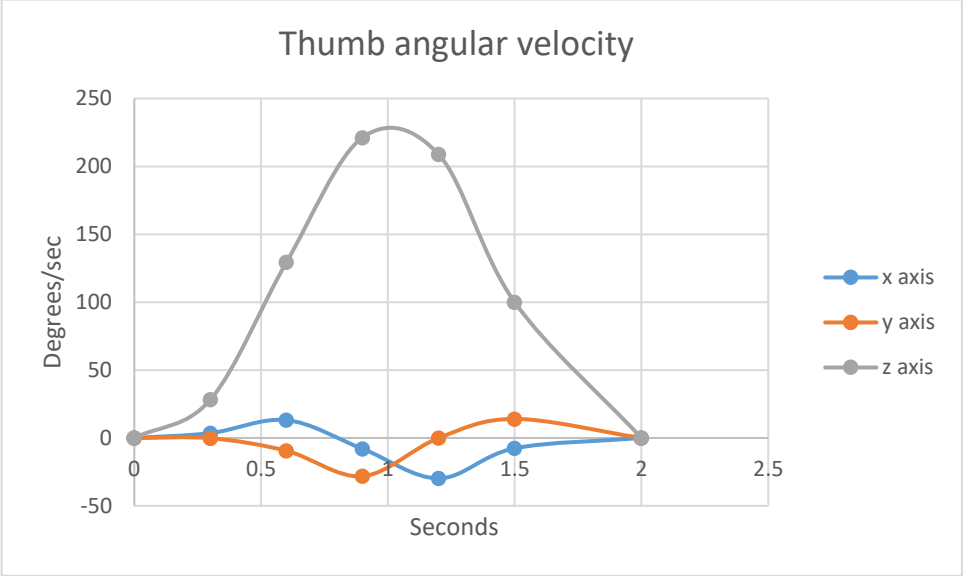

Figure 4.11. Thumb angular velocity

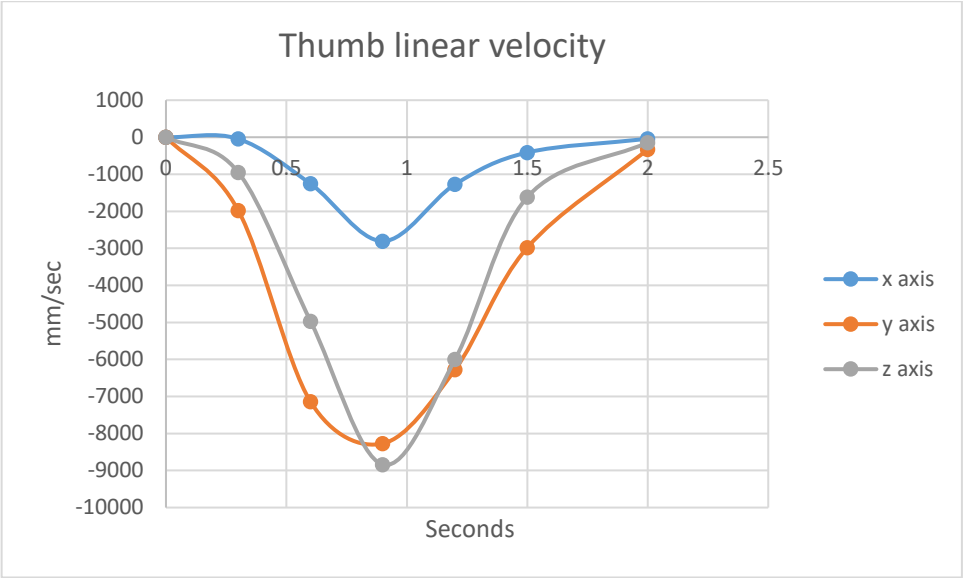

Figure 4.12. Thumb linear velocity

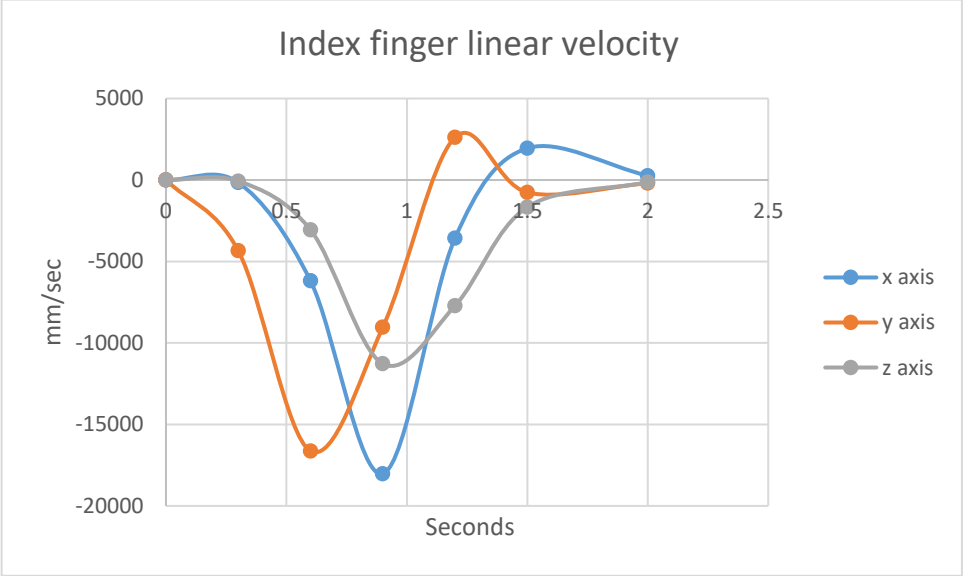

Figure 4.13. Index finger linear velocity

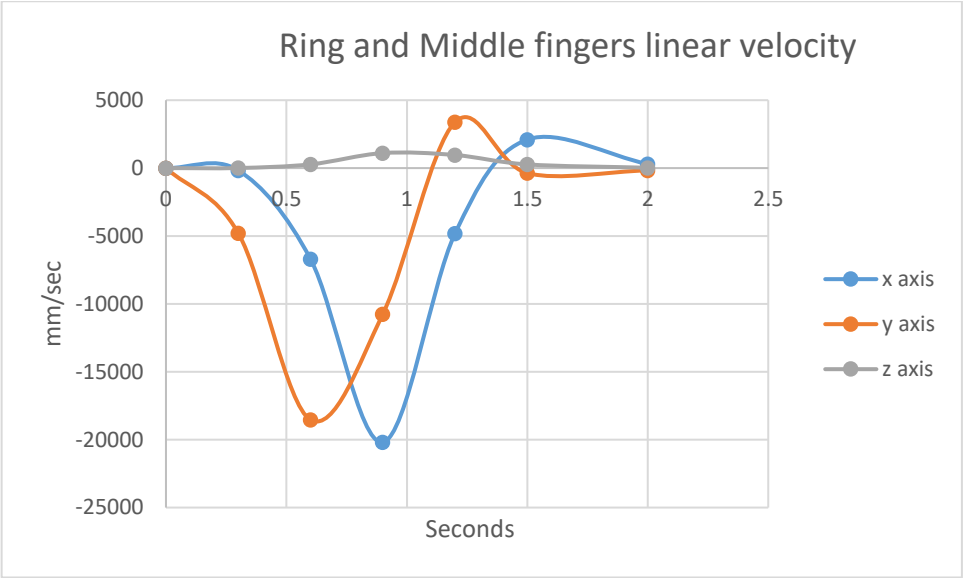

Figure 4.14. Ring and Middle fingers linear velocities

Figures 4.9 to 4.14 are based on the constructed kinematic model and show linear and angular velocity of the fingertips. Specified rapid motion (figure 6.1) is set to occur during 2 seconds for all joints, while 10 N act on each fingertip simultaneously.

4.7. Summary

Kinematic analysis of the proposed robotic hand was completed, equations were successfully obtained and applied to inverse dynamics. It is essential to mention that depending on orientation of the frame, movement can occur with positive or negative sign. As ‘z’ axis is rotated around ‘y’ axis, polynomial equations of angles are sensitive to that.

Chapter 5
Dynamics

5.1. Introduction

Dynamic model gives an in-depth description of mechanical system. Purpose of the dynamic modelling is to find relationship between motion and forces that are causing it. Moreover, the model gives possibility to simulate various scenarios, when external forces are applied to particular places of mechanical system, and to find corresponding force-torque response of the joints.

There are two common strategies that are considered as a dynamic problem solution. Application of dynamic analysis to manipulators could be direct or inverse. Direct dynamics deals with prediction of speed, acceleration and force of the fingertips achieved by the torque applied at joints, whereas inverse dynamics requires a set of conditions for the fingertip motion and force generation as an input and calculates torque in the joints that is expected for the stated task. Each method provides specific benefits and hence is suitable for different objectives. Direct dynamics is a useful approach for computer simulations and study of the system's workspace and behavior under certain operational circumstances. After that, it is then possible to produce predicted control for general-purpose automated activity. However, some mechanical systems do require real-time control for the following reasons: 1) risk for bearings and actuators to face critical load and be damaged during operation (in case there is a chance of extra load conditions and appropriate control loop is responsible for decision-making); 2) optimal efficiency during task execution with significant accuracy assured at high speeds or smooth slow motion; 3) real-time functioning and performance feedback during assignment of various objectives. Consequently, inverse dynamics model is chosen. Also, controller based on inverse dynamics model is superior to the controller using just inverse kinematics, because inertia of manipulator is considered.[70]

In this chapter, Newton-Euler dynamics is presented. Inverse dynamics numerical simulations are produced. Results are discussed and the corresponding conclusions are made.

5.2. Inertia

Inertia of any body could be understood as a property to resist changes of the object's condition – regardless of whether it is a motion state or rest state. Geometry and mass are factors that define moment of inertia. For basic shapes moment of inertia was already calculated, but for complex structures it is necessary to use computer program like SolidWorks or AutoCAD.

For further calculations and overall correctness, it is necessary to make an assumption that all DC motors will have furtherly mentioned moment of inertia. In reality, DC motors have some cavities inside and are not ideally solid objects. This is neglected to reduce the theoretical complexity. Certain inertial impact is approximated as it is not possible to obtain a detailed geometry of the DC motor, because the 3D CAD model provided by manufacturer represents continuous structure without consideration of inner element composition. Hence, scheme 5.1 illustrates the actuator's moment of inertia (applies to gearhead as well).

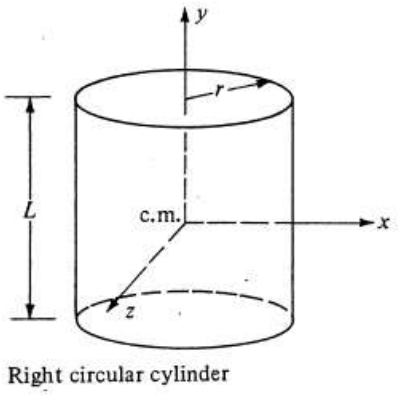

Right circular cylinder

$$\hat{I}_{xx} = \hat{I}_{zz} = \frac{m}{12}(3r^2 + L^2)$$

$$\hat{I}_{yy} = \frac{mr^2}{2}$$

Scheme 5.1. Moment of Inertia of the cylinder[71]

Scheme 5.1 shows equal distribution of the mass density through the body, therefore, it is enough to calculate principal axis.

For all fingers, except thumb, mass of inner DC motor is added to the lower link's mass. Distance between centres of mass is within less than 1 mm range and is neglected. For palm links, everything remains as it is shown on schematics, except link 3 – actuator's mass is included in the link. Inertias of all objects and distances are calculated with measuring tool of the SolidWorks software. Actuator's inertias are also taken into account by the software and included in the general inertia matrix for each link.

When necessary parameters of all present rigid bodies are defined, the next step is to assess which forces and moments each link is withstanding.

5.3. Recursive Newton-Euler Dynamics of the Robotic Hand Mechanism

Advantage of the Newton-Euler set of equations is that accumulated torques and forces at joints are found with respect to the applied force. Hence, not only DC motors can be correctly selected after result analysis, but also bearings. This approach analyzes each link in the mechanical system separately in order to solve appearing torques and forces step by step. Scheme 5.2 shows how the Newton-Euler principle works,

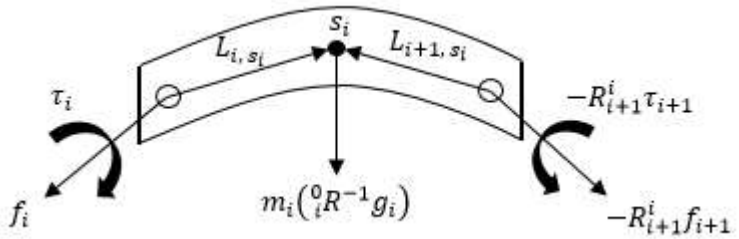

Scheme 5.2. Newton-Euler principle

The following fundamental equations are involved in the process:

$$\sum \mathbf{F} = \mathbf{ma} \qquad (5.1)$$

$$\sum \mathbf{M} = \mathbf{I\alpha} \qquad (5.2)$$

$$\sum \mathbf{M} = \boldsymbol{I}\dot{\omega} + \omega \times (\boldsymbol{I}\omega) \qquad (5.3)$$

It is obligatory to understand that equation 5.1 is only true for the planar motion. Therefore, equations 5.2 and 5.3, denoted as Newton's and Euler's equation respectively, will be used for equation derivation, because proposed mechanical system performs non-planar 3D motion. It is now possible to identify derivation procedure. For scheme that represents free body diagram of the system's arbitrary link, solution follows:

$$f_i - R^i_{i+1}f_{i+1} + m_i({}^0_iR^{-1}g_i) = \mathrm{m}_i\mathrm{a}_{s_i} \qquad (5.4)$$

$$\tau_i - R^i_{i+1}\tau_{i+1} + f_i \times L_{i,s_i} - R^i_{i+1}f_{i+1} \times L_{i+1,s_i} = \left({}^0_iR.I_i.{}^0_iR^T\right).\dot{\omega}_i + \omega_i \times \left(\left({}^0_iR.I_i.{}^0_iR^T\right).\omega_i\right) \qquad (5.5)$$

Involved vectors are described accordingly,

$\boldsymbol{f_i}$ – constraint force from link *i*-1

$\boldsymbol{R^i_{i+1}f_{i+1}}$ – transformation of the neighbouring constraint force from link *i*+1

$\boldsymbol{m_i}$ – mass of link *i*

$\boldsymbol{{}^0_i R^{-1} g_i}$ – gravitational influence in link *i* presented in global coordinates

$\mathbf{a}_{s_i}$ – linear acceleration of the link *i* centre of mass, $\boldsymbol{s_i}$

$\boldsymbol{\tau_i}$ – torque applied by link *i*-1

$\boldsymbol{R^i_{i+1} \tau_{i+1}}$ – torque applied by link *i*+1 is presented in link *i* coordinates

$\boldsymbol{L_{i,\, s_i}}$ –distance from joint *i*-1 to the link *i* centre of mass, $\boldsymbol{s_i}$

$\boldsymbol{L_{i+1,\, s_i}}$ – distance from joint *i*+1 to the link *i* centre of mass, $\boldsymbol{s_i}$

$\boldsymbol{{}^0_i R . I_i . {}^0_i R^T}$ – link *i* moment of Inertia presented in global coordinates

$\dot{\omega}_i$ – angular acceleration of link *i* (same quantity for the $\boldsymbol{s_i}$)

ω_i – angular velocity of link *i* (same quantity for the $\boldsymbol{s_i}$)

Please note that for all further schematics mentioned assignment principle of expression terms remains the same. For better illustration purposes, free body diagrams will be simplified.

5.3.1. Forces and moments in the fingers

Principal abbreviations used:

$m_{d.l.}$ – mass of the driving link

$m_{u.ph.}$ – mass of the upper phalange

$m_{m.ph.}$ – mass of the middle phalange

$m_{l.ph.}$ – mass of the lower phalange

$F_{u.ph.b1}$ and $F_{u.ph.b2}$ – forces at upper phalange bearing 1 and 2

$m_{i.m.}$ – mass of the inner motor

$m_{o.m.}$ – mass of the outer motor

Hence, for fingers 2, 3 and 4 (index, middle and ring), links are analyzed one by one starting from the fingertip. Consider scheme 5.3,

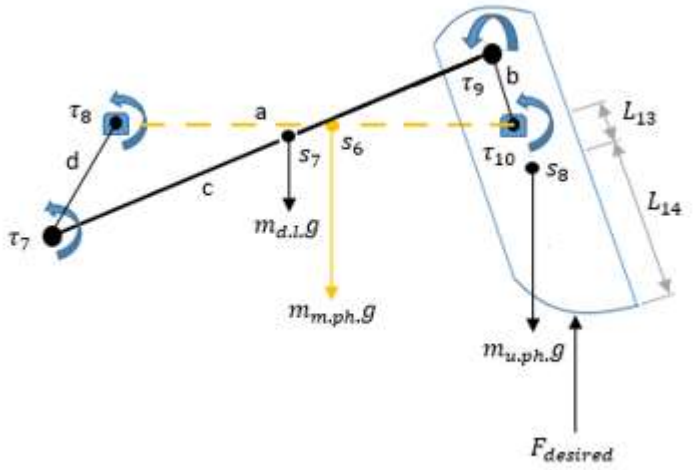

Scheme 5.3. Upper part of the finger

Free body diagram shows what forces should be considered when external force is applied.

Lower phalange with 2 upper joints, as well as driving link, middle and upper phalanges with corresponding joints can be observed in scheme 5.3. This complex problem could be split into several parts. It is important to note that middle and upper phalanges both rely on the driving link. First, using lever principle, tau 9 and 10 are obtained. They are then assigned to the driving link and middle phalange correspondingly. Since there is only one actuator that provides torque, $\boldsymbol{\tau_7}$, all moments are eventually calculated about the joint where that actuator is located. For the upper phalange, scheme 5.4 is constructed,

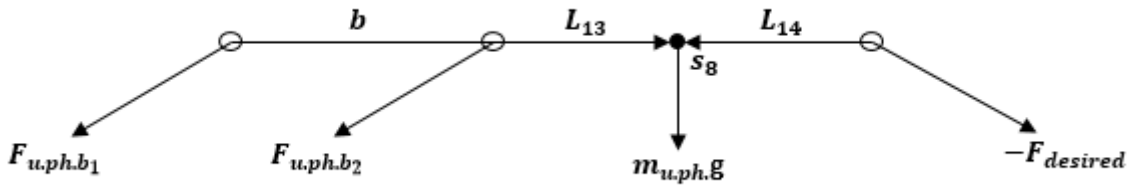

Scheme 5.4. Upper phalange

Applying equations 5.1 and 5.3,

$$\sum \mathbf{F} = \mathbf{ma} \quad => \left(\mathbf{F_{u.ph.b1}} + \mathbf{F_{u.ph.b2}}\right) + \boldsymbol{m_{u.ph.}}\left({}^{\mathbf{0}}_{\boldsymbol{u.ph.}}\boldsymbol{R}^{-1}.\boldsymbol{g}\right) - {}^{\mathbf{0}}_{\boldsymbol{u.ph.}}\boldsymbol{R}^{-1}.\mathbf{F_{desired}}$$
$$= \boldsymbol{m_{u.ph.}a_{s8}}$$

$$\left(\mathbf{F_{total\_1}}\right) = {}^{0}_{u.ph.}\boldsymbol{R}^{-1}.\,\mathbf{F_{desired}} - \boldsymbol{m_{u.ph.}}\left({}^{0}_{u.ph.}\boldsymbol{R}^{-1}.\,\boldsymbol{g}\right) + \boldsymbol{m_{u.ph.}}\boldsymbol{a_{s8}} \qquad (5.6)$$

Lever principle allows to predict amount of force at particular place if distance is known:

$$\left(\mathbf{1} - \left(\frac{\boldsymbol{L_{13}}}{\boldsymbol{L_{13}+b}}\right)\right)\mathbf{F_{total}} = \mathbf{F_{u.ph.b1}} \qquad (5.7)$$

$$\left(\left(\frac{\boldsymbol{L_{13}}}{\boldsymbol{L_{13}+b}}\right)\right)\mathbf{F_{total}} = \mathbf{F_{u.ph.b2}} \qquad (5.8)$$

$$\sum \mathbf{M} = \boldsymbol{I}\dot{\omega} + \omega \times (\boldsymbol{I}\omega) => \ (\boldsymbol{\tau_9} + \boldsymbol{\tau_{10}}) - {}^{0}_{u.ph.}\boldsymbol{R}^{-1}.\,\boldsymbol{M_{desired}} + \left(\mathbf{F_{u.ph.b1}} \times (\boldsymbol{L_{13}} + \boldsymbol{b})\right) + \left(\mathbf{F_{u.ph.b2}} \times \boldsymbol{L_{13}}\right) - \left({}^{0}_{u.ph.}\boldsymbol{R}^{-1}.\,\boldsymbol{F_{desired}} \times \boldsymbol{L_{14}}\right) = \left({}^{0}_{u.ph.}\boldsymbol{R}.\,\boldsymbol{I_{u.ph.}}\cdot {}^{0}_{u.ph.}\boldsymbol{R}^{T}\right).\,\dot{\omega}_{\boldsymbol{u.ph.}} + \omega_{\boldsymbol{u.ph.}} \times \left(\left({}^{0}_{u.ph.}\boldsymbol{R}.\,\boldsymbol{I_{u.ph.}}\cdot {}^{0}_{u.ph.}\boldsymbol{R}^{T}\right).\,\omega_{\boldsymbol{u.ph.}}\right)$$

$$\boldsymbol{\tau_{total\_1}} = {}^{0}_{u.ph.}\boldsymbol{R}^{-1}.\,\boldsymbol{M_{desired}} + \left({}^{0}_{u.ph.}\boldsymbol{R}^{-1}.\,\boldsymbol{F_{desired}} \times \boldsymbol{L_{14}}\right) - \left(\mathbf{F_{u.ph.b1}} \times (\boldsymbol{L_{13}} + \boldsymbol{b})\right) - \left(\mathbf{F_{u.ph.b2}} \times \boldsymbol{L_{13}}\right) + \left({}^{0}_{u.ph.}\boldsymbol{R}.\,\boldsymbol{I_{u.ph.}}\cdot {}^{0}_{u.ph.}\boldsymbol{R}^{T}\right).\,\dot{\omega}_{\boldsymbol{u.ph.}} + \omega_{\boldsymbol{u.ph.}} \times \left(\left({}^{0}_{u.ph.}\boldsymbol{R}.\,\boldsymbol{I_{u.ph.}}\cdot {}^{0}_{u.ph.}\boldsymbol{R}^{T}\right).\,\omega_{\boldsymbol{u.ph.}}\right)$$

In derived equations, external load and gravity were transformed to the reviewed link's frame. Therefore, they are now considered in global coordinates. As for $\boldsymbol{M_{desired}}$ torque, it is equal to zero, because the fingertip does not represent a joint.

Lever principle is used again for torques:

$$\left(\mathbf{1} - \frac{\boldsymbol{L_{13}}}{\boldsymbol{L_{13}+b}}\right)\boldsymbol{\tau_{total}} = \boldsymbol{\tau_9} \qquad (5.9)$$

$$\left(\frac{\boldsymbol{L_{13}}}{\boldsymbol{L_{13}+b}}\right)\boldsymbol{\tau_{total}} = \boldsymbol{\tau_{10}} \qquad (5.10)$$

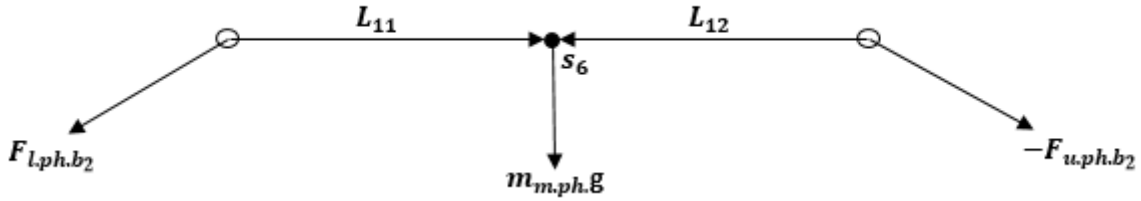

Scheme 5.5. Middle phalange

For the middle phalange,

$$\sum \mathbf{F} = \mathbf{ma} \quad => \mathbf{F_{l.ph.b2}} - {}^{m.ph.}_{u.ph.}\boldsymbol{R}.\,\boldsymbol{F_{u.ph.b2}} + \mathbf{m_{m.ph.}}\left({}^{0}_{m.ph.}\boldsymbol{R}^{-1}.\,\mathbf{g}\right) = \boldsymbol{m_{m.ph.}}\boldsymbol{a_{s6}}$$

$$\mathbf{F_{l.ph.b2}} = {}^{m.ph.}_{u.ph.}\boldsymbol{R}.\boldsymbol{F_{u.ph.b2}} - \mathbf{m_{m.ph.}}\left({}^{0}_{m.ph.}\boldsymbol{R}^{-1}.\mathbf{g}\right) + \boldsymbol{m_{m.ph.}a_{s6}} \tag{5.11}$$

$$\sum \mathbf{M} = \boldsymbol{I}\dot{\omega} + \omega \times (\boldsymbol{I}\omega) \quad => \boldsymbol{\tau_8} - {}^{m.ph.}_{u.ph.}\boldsymbol{R}.\boldsymbol{\tau_{10}} + \left(\mathbf{F_{l.ph.b2}} \times \boldsymbol{L_{11}}\right) - \left({}^{m.ph.}_{u.ph.}\boldsymbol{R}.\boldsymbol{F_{u.ph.b2}} \times \boldsymbol{L_{12}}\right) =$$
$$\left({}^{0}_{m.ph.}\boldsymbol{R}.\boldsymbol{I_{m.ph.}}\cdot {}^{0}_{m.ph.}\boldsymbol{R}^{T}\right).\dot{\omega}_{m.ph.} + \omega_{m.ph.} \times \left(\left({}^{0}_{m.ph.}\boldsymbol{R}.\boldsymbol{I_{m.ph.}}\cdot {}^{0}_{m.ph.}\boldsymbol{R}^{T}\right).\omega_{m.ph.}\right) \tag{5.12}$$

$$\boldsymbol{\tau_8} = {}^{m.ph.}_{u.ph.}\boldsymbol{R}.\boldsymbol{\tau_{10}} + \left({}^{m.ph.}_{u.ph.}\boldsymbol{R}.\boldsymbol{F_{u.ph.b2}} \times \boldsymbol{L_{12}}\right) - \left(\mathbf{F_{l.ph.b2}} \times \boldsymbol{L_{11}}\right) +$$
$$\left({}^{0}_{m.ph.}\boldsymbol{R}.\boldsymbol{I_{m.ph.}}\cdot {}^{0}_{m.ph.}\boldsymbol{R}^{T}\right).\dot{\omega}_{m.ph.} + \omega_{m.ph.} \times \left(\left({}^{0}_{m.ph.}\boldsymbol{R}.\boldsymbol{I_{m.ph.}}\cdot {}^{0}_{m.ph.}\boldsymbol{R}^{T}\right).\omega_{m.ph.}\right) \tag{5.13}$$

Now, when $\boldsymbol{\tau_8}$ is calculated, it is possible obtain its influence on the actuator:

$$\boldsymbol{\tau_{7_{ph.}}} = {}^{l.ph.}_{m.ph.}\boldsymbol{R}.\boldsymbol{\tau_8} + \left({}^{l.ph.}_{m.ph.}\boldsymbol{R}.\boldsymbol{F_{l.ph.b2}} \times \boldsymbol{d}\right) \tag{5.14}$$

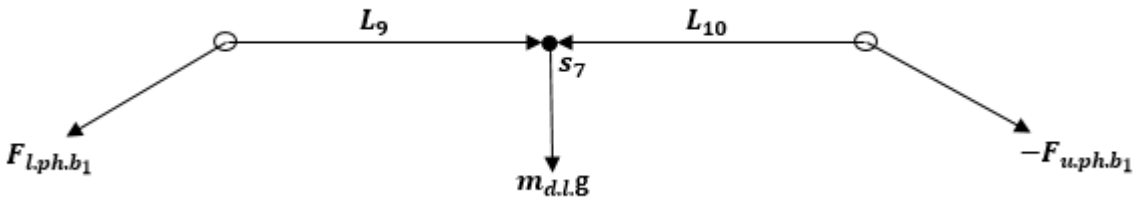

Scheme 5.6. Driving link

$$\sum \mathbf{F} = \mathbf{ma} \quad => \mathbf{F_{l.ph.b1}} - {}^{d.l.}_{u.ph.}\boldsymbol{R}.\boldsymbol{F_{u.ph.b1}} + \mathbf{m_{d.l.}}\left({}^{0}_{d.l.}\boldsymbol{R}^{-1}.\mathbf{g}\right) = \boldsymbol{m_{d.l.}a_{s7}}$$

$$\mathbf{F_{l.ph.b1}} = {}^{d.l.}_{u.ph.}\boldsymbol{R}.\boldsymbol{F_{u.ph.b1}} - \mathbf{m_{d.l.}}\left({}^{0}_{d.l.}\boldsymbol{R}^{-1}.\mathbf{g}\right) + \boldsymbol{m_{d.l.}a_{s7}} \tag{5.15}$$

$$\sum \mathbf{M} = \boldsymbol{I}\dot{\omega} + \omega \times (\boldsymbol{I}\omega) \quad => \boldsymbol{\tau_{7_{d.l.}}} - {}^{d.l.}_{u.ph.}\boldsymbol{R}.\boldsymbol{\tau_9} + \left(\boldsymbol{F_{l.ph.b1}} \times \boldsymbol{L_9}\right) - \left({}^{d.l.}_{u.ph.}\boldsymbol{R}.\boldsymbol{F_{u.ph.b1}} \times \boldsymbol{L_{10}}\right) =$$
$$\left({}^{0}_{d.l.}\boldsymbol{R}.\boldsymbol{I_{d.l.}}\cdot {}^{0}_{d.l.}\boldsymbol{R}^{T}\right).\dot{\omega}_{d.l.} + \omega_{d.l.} \times \left(\left({}^{0}_{d.l.}\boldsymbol{R}.\boldsymbol{I_{d.l.}}\cdot {}^{0}_{d.l.}\boldsymbol{R}^{T}\right).\omega_{d.l.}\right) \tag{5.16}$$

$$\boldsymbol{\tau_{7_{d.l.}}} = {}^{d.l.}_{u.ph.}\boldsymbol{R}.\boldsymbol{\tau_9} + \left({}^{d.l.}_{u.ph.}\boldsymbol{R}.\boldsymbol{F_{u.ph.b1}} \times \boldsymbol{L_{10}}\right) - \left(\boldsymbol{F_{l.ph.b1}} \times \boldsymbol{L_9}\right) + \left({}^{0}_{d.l.}\boldsymbol{R}.\boldsymbol{I_{d.l.}}\cdot {}^{0}_{d.l.}\boldsymbol{R}^{T}\right).\dot{\omega}_{d.l.} +$$
$$\omega_{d.l.} \times \left(\left({}^{0}_{d.l.}\boldsymbol{R}.\boldsymbol{I_{d.l.}}\cdot {}^{0}_{d.l.}\boldsymbol{R}^{T}\right).\omega_{d.l.}\right) \tag{5.17}$$

Finally, $\boldsymbol{\tau_7}$ is found:

$$\boldsymbol{\tau_7} = \boldsymbol{\tau_{7_{ph.}}} + {}^{l.ph.}_{d.l.}\boldsymbol{R}.\boldsymbol{\tau_{7_{d.l.}}} \tag{5.18}$$

For general case, scheme 5.7 and 5.8, there is only one last joint left in the finger. All accumulated up to this moment torques and forces should be applied to the last joint, so that $\boldsymbol{\tau_6}$ is obtained. It can be noted that the lower phalange is carrying a DC motor. Therefore, its inertial contribution also has to be included into the link's moment of inertia.

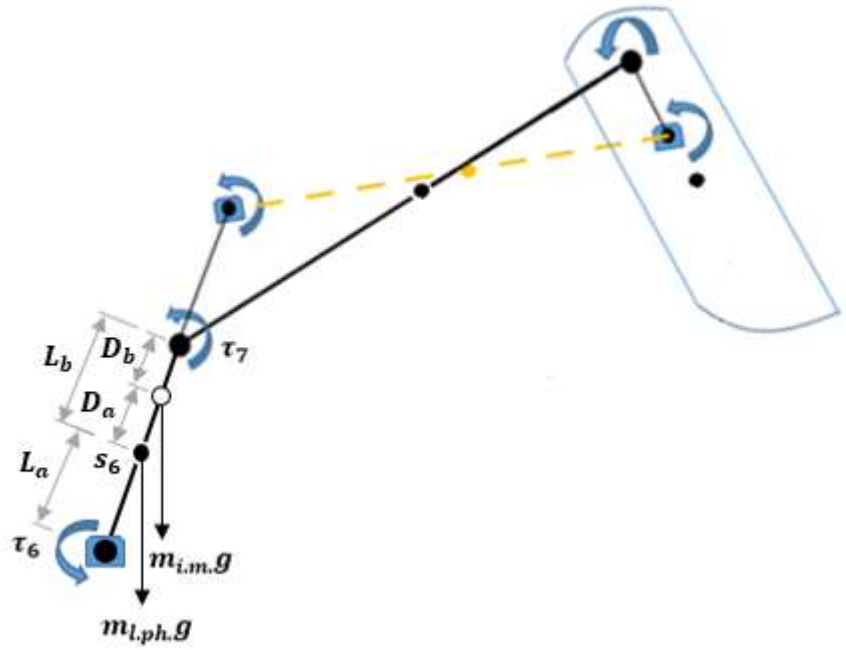

Scheme 5.7. General case

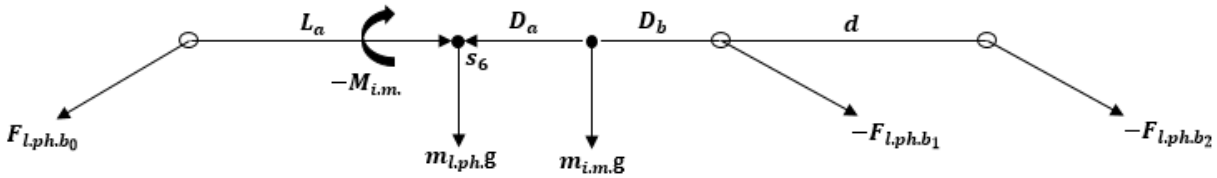

Scheme 5.8. Lower phalange

Since moment occurring at bearing 2 was previously included as a load for actuator that is located at bearing 1, in the next sum of moments calculation, it is not present. From scheme 5.7, it is evident that $\boldsymbol{\tau_7}$ operates the four-bar linkage and this mechanism requires separate analysis. However, force at bearing 2 should be still considered for the overall lower link's sum of forces.

For the lower phalange:

$$\sum \mathbf{F} = \mathbf{ma} \Rightarrow \mathbf{F}_{\mathbf{l.ph.b_0}} - {}^{l.ph.}_{d.l.}\boldsymbol{R}.\mathbf{F}_{l.ph.b_1} - {}^{l.ph.}_{m.ph.}\boldsymbol{R}.\boldsymbol{F}_{l.ph.b2} + \mathbf{m}_{\mathbf{l.ph.}}\left({}^{0}_{l.ph}\boldsymbol{R}^{-1}.\mathbf{g}\right) + \mathbf{m}_{i.m.}\left({}^{0}_{l.ph}\boldsymbol{R}^{-1}.\boldsymbol{g}\right) = \mathbf{m}_{l.ph.}\mathbf{a}_{s6}$$

$$\mathbf{F}_{\mathbf{l.ph.b_0}} = {}^{l.ph.}_{d.l.}\boldsymbol{R}.\mathbf{F}_{l.ph.b_1} + {}^{l.ph.}_{m.ph.}\boldsymbol{R}.\boldsymbol{F}_{l.ph.b2} - \mathbf{m}_{\mathbf{l.ph.}}\left({}^{0}_{l.ph}\boldsymbol{R}^{-1}.\mathbf{g}\right) - \mathbf{m}_{i.m.}\left({}^{0}_{l.ph}\boldsymbol{R}^{-1}.\boldsymbol{g}\right) + \mathbf{m}_{l.ph.}\mathbf{a}_{s6} \quad (5.19)$$

$$\sum \mathbf{M} = \boldsymbol{I}\dot{\omega} + \omega \times (\boldsymbol{I}\omega) \Rightarrow \boldsymbol{\tau_6} - \boldsymbol{\tau_7} + \left(\boldsymbol{F}_{l.ph.b_0} \times \boldsymbol{L_a}\right) - \left({}^{l.ph.}_{d.l.}\boldsymbol{R}.\boldsymbol{F}_{l.ph.b_1} \times \boldsymbol{L_b}\right) - \boldsymbol{M}_{i.m.} = \left({}^{0}_{l.ph.}\boldsymbol{R}.\boldsymbol{I}_{l.ph.}.{}^{0}_{l.ph.}\boldsymbol{R}^{T}\right).\dot{\omega}_{l.ph.} + \omega_{l.ph.} \times \left(\left({}^{0}_{l.ph.}\boldsymbol{R}.\boldsymbol{I}_{l.ph.}.{}^{0}_{l.ph.}\boldsymbol{R}^{T}\right).\omega_{l.ph.}\right) \quad (5.20)$$

In the sum of moments equation 5.20, $\boldsymbol{\tau_7}$ does not require transformation, because it consists of two already transformed to the lower phalange torques.

In addition, $\boldsymbol{M}_{i.m.} = \mathbf{m}_{i.m.}\left({}^{0}_{l.ph}\boldsymbol{R}^{-1}.\boldsymbol{g}\right) \times \boldsymbol{D_a}$ (5.21)

Therefore, torque 6 is obtained:

$$\boldsymbol{\tau_6} = \boldsymbol{\tau_7} - \left(\boldsymbol{F}_{l.ph.b_0} \times \boldsymbol{L_a}\right) + \left({}^{l.ph.}_{d.l.}\boldsymbol{R}.\boldsymbol{F}_{l.ph.b_1} \times \boldsymbol{L_b}\right) + \boldsymbol{M}_{i.m.} + \left({}^{0}_{l.ph.}\boldsymbol{R}.\boldsymbol{I}_{l.ph.}.{}^{0}_{l.ph.}\boldsymbol{R}^{T}\right).\dot{\omega}_{l.ph.} + \omega_{l.ph.} \times \left(\left({}^{0}_{l.ph.}\boldsymbol{R}.\boldsymbol{I}_{l.ph.}.{}^{0}_{l.ph.}\boldsymbol{R}^{T}\right).\omega_{l.ph.}\right) \quad (5.22)$$

It is also necessary to consider special case of the finger's structure – thumb. It has another four-bar linkage that is placed outside the thumb and drives it. Four-bar linkage allows the DC motor not to contradict with bearings and rotary parts, so it is shifted away from direct actuation. Scheme 5.9 presents the case:

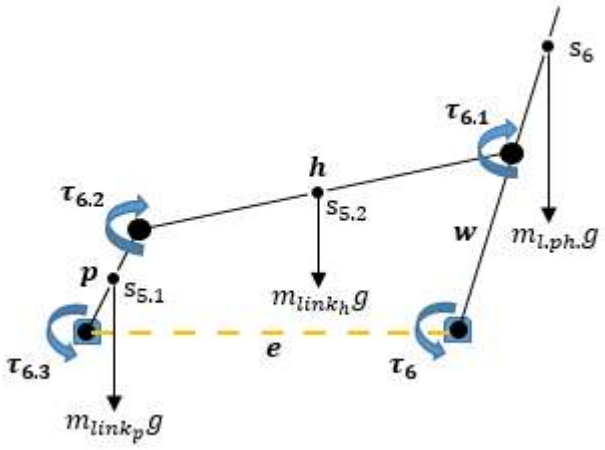

Scheme 5.9. Special Case of the Lower Phalange.

Generated load at the lower phalange of the thumb is assigned to the four-bar linkage and bearing 0, so that $\boldsymbol{\tau_6}$ with $\boldsymbol{\tau_{6.1(1)}}$ are found. Thumb has no actuator located at bearing 0 – joint is passive, hence required torque, $\boldsymbol{\tau_{Total\_2}}$, is added to the driving linkage.

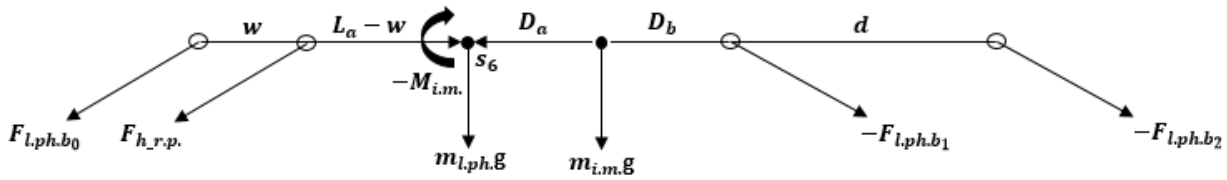

Scheme 5.10. Special Case of the Lower Phalange.

Equations are reworked to satisfy changes to the scheme,

$$\sum \mathbf{F} = \mathbf{ma} => \mathbf{F}_{\mathbf{l.ph.b_0}} + \mathbf{F}_{\mathbf{h\_r.p.}} - {}^{l.ph.}_{d.l.}\boldsymbol{R}.\mathbf{F}_{l.ph.b_1} - {}^{l.ph.}_{m.ph.}\boldsymbol{R}.\boldsymbol{F}_{l.ph.b2} + \mathbf{m}_{\mathbf{l.ph.}}\left({}^{0}_{l.ph}\boldsymbol{R}^{-1}.\mathbf{g}\right) + \mathbf{m}_{i.m.}\left({}^{0}_{l.ph}\boldsymbol{R}^{-1}.\boldsymbol{g}\right) = \mathbf{m}_{l.ph.}\mathbf{a}_{s6}$$

$$\mathbf{F}_{\mathbf{Total\_2}} = {}^{l.ph.}_{d.l.}\boldsymbol{R}.\mathbf{F}_{l.ph.b_1} + {}^{l.ph.}_{m.ph.}\boldsymbol{R}.\boldsymbol{F}_{l.ph.b2} - \mathbf{m}_{\mathbf{l.ph.}}\left({}^{0}_{l.ph}\boldsymbol{R}^{-1}.\mathbf{g}\right) - \mathbf{m}_{i.m.}\left({}^{0}_{l.ph}\boldsymbol{R}^{-1}.\boldsymbol{g}\right) + \mathbf{m}_{l.ph.}\mathbf{a}_{s6} \quad (5.23)$$

Using lever principle again,

$$\mathbf{F}_{\mathbf{l.ph.b_0}} = \left(\mathbf{1} - \frac{L_a - w}{L_a}\right)\mathbf{F}_{\mathbf{Total\_2}} \quad (5.24)$$

$$\mathbf{F}_{\mathbf{h\_r.p.}} = \left(\frac{L_a - w}{L_a}\right)\mathbf{F}_{\mathbf{Total\_2}} \quad (5.25)$$

$$\sum \mathbf{M} = \boldsymbol{I}\dot{\omega} + \omega \times (\boldsymbol{I}\omega) \quad => \boldsymbol{\tau_6} + \boldsymbol{\tau_{6.1(1)}} - \boldsymbol{\tau_7} + \left(\boldsymbol{F}_{l.ph.b_0} \times \boldsymbol{L_a}\right) - \left({}^{l.ph.}_{d.l.}\boldsymbol{R}.\boldsymbol{F}_{l.ph.b_1} \times \boldsymbol{L_b}\right) - \boldsymbol{M}_{i.m.} = \left({}^{0}_{l.ph.}\boldsymbol{R}.\boldsymbol{I}_{l.ph.}.{}^{0}_{l.ph.}\boldsymbol{R}^{T}\right).\dot{\omega}_{l.ph.} + \omega_{l.ph.} \times \left(\left({}^{0}_{l.ph.}\boldsymbol{R}.\boldsymbol{I}_{l.ph.}.{}^{0}_{l.ph.}\boldsymbol{R}^{T}\right).\omega_{l.ph.}\right) \quad (5.26)$$

$$\boldsymbol{\tau_{Total\_2}} = \boldsymbol{\tau_7} - \left(\boldsymbol{F}_{l.ph.b_0} \times \boldsymbol{L_a}\right) + \left({}^{l.ph.}_{d.l.}\boldsymbol{R}.\boldsymbol{F}_{l.ph.b_1} \times \boldsymbol{L_b}\right) + \boldsymbol{M}_{i.m.} + \left({}^{0}_{l.ph.}\boldsymbol{R}.\boldsymbol{I}_{l.ph.}.{}^{0}_{l.ph.}\boldsymbol{R}^{T}\right).\dot{\omega}_{l.ph.} + \omega_{l.ph.} \times \left(\left({}^{0}_{l.ph.}\boldsymbol{R}.\boldsymbol{I}_{l.ph.}.{}^{0}_{l.ph.}\boldsymbol{R}^{T}\right).\omega_{l.ph.}\right) \quad (5.27)$$

$$\boldsymbol{\tau_6} = \left(\mathbf{1} - \frac{L_a - w}{L_a}\right)\boldsymbol{\tau_{Total\_2}} \quad (5.28)$$

$$\boldsymbol{\tau_{6.1(1)}} = \left(\frac{L_a - w}{L_a}\right)\boldsymbol{\tau_{Total\_2}} \quad (5.29)$$

It is now possible to figure out what load actuator is taking, $\boldsymbol{\tau_{6.3}}$. As thumb's lowest joint is passive (if active, then $\boldsymbol{\tau_{6.1(1)}}$ should be considered), torque that is required for it is passed to the linkage:

$$\boldsymbol{\tau_{6.1} = \tau_{Total\_2}} \qquad (5.30)$$

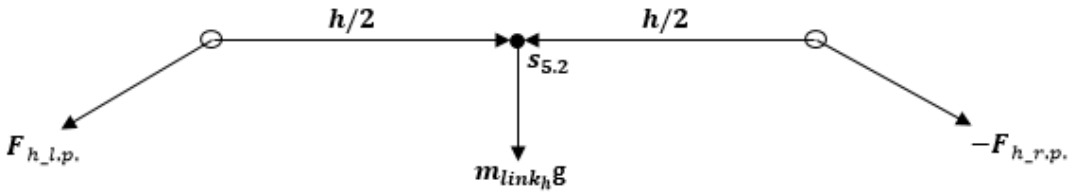

Scheme 5.11. Situation in link h

$$\sum \mathbf{F} = \mathbf{ma} \quad => \mathbf{F_{h\_l.p.}} - {}^{link_h}_{l.ph.}\boldsymbol{R}.\boldsymbol{F_{h\_r.p.}} + \mathbf{m_{link_h}}\left({}^{0}_{link_h}\boldsymbol{R^{-1}}.\mathbf{g}\right) = \boldsymbol{m_{link_h}a_{s5.2}}$$

$$\mathbf{F_{h\_l.p.}} = {}^{link_h}_{l.ph.}\boldsymbol{R}.\boldsymbol{F_{h\_r.p}} - \mathbf{m_{link_h}}\left({}^{0}_{link_h}\boldsymbol{R^{-1}}.\mathbf{g}\right) + \boldsymbol{m_{link_h}a_{s5.2}} \qquad (5.31)$$

$$\sum \mathbf{M} = \boldsymbol{I}\dot{\omega} + \omega \times (\boldsymbol{I}\omega) \quad => \boldsymbol{\tau_{6.2}} - {}^{link_h}_{l.ph.}\boldsymbol{R}.\boldsymbol{\tau_{6.1}} + \left(\mathbf{F_{h\_l.p.}} \times \frac{\boldsymbol{h}}{\mathbf{2}}\right) - \left({}^{link_h}_{l.ph.}\boldsymbol{R}.\boldsymbol{F_{h\_r.p}} \times \frac{\boldsymbol{h}}{\mathbf{2}}\right) =$$
$$\left({}^{0}_{link_h}\boldsymbol{R}.\boldsymbol{I_{link_h}}.{}^{0}_{link_h}\boldsymbol{R^{T}}\right).\dot{\omega}_{link_h} + \omega_{link_h} \times \left(\left({}^{0}_{link_h}\boldsymbol{R}.\boldsymbol{I_{link_h}}.{}^{0}_{link_h}\boldsymbol{R^{T}}\right).\omega_{link_h}\right) \qquad (5.32)$$

$$\boldsymbol{\tau_{6.2}} = {}^{link_h}_{l.ph.}\boldsymbol{R}.\boldsymbol{\tau_{6.1}} - \left(\mathbf{F_{h\_l.p.}} \times \frac{\boldsymbol{h}}{\mathbf{2}}\right) + \left({}^{link_h}_{l.ph.}\boldsymbol{R}.\boldsymbol{F_{h\_r.p}} \times \frac{\boldsymbol{h}}{\mathbf{2}}\right) + \left({}^{0}_{link_h}\boldsymbol{R}.\boldsymbol{I_{link_h}}.{}^{0}_{link_h}\boldsymbol{R^{T}}\right).\dot{\omega}_{link_h} +$$
$$\omega_{link_h} \times \left(\left({}^{0}_{link_h}\boldsymbol{R}.\boldsymbol{I_{link_h}}.{}^{0}_{link_h}\boldsymbol{R^{T}}\right).\omega_{link_h}\right) \qquad (5.33)$$

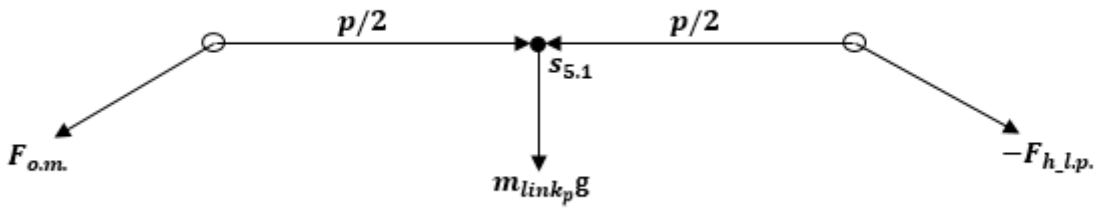

Scheme 5.12. Situation in link p

$$\sum \mathbf{F} = \mathbf{ma} \quad => \mathbf{F_{o.m.}} - {}^{link_p}_{link_h}\boldsymbol{R}.\boldsymbol{F_{h\_l.p.}} + \mathbf{m_{link_p}}\left({}^{0}_{link_p}\boldsymbol{R^{-1}}.\mathbf{g}\right) = \boldsymbol{m_{link_p}a_{s5.1}}$$
$$\mathbf{F_{o.m.}} = {}^{link_p}_{link_h}\boldsymbol{R}.\boldsymbol{F_{h\_l.p.}} - \mathbf{m_{link_p}}\left({}^{0}_{link_p}\boldsymbol{R^{-1}}.\mathbf{g}\right) + \boldsymbol{m_{link_p}a_{s5.1}} \qquad (5.34)$$

$$\sum \mathbf{M} = \boldsymbol{I}\dot{\omega} + \omega \times (\boldsymbol{I}\omega) \quad => \quad \boldsymbol{\tau_{6.3}} - {}^{link_p}_{link_h}\boldsymbol{R}.\boldsymbol{\tau_{6.2}} + \left(\boldsymbol{F_{o.m.}} \times \frac{\boldsymbol{p}}{\boldsymbol{2}}\right) - \left({}^{link_p}_{link_h}\boldsymbol{R}.\boldsymbol{F_{h\_l.p.}} \times \frac{\boldsymbol{p}}{\boldsymbol{2}}\right) =$$

$$\left({}^{0}_{link_p}\boldsymbol{R}.\boldsymbol{I}_{link_p}.\,{}^{0}_{link_p}\boldsymbol{R}^{T}\right).\dot{\omega}_{link_p} + \omega_{link_p} \times \left(\left({}^{0}_{link_p}\boldsymbol{R}.\boldsymbol{I}_{link_p}.\,{}^{0}_{link_p}\boldsymbol{R}^{T}\right).\omega_{link_p}\right) \quad (5.35)$$

$$\boldsymbol{\tau_{6.3}} = {}^{link_p}_{link_h}\boldsymbol{R}.\boldsymbol{\tau_{6.2}} - \left(\boldsymbol{F_{o.m.}} \times \frac{\boldsymbol{p}}{\boldsymbol{2}}\right) + \left({}^{link_p}_{link_h}\boldsymbol{R}.\boldsymbol{F_{h\_l.p.}} \times \frac{\boldsymbol{p}}{\boldsymbol{2}}\right) + \left({}^{0}_{link_p}\boldsymbol{R}.\boldsymbol{I}_{link_p}.\,{}^{0}_{link_p}\boldsymbol{R}^{T}\right).\dot{\omega}_{link_p} +$$

$$\omega_{link_p} \times \left(\left({}^{0}_{link_p}\boldsymbol{R}.\boldsymbol{I}_{link_p}.\,{}^{0}_{link_p}\boldsymbol{R}^{T}\right).\omega_{link_p}\right) \quad (5.36)$$

5.3.2. Behavior of passive links

After solution for the fingers' torques and forces is obtained, it is necessary to assign these values to the actuators located in the palm. Structure of the palm has two passive links (carrying thumb and index finger) that apply load to the left and right parts, where driven links are located. In order to define amount of load taken by particular side, passive links' common centre of mass is found using SolidWorks software. Hence, load distribution is calculated according to how far away is passive links' common centre of mass from the symmetry axis of active links' edge joints. When common centre of mass lies on the symmetry axis, it is assumed that the overall load from passive links is transferred equally, i.e. 50% to the left active link and 50% to the right active link. From figures 5.1 and 5.2, it is possible to approximate force-torque distribution changes according to particular configuration of the mechanism.

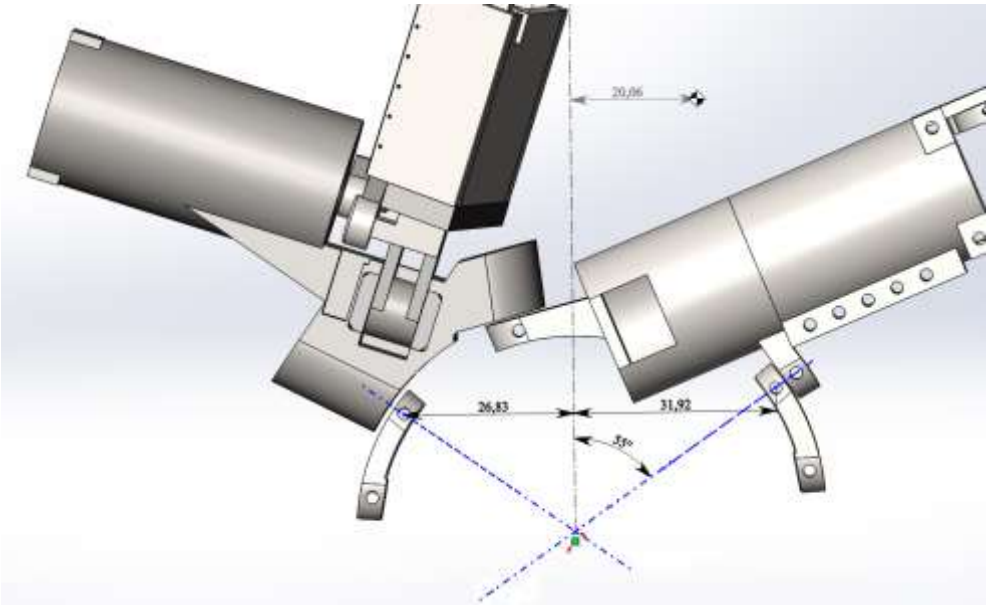

Figure 5.1. Centre of mass when fingers are flat

Figure 5.1 illustrates that at flat finger position common centre of mass is shifted to the right active link's side for 20.06 mm or for ≈34% of the distance between actuated links. It is now possible to obtain ratio to approximate load taken by active links. Therefore, in these conditions, right active link will take 66% of the overall torque and force accumulated by passive links, whereas left active link will take only 34%.

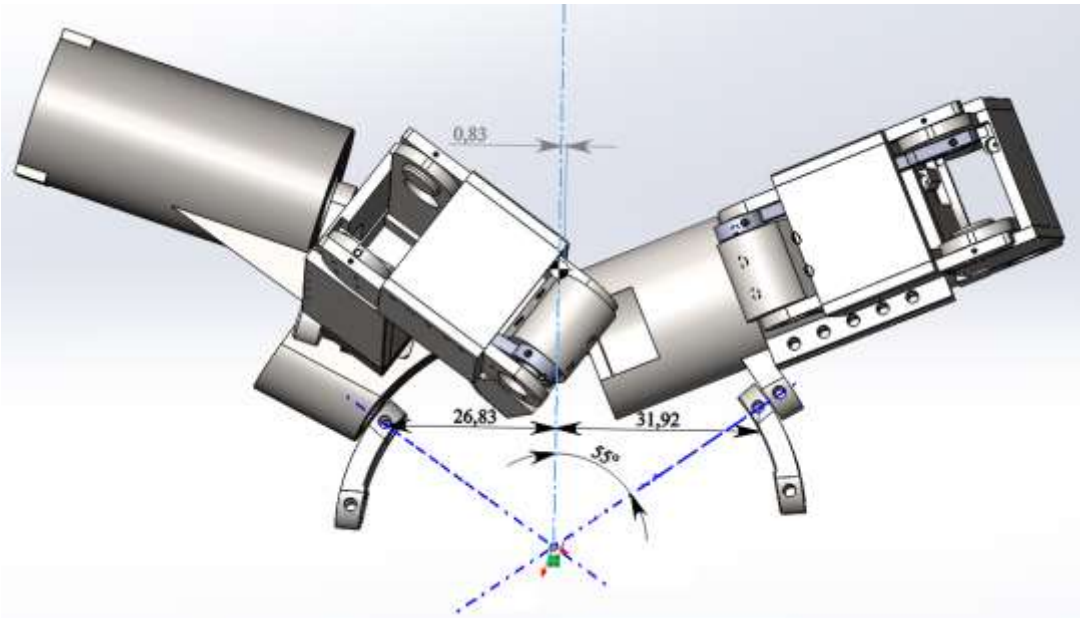

Figure 5.2. Centre of mass when index finger and thumb are bent

Figure 5.2 highlights that when both index finger and thumb are bent, active links in the palm are almost equally loaded. Insignificant deviation will be neglected, so at maximum bending active links take 50% of the load each.

Figures 9.2 to 9.5 in appendix show that different configurations have relatively small impact on the centre of mass location change – hence, major influence was noted and considered.

For numerical simulation, the following basic assumption will be used: torque and force influence on the right active link will increase from 50% to 66% depending on the phalange flexion amplitude.

5.3.3. Calculations for torque 1 and F_{B01}

When position of the passive links' common centre of mass is taken into account, now forces and torques can be calculated for the left and right actuated joints accordingly.

For the left actuator, scheme 5.13 is considered first.

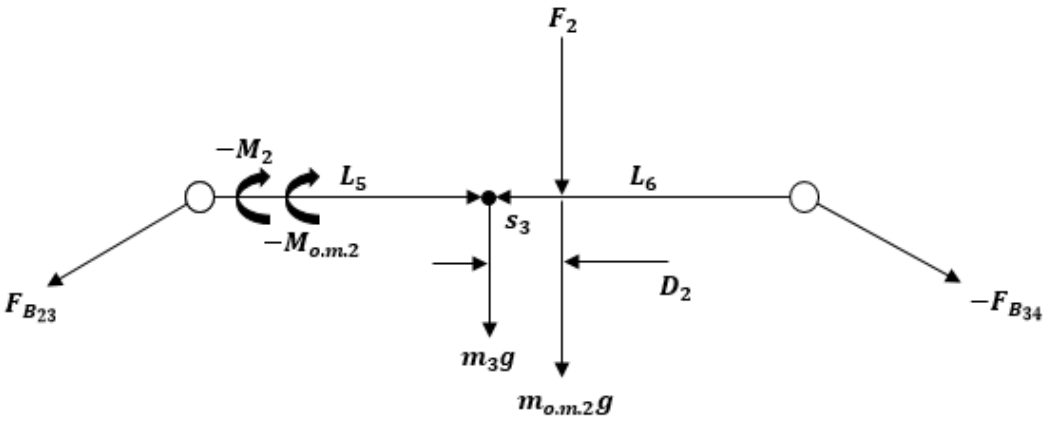

Scheme 5.13. Free body diagram of the link 3

It is possible to observe forces and moments acting on link 3. $\mathbf{F_{B23}}$ **and** $\mathbf{F_{B34}}$ stand for pulling forces of the left link and right link in respect to the reviewed one respectively. Resultant vectors of these forces are strictly defined by position of the neighboring elements. Also, $\mathbf{L_5}$ ***and*** $\mathbf{L_6}$ are position vectors from the bearing's center to the link's center of mass. Force $\mathbf{F_2}$ is cause by the index finger that is connected to the link; consequently, moment $\boldsymbol{M_2}$ arises from the finger as well. This particular link is actuated by external DC motor, so $-\boldsymbol{M}_{o.m.2}$ is taken into account. Distances, D, are indicating interval between centers of mass. $\boldsymbol{S_1}$ stands for link's center of mass. All moments are taken about link's center of mass. It will be necessary to note that analysed problem is not a planar case, hence outcome final equations are related to each axis – x, y and z.

$$\sum \mathrm{F} = \mathrm{ma} \quad => \quad \mathrm{F_{B23}} - {}^{link3}_{link4}\mathrm{R}.\,\mathrm{F_{B34}} + \mathrm{m_3}({}^{0}_{link3}\mathrm{R}^{-1}.\,\mathrm{g}) + {}^{link3}_{i.l.ph.}\mathrm{R}.\,\mathrm{F_2} + m_{o.m.2}({}^{0}_{link3}\mathrm{R}^{-1}.\,\mathrm{g}) = m_3 a_{s3} \tag{5.36}$$

To apply load of the passive links with appropriate proportion, they are disconnected from the closed chain, i.e.

$${}^{link3}_{link4}\mathrm{R}.\,\mathrm{F_{B34}} = 0; \qquad {}^{link3}_{link4}\mathrm{R}.\,\tau_4 = 0 \tag{5.37}$$

$$\mathrm{F_{B23}} = -\mathrm{m_3}({}^{0}_{link3}\mathrm{R}^{-1}.\,\mathrm{g}) - {}^{link3}_{i.l.ph.}\mathrm{R}.\,\mathrm{F_2} - m_{o.m.2}({}^{0}_{link3}\mathrm{R}^{-1}.\,\mathrm{g}) + m_3 a_{s3} \tag{5.38.1}$$

$$\sum \mathrm{M} = I\dot{\omega} + \omega \times (I\omega) \quad => \ \tau_3 - {}^{link3}_{link4}\mathrm{R}.\tau_4 + \left(F_{B_{23}} \times L_5\right) - \left({}^{link3}_{link4}\mathrm{R}.F_{B_{34}} \times L_6\right) - {}^{link3}_{i.l.ph.}\mathrm{R}.M_2 - M_{o.m.2} = \left({}^{0}_{link_3}R.I_{link_3}.{}^{0}_{link_3}R^T\right).\dot{\omega}_{link_3} + \omega_{link_3} \times \left(\left({}^{0}_{link_3}R.I_{link_3}.{}^{0}_{link_3}R^T\right).\omega_{link_3}\right) \quad (5.38.2)$$

$$\tau_3 = {}^{link3}_{i.l.ph.}\mathrm{R}.M_2 - \left(F_{B_{23}} \times L_5\right) + M_{o.m.2} + \left({}^{0}_{link_3}R.I_{link_3}.{}^{0}_{link_3}R^T\right).\dot{\omega}_{link_3} + \omega_{link_3} \times \left(\left({}^{0}_{link_3}R.I_{link_3}.{}^{0}_{link_3}R^T\right).\omega_{link_3}\right) \quad (5.39)$$

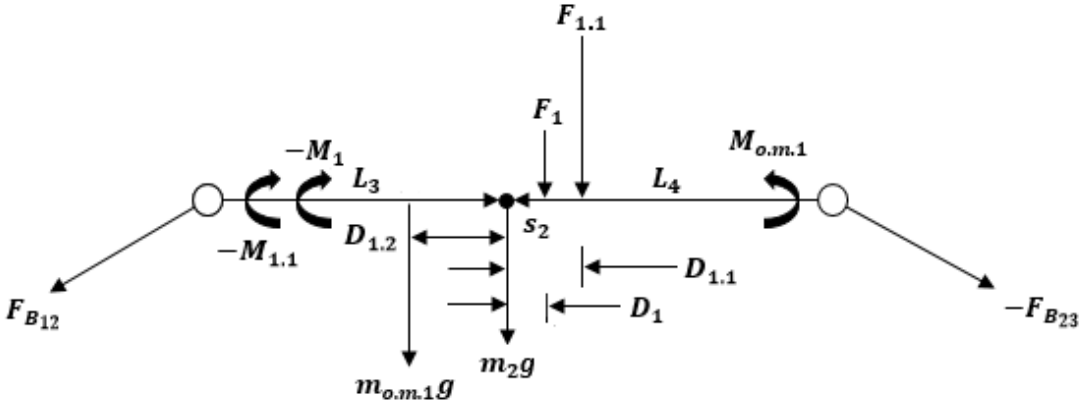

Scheme 5.14. Free body diagram of the link 2

Scheme 5.14 shows link with the thumb force acting on it. This link is unique as thumb is attached at two points, applying $\mathbf{F_1}$ and $\mathbf{F_{1.1}}$ due to implemented four-bar linkage.

$$\sum \mathrm{F} = \mathrm{ma} \ => \mathrm{F_{B12}} - {}^{link2}_{link3}\mathrm{R}.\mathrm{F_{B23}} + \mathrm{m_2}({}^{0}_{link2}\mathrm{R}^{-1}.\mathrm{g}) + {}^{link2}_{t.l.ph.}\mathrm{R}.\mathrm{F_1} + {}^{link2}_{o.dr.l}\mathrm{R}.\mathrm{F_{1.1}} + m_{o.m.1}({}^{0}_{link2}\mathrm{R}^{-1}.\mathrm{g}) = m_2 a_{s2}$$

$$\mathrm{F_{B12}} = {}^{link2}_{link3}\mathrm{R}.\mathrm{F_{B23}} - \mathrm{m_2}({}^{0}_{link2}\mathrm{R}^{-1}.\mathrm{g}) - {}^{link2}_{t.l.ph.}\mathrm{R}.\mathrm{F_1} - {}^{link2}_{o.dr.l}\mathrm{R}.\mathrm{F_{1.1}} - m_{o.m.1}({}^{0}_{link2}\mathrm{R}^{-1}.\mathrm{g}) + m_2 a_{s2} \quad (5.40)$$

$$\sum \mathrm{M} = I\dot{\omega} + \omega \times (I\omega) => \ \tau_2 - {}^{link2}_{link3}\mathrm{R}.\tau_3 + \left(F_{B_{12}} \times L_3\right) - \left({}^{link2}_{link3}\mathrm{R}.F_{B_{23}} \times L_4\right) - {}^{link2}_{t.l.ph.}\mathrm{R}.M_1 - {}^{link2}_{o.dr.l}\mathrm{R}.M_{1.1} + M_{o.m.1} = \left({}^{0}_{link_2}R.I_{link_2}.{}^{0}_{link_2}R^T\right).\dot{\omega}_{link2} + \omega_{link2} \times \left(\left({}^{0}_{link_2}R.I_{link_2}.{}^{0}_{link_2}R^T\right).\omega_{link2}\right) \quad (5.41)$$

$$\tau_2 = {}^{link2}_{link3}\mathrm{R}.\tau_3 - \left(F_{B_{12}} \times L_3\right) + \left({}^{link2}_{link3}\mathrm{R}.F_{B_{23}} \times L_4\right) + {}^{link2}_{t.l.ph.}\mathrm{R}.M_1 + {}^{link2}_{o.dr.l}\mathrm{R}.M_{1.1} - M_{o.m.1} +$$
$$\left({}^{0}_{link2}R.I_{link2}.{}^{0}_{link2}R^T\right).\dot{\omega}_{link2} + \omega_{link2} \times \left(\left({}^{0}_{link2}R.I_{link2}.{}^{0}_{link2}R^T\right).\omega_{link2}\right) \qquad (5.42)$$

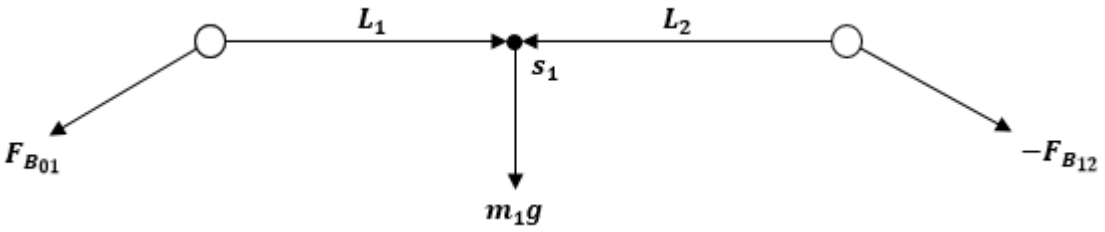

Scheme 5.15. Free body diagram of the link 1

On Scheme 5.15, crank is schematically represented. It is actuated by the second DC motor located within the 'stationary' fifth link. There are no fingers on this link; it serves as a rotary motion translator.

$$\sum \mathbf{F} = \mathbf{ma} \quad => \mathbf{F_{B01}} - {}^{link1}_{link2}\mathbf{R}.\mathbf{F_{B12}} + \mathbf{m_1}\left({}^{0}_{link1}\mathbf{R}^{-1}.\mathbf{g}\right) = \boldsymbol{m_1 a_{s1}}$$
$$\mathbf{F_{B01}} = \boldsymbol{ratio_3} * \left({}^{link1}_{link2}\mathbf{R}.\mathbf{F_{B12}} - \mathbf{m_1}\left({}^{0}_{link1}\mathbf{R}^{-1}.\mathbf{g}\right) + \boldsymbol{m_1 a_{s1}}\right) \qquad (5.43)$$

$$\sum \mathbf{M} = \boldsymbol{I}\dot{\omega} + \omega \times (\boldsymbol{I}\omega) \quad => \boldsymbol{\tau_1} - {}^{link1}_{link2}\mathbf{R}.\boldsymbol{\tau_2} + \left(\boldsymbol{F_{B_{01}}} \times \boldsymbol{L_1}\right) - \left({}^{link1}_{link2}\mathbf{R}.\boldsymbol{F_{B_{12}}} \times \boldsymbol{L_2}\right) =$$
$$\left({}^{0}_{link1}\boldsymbol{R}.\boldsymbol{I_{link1}}.{}^{0}_{link1}\boldsymbol{R^T}\right).\dot{\omega}_{\boldsymbol{link1}} + \omega_{\boldsymbol{link1}} \times \left(\left({}^{0}_{link1}\boldsymbol{R}.\boldsymbol{I_{link1}}.{}^{0}_{link1}\boldsymbol{R^T}\right).\omega_{\boldsymbol{link1}}\right) \qquad (5.44)$$

$$\boldsymbol{\tau_1} = \boldsymbol{ratio_3} * \left({}^{link1}_{link2}\mathbf{R}.\boldsymbol{\tau_2} - \left(\boldsymbol{F_{B_{01}}} \times \boldsymbol{L_1}\right) + \left({}^{link1}_{link2}\mathbf{R}.\boldsymbol{F_{B_{12}}} \times \boldsymbol{L_2}\right) +\right.$$
$$\left.\left({}^{0}_{link1}\boldsymbol{R}.\boldsymbol{I_{link1}}.{}^{0}_{link1}\boldsymbol{R^T}\right).\dot{\omega}_{\boldsymbol{link1}} + \omega_{\boldsymbol{link1}} \times \left(\left({}^{0}_{link1}\boldsymbol{R}.\boldsymbol{I_{link1}}.{}^{0}_{link1}\boldsymbol{R^T}\right).\omega_{\boldsymbol{link1}}\right)\right) \qquad (5.45)$$

5.3.4. Calculations for torque 5 and F_{B40}

Scheme 5.14 will be used again, but now the closed loop is disconnected from the left side, i.e. $\mathrm{F_{B12}} = 0$.

$$-\mathrm{F_{B23}} + \mathrm{m_2}\left({}^{0}_{link2}\mathrm{R}^{-1}.\mathrm{g}\right) + {}^{link2}_{t.l.ph.}\mathrm{R}.\mathrm{F_1} + {}^{link2}_{o.dr.l}\mathrm{R}.\mathrm{F_{1.1}} + m_{o.m.1}\left({}^{0}_{link2}\mathrm{R}^{-1}.\mathrm{g}\right) = m_2 a_{s2}$$
$$\mathrm{F_{B23}} = \mathrm{m_2}\left({}^{0}_{link2}\mathrm{R}^{-1}.\mathrm{g}\right) + {}^{link2}_{t.l.ph.}\mathrm{R}.\mathrm{F_1} + {}^{link2}_{o.dr.l}\mathrm{R}.\mathrm{F_{1.1}} + m_{o.m.1}\left({}^{0}_{link2}\mathrm{R}^{-1}.\mathrm{g}\right) - m_2 a_{s2} \qquad (5.46)$$

$$-\tau_3 - \left(F_{B_{23}} \times L_4\right) - {}^{link2}_{t.l.ph.}\mathrm{R}.M_1 - {}^{link2}_{o.dr.l}\mathrm{R}.M_{1.1} + M_{o.m.1} = \left({}^{0}_{link2}R.I_{link2}.{}^{0}_{link2}R^T\right).\dot{\omega}_{link2} + \omega_{link2} \times \left(\left({}^{0}_{link2}R.I_{link2}.{}^{0}_{link2}R^T\right).\omega_{link2}\right)$$

$$\tau_3 = -\left(F_{B_{23}} \times L_4\right) - {}^{link2}_{t.l.ph.}\mathrm{R}.M_1 - {}^{link2}_{o.dr.l}\mathrm{R}.M_{1.1} + M_{o.m.1} - \left({}^{0}_{link2}R.I_{link2}.{}^{0}_{link2}R^T\right).\dot{\omega}_{link2} - \omega_{link2} \times \left(\left({}^{0}_{link2}R.I_{link2}.{}^{0}_{link2}R^T\right).\omega_{link2}\right) \quad (5.47)$$

Inspecting scheme 5.13 and moving to the right,

$${}^{link3}_{link2}\mathrm{R}.\mathrm{F}_{\mathrm{B23}} - \mathrm{F}_{\mathrm{B34}} + \mathrm{m}_3\left({}^{0}_{link3}\mathrm{R}^{-1}.\mathrm{g}\right) + {}^{link3}_{i.l.ph.}\mathrm{R}.\mathrm{F}_2 + m_{o.m.2}\left({}^{0}_{link3}\mathrm{R}^{-1}.\mathrm{g}\right) = m_3 a_{s3}$$

$$\mathrm{F}_{\mathrm{B34}} = {}^{link3}_{link2}\mathrm{R}.\mathrm{F}_{\mathrm{B23}} + \mathrm{m}_3\left({}^{0}_{link3}\mathrm{R}^{-1}.\mathrm{g}\right) + {}^{link3}_{i.l.ph.}\mathrm{R}.\mathrm{F}_2 + m_{o.m.2}\left({}^{0}_{link3}\mathrm{R}^{-1}.\mathrm{g}\right) - m_3 a_{s3} \quad (5.48)$$

$${}^{link3}_{link2}\mathrm{R}.\tau_3 - \tau_4 + \left({}^{link3}_{link2}\mathrm{R}.F_{B_{23}} \times L_5\right) - \left(F_{B_{34}} \times L_6\right) - {}^{link3}_{i.l.ph.}\mathrm{R}.M_2 - M_{o.m.2} = \left({}^{0}_{link3}R.I_{link3}.{}^{0}_{link3}R^T\right).\dot{\omega}_{link3} + \omega_{link3} \times \left(\left({}^{0}_{link3}R.I_{link3}.{}^{0}_{link3}R^T\right).\omega_{link3}\right) \quad (5.49)$$

$$\tau_4 = {}^{link3}_{link2}\mathrm{R}.\tau_3 + \left({}^{link3}_{link2}\mathrm{R}.F_{B_{23}} \times L_5\right) - \left(F_{B_{34}} \times L_6\right) - {}^{link3}_{i.l.ph.}\mathrm{R}.M_2 - M_{o.m.2} - \left({}^{0}_{link3}R.I_{link3}.{}^{0}_{link3}R^T\right).\dot{\omega}_{link3} - \omega_{link3} \times \left(\left({}^{0}_{link3}R.I_{link3}.{}^{0}_{link3}R^T\right).\omega_{link3}\right) \quad (5.50)$$

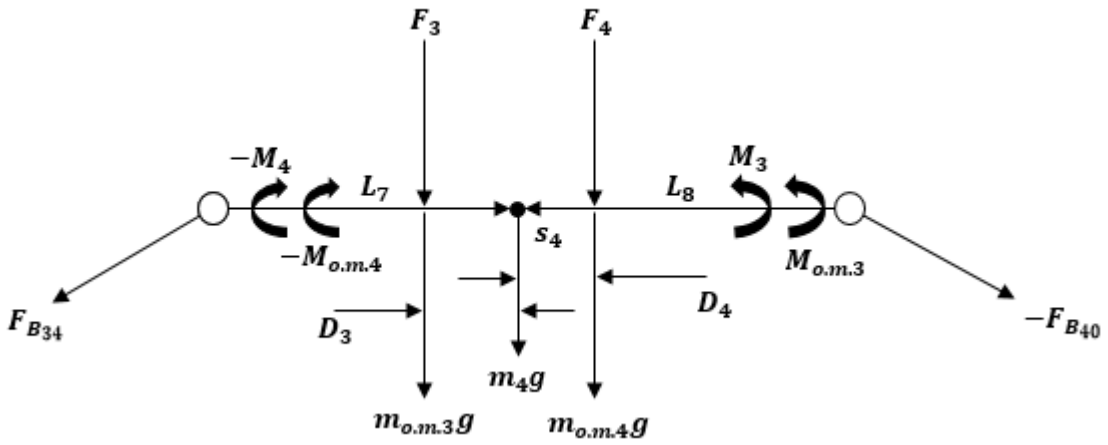

Scheme 5.16. Free body diagram of the link 4

Now, scheme 5.16 is used to show situation in link 4. This link carries middle and ring fingers that are located on both sides of the link's centre of mass.

$${}^{link4}_{link3}\mathrm{R}.\mathrm{F}_{\mathrm{B34}} - \mathrm{F}_{\mathrm{B40}} + \mathrm{m}_4\left({}^{0}_{link4}\mathrm{R}^{-1}.\mathrm{g}\right) + {}^{link4}_{m.f..l.ph.}\mathrm{R}.\mathrm{F}_3 + {}^{link4}_{r.f..l.ph.}\mathrm{R}.\mathrm{F}_4 + m_{o.m.3}\left({}^{0}_{link4}\mathrm{R}^{-1}.\mathrm{g}\right) + m_{o.m.4}\left({}^{0}_{link4}\mathrm{R}^{-1}.\mathrm{g}\right) = m_4 a_{s4} \quad (5.51)$$

$$\mathrm{F_{B40}} = ratio_4 * \left({}^{link4}_{link3}\mathrm{R}.\,\mathrm{F_{B34}} + \mathrm{m_4}({}^{0}_{link4}\mathrm{R}^{-1}.\,\mathrm{g}) + {}^{link4}_{m.f.l.ph.}\mathrm{R}.\,\mathrm{F_3} + {}^{link4}_{r.f.l.ph.}\mathrm{R}.\,\mathrm{F_4} + m_{o.m.3}({}^{0}_{link4}\mathrm{R}^{-1}.\,\mathrm{g}) + m_{o.m.4}({}^{0}_{link4}\mathrm{R}^{-1}.\,\mathrm{g}) - m_4 a_{s4} \right) \quad (5.52)$$

$${}^{link4}_{link3}\mathrm{R}.\,\tau_4 - \tau_5 + \left({}^{link4}_{link3}\mathrm{R}.\,F_{B34} \times L_7\right) - (F_{B40} \times L_8) + {}^{link4}_{m.f.l.ph.}\mathrm{R}.\,M_3 - {}^{link4}_{r.f.l.ph.}\mathrm{R}.\,\mathrm{M_4} - M_{o.m.4} + M_{o.m.3} = ({}^{0}_{link4}R.\,I_{link4}.\,{}^{0}_{link4}R^T).\,\dot{\omega}_{link4} + \omega_{link4} \times \left(({}^{0}_{link4}R.\,I_{link4}.\,{}^{0}_{link4}R^T).\,\omega_{link4}\right) \quad (5.53)$$

$$\tau_5 = ratio_4 * \left({}^{link4}_{link3}\mathrm{R}.\,\tau_4 + \left({}^{link4}_{link3}\mathrm{R}.\,F_{B34} \times L_7\right) - (F_{B40} \times L_8) + {}^{link4}_{m.f.l.ph.}\mathrm{R}.\,M_3 - {}^{link4}_{r.f.l.ph.}\mathrm{R}.\,\mathrm{M_4} - M_{o.m.4} + M_{o.m.3} - ({}^{0}_{link4}R.\,I_{link4}.\,{}^{0}_{link4}R^T).\,\dot{\omega}_{link4} - \omega_{link4} \times \left(({}^{0}_{link4}R.\,I_{link4}.\,{}^{0}_{link4}R^T).\,\omega_{link4}\right)\right) \quad (5.54)$$

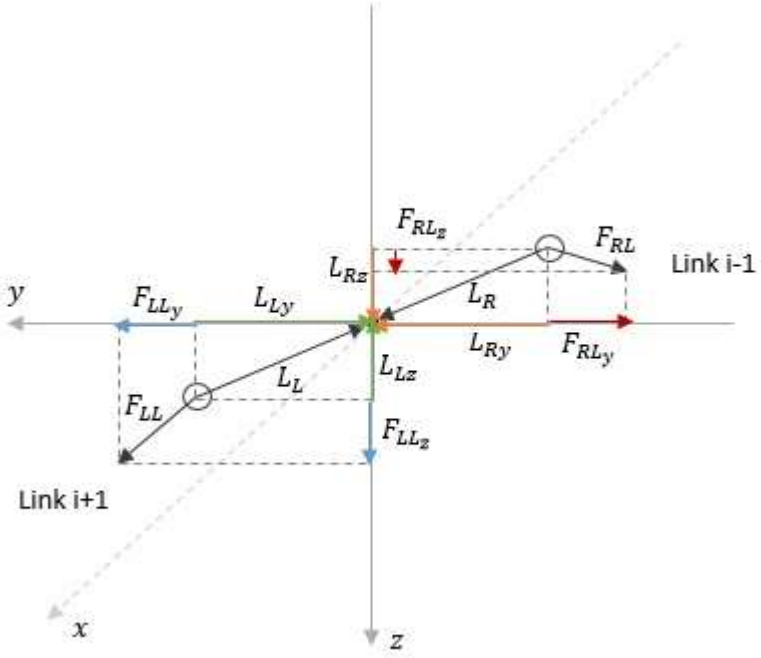

Scheme 5.17. Vector projections

Although all calculations are processed in computer, scheme 5.17 will be used to explain cross product outcomes for each of the axis. For moment equations in non-planar space, when $\boldsymbol{F_{LeftLink} \times L_{Left}}$ ***and*** $\boldsymbol{F_{RightLink} \times L_{Rright}}$, vector product formula is used:

$$\boldsymbol{c_x = a_y b_z - a_z b_y}$$

$$\boldsymbol{c_y = a_z b_x - a_x b_z}$$

$$\boldsymbol{c_z = a_x b_y - a_y b_x}$$

It is now possible to produce resultant vector equations (specifically, moment):

$$\boldsymbol{Terms\ related\ to\ neighbor\ link's\ influence,\ for\ the\ link\ i}$$

$$+\mathbf{1}:\ \begin{matrix} x \\ y \\ z \end{matrix}\begin{cases} \mathbf{F_{RL_y}.L_{Rz}} - \mathbf{F_{RL_z}.L_{Ry}} \\ \mathbf{F_{RL_z}.L_{Rx}} - \mathbf{F_{RL_x}.L_{Rz}} \\ \mathbf{F_{RL_x}.L_{Ry}} - \mathbf{F_{RL_y}.L_{Rx}} \end{cases}$$

$$\boldsymbol{Terms\ related\ to\ neighbor\ link's\ influence,\ for\ the\ link\ i}:\ \begin{matrix} x \\ y \\ z \end{matrix}\begin{cases} \mathbf{F_{LL_y}.L_{Lz}} - \mathbf{F_{LL_z}.L_{Ly}} \\ \mathbf{F_{LL_z}.L_{Lx}} - \mathbf{F_{LL_x}.L_{Lz}} \\ \mathbf{F_{LL_x}.L_{Ly}} - \mathbf{F_{LL_y}.L_{Lx}} \end{cases}$$

5.3.5. Simulation results

When flexion occurs, i.e. theta 5 is negative and theta 1 is positive, spherical triangle is assembled below. Grasping happens when link's inertias are helping motion, i.e. the hand is upside down. Material is set to be aluminium, however some vital parts are set to be from carbon steel. These include link 1 of the palm's mechanism, driving links in the fingers and 2 small links that are part of the thumb's outer actuation system.

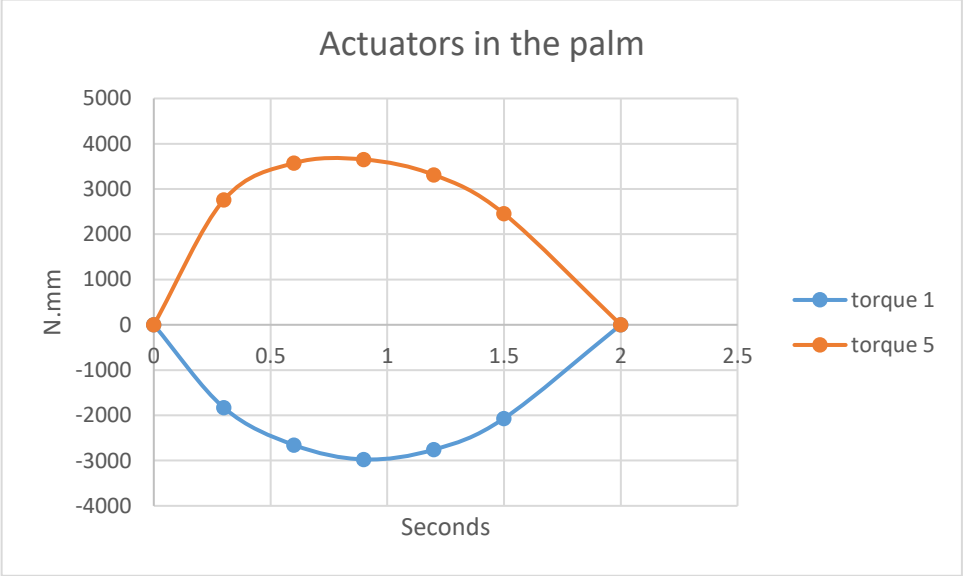

Figure 5.3. Load taken by palm's DC motors

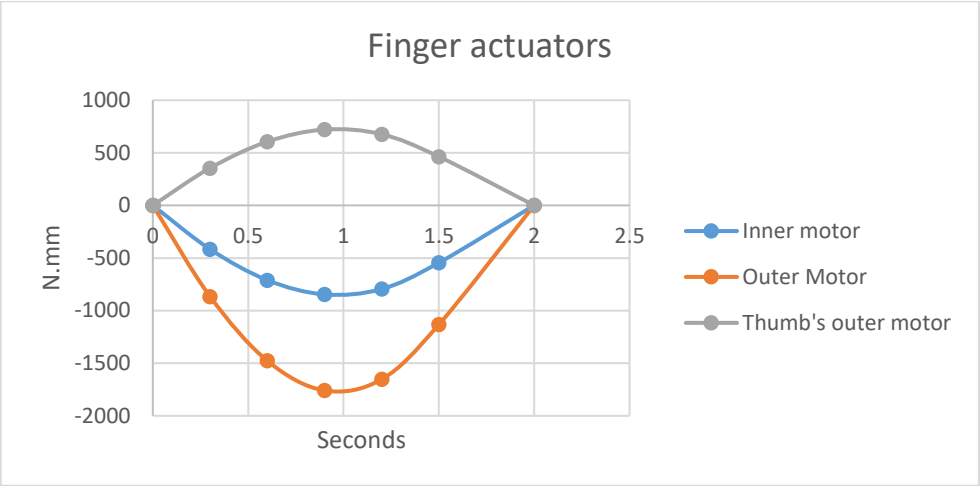

Figure 5.3. Load taken by fingers' DC motors

Figures 5.4 and 5.5 prove that 2-second rapid motion is very demanding in terms of required torque. However, it is still possible to follow the same route, but with longer time – that will reduce torque requirement accordingly and will make realistic conditions for motor operation. It is necessary to say that backward motion will require even higher torque due to inertias acting in the opposite direction. Results are based on conditions when all fingertips meet simultaneous 10 N force resistance and motion is determined by path planning instructions.

5.4. Summary

Obtained results are expected and final comment on the performance can be made. Proposed design is limited in terms of power grasp and also rapid motion under considerable stress is not possible. However, operation under simultaneous 10N-fingertip load with moderate speed is attainable. In addition, the robotic hand was pushed to its limits in terms of chosen actuator's torque affordability and according to the results, the metamorphic anthropomorphic robotic hand with integrated motors shows reasonable performance. Considering the fact that controlled hand's structure is complicated, this is compensated by grasping capabilities and acceptable force generation. Without force acting on each fingertip, i.e. while the object is not yet carried, the proposed hand is able to be dexterous and obtain the posture within short period of time. Then, when the force is applied to the object and its inertia is included to the manipulator, stable smooth motion (and slow if the object is heavy) is recommended to avoid high torque demands.

Chapter 6

Control

6.1. Introduction

Control engineering allows mathematical description of the system variables to achieve the desired motion for continuously operating mechanism. It is an indispensable method for analysing kinematic and dynamic behaviour of the mechanism (robot) and relating it to the desired motion by introducing appropriate controller. For example, forces acting on the mechanism required to achieve the desired robot configuration in a minimum time can be found based on the control model. Such implementation of control theory allows modelling of corrective controller which acts differently with respect to an error signal, optimizing the system to make the desired process possible.

In this chapter, control techniques and route planning are discussed for further implementation into the controller.

6.2. Path Planning

Path planning – is a branch of control science, that describes the trajectory of manipulator motion through obstacles in the set time profile. Path planning defines the curve followed by end-effector between initial and terminate positions, rotational motion between two orientations and the time-dependence function of coordinate variation. Path planning is a challenging problem in robotics, especially when dealing with robot's design for dynamic environments. Changing environment introduces the need of automatic obstacle avoidance feature, which complicates the path planning process.

Path planning process consists of two tasks: determination of geometric path and avoiding the excessive time, energy and jerk. Several approaches dedicated to minimization of each of the parameters alone, depending on the goal set for each robot.

Time is the first criteria for judging system's performance as it is directly proportional to the productivity of the system. Minimization of the execution time is especially important in automated robotics.

Although there are various methods available for path planning, i.e. cubic path, non-polynomial path, Cartesian path, rotation path (rotation matrices), polynomial method is widely used and acknowledged for its simplicity and efficiency. It provides enough control for variety of tasks and also path can be split into segments and checkpoints set.

A seven-degree polynomial has maintenance of jerk parameters in comparison to the five-degree polynomial, which represents a simplified version without jerk consideration and hence is faster in terms of computation time if huge calculation sequences should be performed. However, for precision actuation a seven-degree polynomial must be used to set particular conditions of the start and end points of the described route that are meant to have no jerk. In addition, when requirements for route checkpoints are being assessed, for some points admitted amount of jerk may take place if task requires so.

Consider a seven-degree polynomial's final form,

$$\theta(t) = k_0 + k_1 t + k_2 t^2 + k_3 t^3 + k_4 t^4 + k_5 t^5 + k_6 t^6 + k_7 t^7 \quad (6.1)$$

where 'k' – constant coefficient.

A general seven-degree polynomial can be presented by the following matrices, containing start motion and end motion parameters:

$$\begin{bmatrix} 1 & t_s & t_s^2 & t_s^3 & t_s^4 & t_s^5 & t_s^6 & t_s^7 \\ 0 & 1 & 2t_s & 3t_s^2 & 4t_s^3 & 5t_s^4 & 6t_s^5 & 7t_s^6 \\ 0 & 0 & 2 & 6t_s & 12t_s^2 & 20t_s^3 & 30t_s^4 & 42t_s^5 \\ 0 & 0 & 0 & 6 & 24t_s & 60t_s^2 & 120t_s^3 & 210t_s^4 \\ 1 & t_e & t_e^2 & t_e^3 & t_e^4 & t_e^5 & t_e^6 & t_e^7 \\ 0 & 1 & 2t_e & 3t_e^2 & 4t_e^3 & 5t_e^4 & 6t_e^5 & 7t_e^6 \\ 0 & 0 & 2 & 6t_e & 12t_e^2 & 20t_e^3 & 30t_e^4 & 42t_e^5 \\ 0 & 0 & 0 & 6 & 24t_e & 60t_e^2 & 120t_e^3 & 210t_e^4 \end{bmatrix} \cdot \begin{bmatrix} k_0 \\ k_1 \\ k_2 \\ k_3 \\ k_4 \\ k_5 \\ k_6 \\ k_7 \end{bmatrix} = \begin{bmatrix} \theta(t_s) \\ \dot{\theta}(t_s) \\ \ddot{\theta}(t_s) \\ \dddot{\theta}(t_s) \\ \theta(t_e) \\ \dot{\theta}(t_e) \\ \ddot{\theta}(t_e) \\ \dddot{\theta}(t_e) \end{bmatrix} \quad (6.2)$$

Coefficients are therefore found:

$$\begin{bmatrix} k_0 \\ k_1 \\ k_2 \\ k_3 \\ k_4 \\ k_5 \\ k_6 \\ k_7 \end{bmatrix} = \begin{bmatrix} 1 & t_s & t_s^2 & t_s^3 & t_s^4 & t_s^5 & t_s^6 & t_s^7 \\ 0 & 1 & 2t_s & 3t_s^2 & 4t_s^3 & 5t_s^4 & 6t_s^5 & 7t_s^6 \\ 0 & 0 & 2 & 6t_s & 12t_s^2 & 20t_s^3 & 30t_s^4 & 42t_s^5 \\ 0 & 0 & 0 & 6 & 24t_s & 60t_s^2 & 120t_s^3 & 210t_s^4 \\ 1 & t_e & t_e^2 & t_e^3 & t_e^4 & t_e^5 & t_e^6 & t_e^7 \\ 0 & 1 & 2t_e & 3t_e^2 & 4t_e^3 & 5t_e^4 & 6t_e^5 & 7t_e^6 \\ 0 & 0 & 2 & 6t_e & 12t_e^2 & 20t_e^3 & 30t_e^4 & 42t_e^5 \\ 0 & 0 & 0 & 6 & 24t_e & 60t_e^2 & 120t_e^3 & 210t_e^4 \end{bmatrix}^{-1} \cdot \begin{bmatrix} \theta(t_s) \\ \dot{\theta}(t_s) \\ \ddot{\theta}(t_s) \\ \dddot{\theta}(t_s) \\ \theta(t_e) \\ \dot{\theta}(t_e) \\ \ddot{\theta}(t_e) \\ \dddot{\theta}(t_e) \end{bmatrix} \quad (6.3)$$

For all actuators the following simulation requirements will be set:

$\gamma(0) = 0$ $\quad \dot{\gamma}(0) = 0$ $\quad \ddot{\gamma}(0) = 0$ $\quad \dddot{\gamma}(0) = 0$

$\gamma(2) = 78.5$ $\quad \dot{\gamma}(2) = 0$ $\quad \ddot{\gamma}(2) = 0$ $\quad \dddot{\gamma}(2) = 0$

where γ is an input from figure 6.1 below.

Therefore,

$$\begin{bmatrix} 1 & 0 & 0 & 0 & 0 & 0 & 0 & 0 \\ 0 & 1 & 0 & 0 & 0 & 0 & 0 & 0 \\ 0 & 0 & 2 & 0 & 0 & 0 & 0 & 0 \\ 0 & 0 & 0 & 6 & 0 & 0 & 0 & 0 \\ 1 & 2 & 4 & 8 & 16 & 32 & 64 & 128 \\ 0 & 1 & 4 & 12 & 32 & 80 & 192 & 448 \\ 0 & 0 & 2 & 12 & 48 & 160 & 480 & 1344 \\ 0 & 0 & 0 & 6 & 48 & 240 & 960 & 3360 \end{bmatrix} \cdot \begin{bmatrix} k_0 \\ k_1 \\ k_2 \\ k_3 \\ k_4 \\ k_5 \\ k_6 \\ k_7 \end{bmatrix} = \begin{bmatrix} 0 \\ 0 \\ 0 \\ 0 \\ 78.5 \\ 0 \\ 0 \\ 0 \end{bmatrix} \quad (6.4)$$

The final polynomial is: $\gamma(t) = 171.719t^4 - 206.062t^5 + 85.8594t^6 - 12.2656t^7$ (6.5)

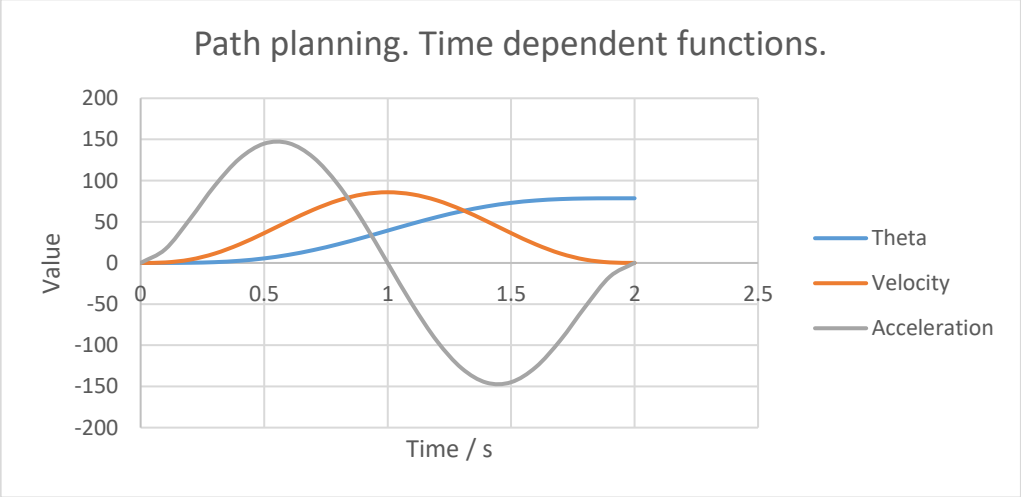

Figure 6.1. Conditions for set motion

Figure 6.1 shows that no jerk takes place and therefore motion is smooth and accurate.

The studied example shows implementation of higher order polynomial functions for satisfaction of set boundary conditions. One of the main advantages for using single high degree polynomial function is the smoothness of produced path, which takes into account many conditions (i.e. n-degree polynomial considers n+1 conditions, including constraints on accelerations and sometimes jerk).[68] On the other hand, single function can be split into few lower degree polynomials with their own boundary conditions. The results from all segments are then combined to produce the path. The main disadvantage of the split-path planning is that produced trajectory is absence of a single continuous differentiable function, which results in not a continuous velocity and acceleration, hence, jumps in accelerations are possible and the main requirement for path smoothness (continuous acceleration) is not met.[68] The main disadvantage of high degree polynomial employment is the mathematical complexity. Despite that smoothness of the path is important for reduction of motor wear, the difference in effectiveness may not be strongly noticeable and hence the time- and cost-consuming computing could be eliminated by using the piecewise approach.[72]

6.3. Collision Avoidance and Checkpoint Trajectory[73]

Assessment of workspace can be executed using various techniques. One of the most convenient methods is to upload CAD models of the robotic arm and its nearby environment to the specialized for these purposes software. Although this process can be resource demanding, another approach would involve specific treatment of the operation area when it is split into free and reserved (for obstacles) sectors and constraints are assigned to each robotic arm joint.

The free space is determined as C_{free} and the obstacle space is considered as C_{obst}.

$$C = C_{free} \cup C_{obst} \quad (6.6)$$

If distance, d, is defined by configuration ‘k’ and obstacle ‘O’, then the following circumstances are taken into account:

$$d(k, O) = 0 \quad \text{, when the contact is present} \quad (6.7)$$

$$d(k, O) > 0 \quad \text{, when there is no contact} \quad (6.8)$$

$$d(k, O) < 0 \quad \text{, when manipulator is intersecting with an obstacle} \quad (6.9)$$

Required data can be obtained from sensorial hardware or algorithms utilising real-time vision analysis. In addition, common approach is to represent robotic arm and obstacles as spheres of radiuses Z_i (centre at $z_i(k)$) and $O_j(\text{centre at } o_j)$ respectively. Quality of measurements

depends on the amount of spheres involved in the mesh construction. Hence, distance is found:

$$d(k, O) = \min_{i,j} \left\| z_i(k) - o_j \right\| - Z_i - O_j \quad (6.10)$$

Once the environment is studied and free space allocated, a set of checkpoints can be therefore selected in order to achieve the final destination of motion through the safe route. Also, it is important to have a time control for optimisation or task purposes.

6.4. Closed-Loop Feedback Control

When inverse dynamics is determined, there are several ways to control desired motion. Linear and non-linear methods. Linear method is appropriate and may be used in case if acceleration is constant, therefore it would be enough velocity and position errors to stabilize system's performance. Disturbances always occur due to external factors, modelling inaccuracies, etc. Hence, control unit has to take that into account.

Proportional-derivative control offers optimisation when this unit is subtracted from dynamics equation. Consider equation 6.11:

$$Q = -k_D \dot{e} - k_P e \quad (6.11)$$

$$e = q_a - q_d \quad (6.12)$$

$$\dot{e} = \dot{q}_a - \dot{q}_d \quad (6.13)$$

where q_a and $\dot{q}_a$ stand for actual values, but $\dot{q}_a$ and $\dot{q}_d$ stand for desired values.

If acceleration takes places, PD control cannot ensure stability of the system. For this adjustment, results from open-loop of inverse dynamics are used as a feedback for continuous comparison:

$$Q = D(q)\ddot{q_d} + H(q, \dot{q}) + G(q) + D(q)(-k_D \dot{e} - k_P e) \quad (6.14)$$

$$Q = D(q)(\ddot{q_d} - k_D \dot{e} - k_P e) + H(q, \dot{q}) + G(q) \quad (6.15)$$

Further manipulations decrease overall equation to error equation:

$$\ddot{e} + k_D \dot{e} + k_P e = 0 \quad (6.16)$$

Now, finally, solution is obtained:

$$e = Ae^{\lambda_1 t} + Be^{\lambda_2 t} \quad (6.17)$$

$$\lambda_{1,2} = -k_D \pm \sqrt{k^2{}_D - 4k_P} \quad (6.18)$$

In terms of stability, while eigenvalues of matrix A have real parts and are negative, the system is asymptotically stable.

$$\begin{bmatrix} 0 & I \\ -k_P & -k_D \end{bmatrix} \begin{bmatrix} e \\ \dot{e} \end{bmatrix} = [A] \begin{bmatrix} e \\ \dot{e} \end{bmatrix} \qquad (6.19)$$

Closed-loop control algorithms have several advantages over open-loop control. As shown above, the control commands in closed-loop control algorithms are adjusted based on the calculated error, summarised in equation 6.6. Application of new commands changes the dynamic equations of the system and the process is repeated constantly to control the following of designed path.[68] The open-loop control algorithms do not consider any possible error and expect a robot to follow the path only by computing the motion equations. It is, however, a much simpler approach and the open-loop control system is more cost-effective and easier to construct.

6.5. Summary

Control engineering has a vital role in any robot successful and safe functioning. First of the issues addressed in the chapter was path planning: while there exist several methods for path establishment, polynomial approach is considered the most convenient due to sufficient accuracy of the results, prospective to jerk elimination with production of a smooth path with continuous velocity and acceleration. While the high order polynomial function provides the smoothest path, it may be cost-inefficient and the piecewise approach may be preferred. However, choice of path planning approach must be performed by consideration of several factors: the number of conditions to be met, the length of the path, presence of obstacles or geometric constrains.

Closed-loop feedback control was also reviewed in the chapter as it is a reliable control system with high level of accuracy.[74] However, despite the strong advantage, as closed-loop system considers external errors, it is also an expensive complex system for construction. Stability of the closed-loop system is harder to achieve due to the sensitivity of the feedback mechanism. Open-loop control system lacks the accuracy due to the absence of error consideration, but is simple, more stable and easier to construct and maintain. While both of the control systems are widely used, it is important to take into account the target environment for robot employment.

Chapter 7

Finite Element Analysis of Vulnerable Parts

7.1. Introduction

Finite element analysis is often used to inspect behavior of mechanical systems and parts under various stress conditions. It is reliable and cost-effective method to determine drawbacks of design or just to verify expectations – prototyping for analysis becomes less essential and time can be saved at earlier stages of the manipulator development.

In this chapter, changes to the thumb design are assessed. Simulation results are briefly discussed. Thumb is stressed in conditions within which it is expected to perform. Suggestions for design improvements are made.

7.2. Simulations

In general, thumb with its base are made from aluminium in order to reduce load on the actuators. In the model, aluminium alloy 1060 is considered. It has a 27574200 N/m^2 yield strength. As for driving link in the fingers, driving link of the palm (link 1) and thumb's outer linkage small links – they are made out of simple carbon steel, 220594000 N/m^2.

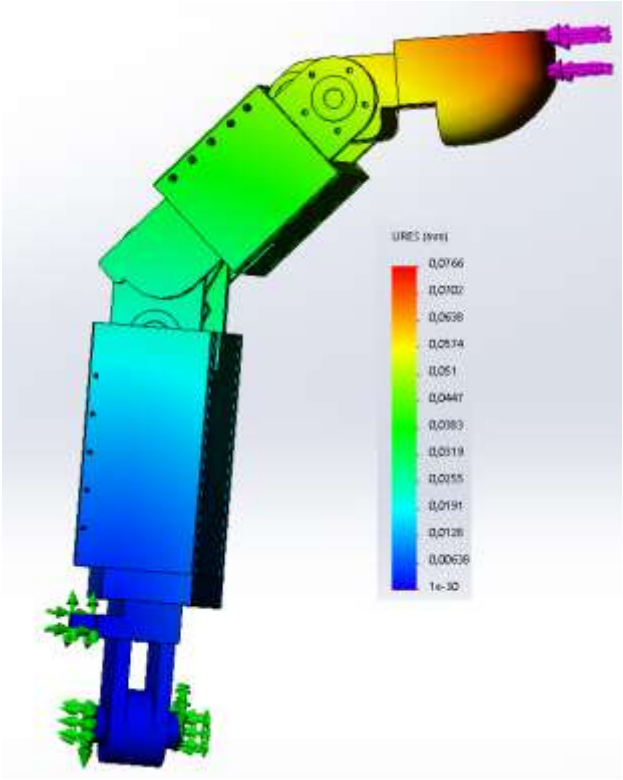

Figure 7.1. Finger is subjected to 10 N

Figure 7.1 illustrates that when thumb's fingertip is subjected to 10 N force, no deformation of material occurs – parts withstand the stress and remain on the same position. It is necessary to mention that despite other fingers have their joint's 'z' axis being parallel, thumb's lower joint is turned for 72 degrees from middle and upper joints. Hence, force is applied from the side and torque required for motion is less. This fact is beneficial for small links that drive the finger as they cannot withstand high torques.

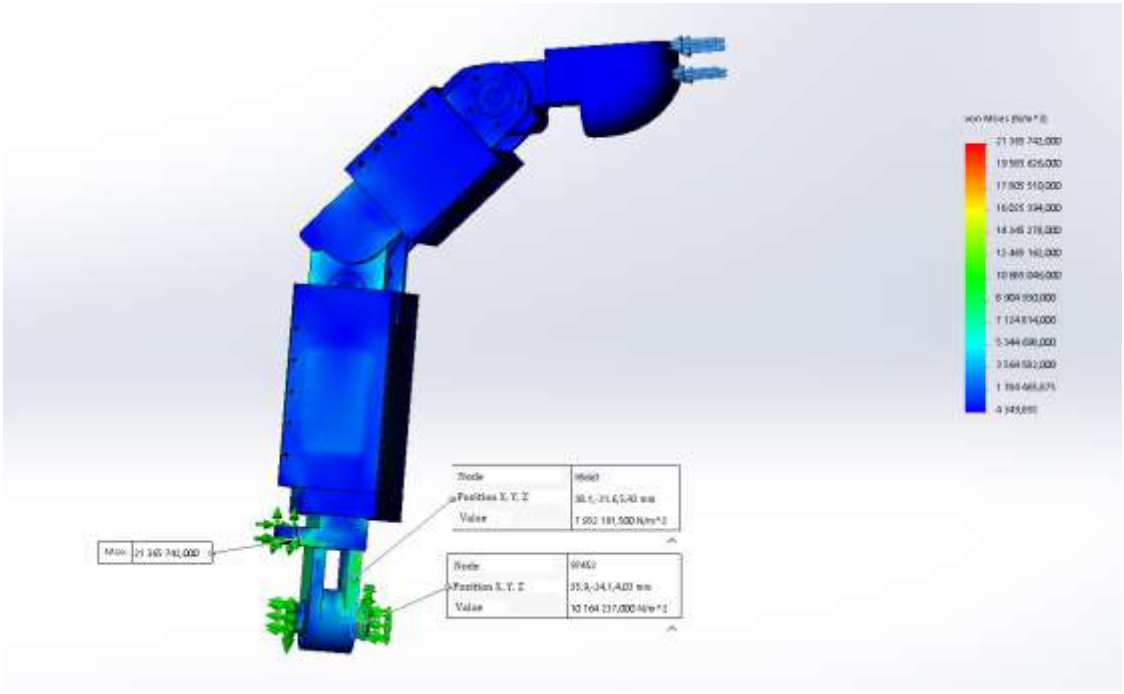

Figure 7.2. Stress at lower joint during 10 N

It is possible to observe on figure 7.2 maximum stress of 21365742 N/m^2. As lower phalange was modeled to be made from aluminium, this stress is near to the critical. Therefore, it may be considered that 10 N at fingertip is maximum force that should be applied to the thumb. Right part of the bottom joint is at higher load than the left part – this is caused by the difference of joint's 'z' axis orientation and is expected result.

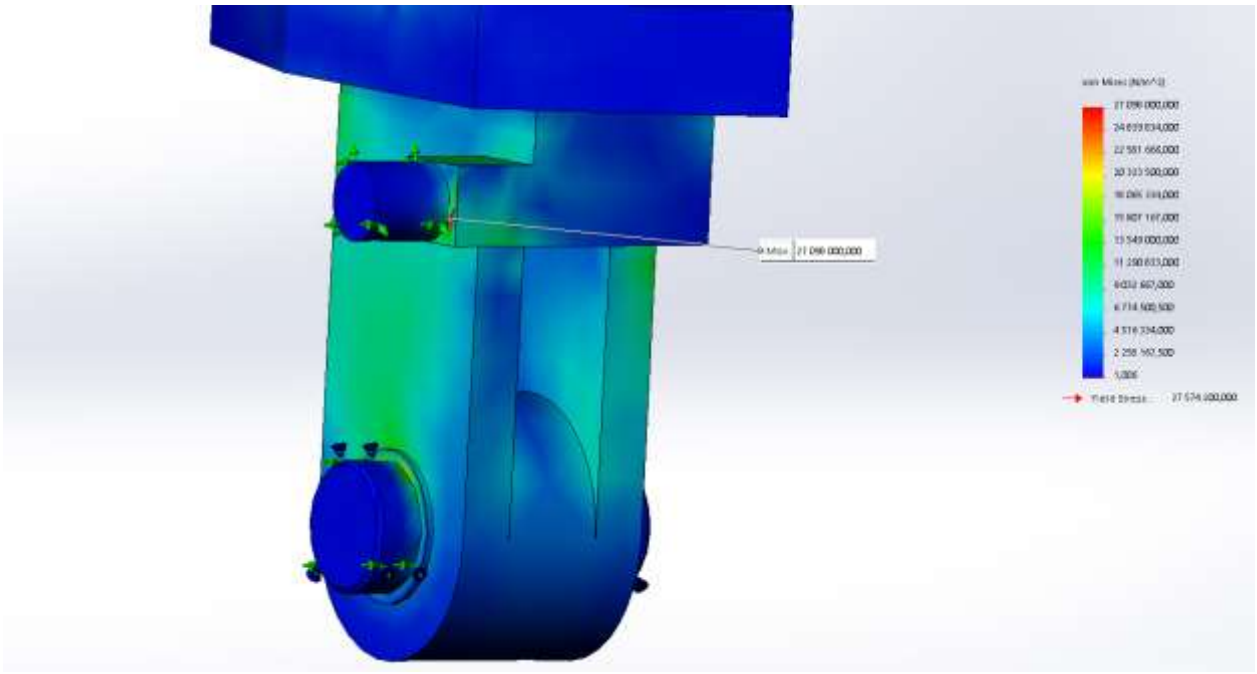

Figure 7.3. 700 N.mm applied to the joint driven by outer linkage

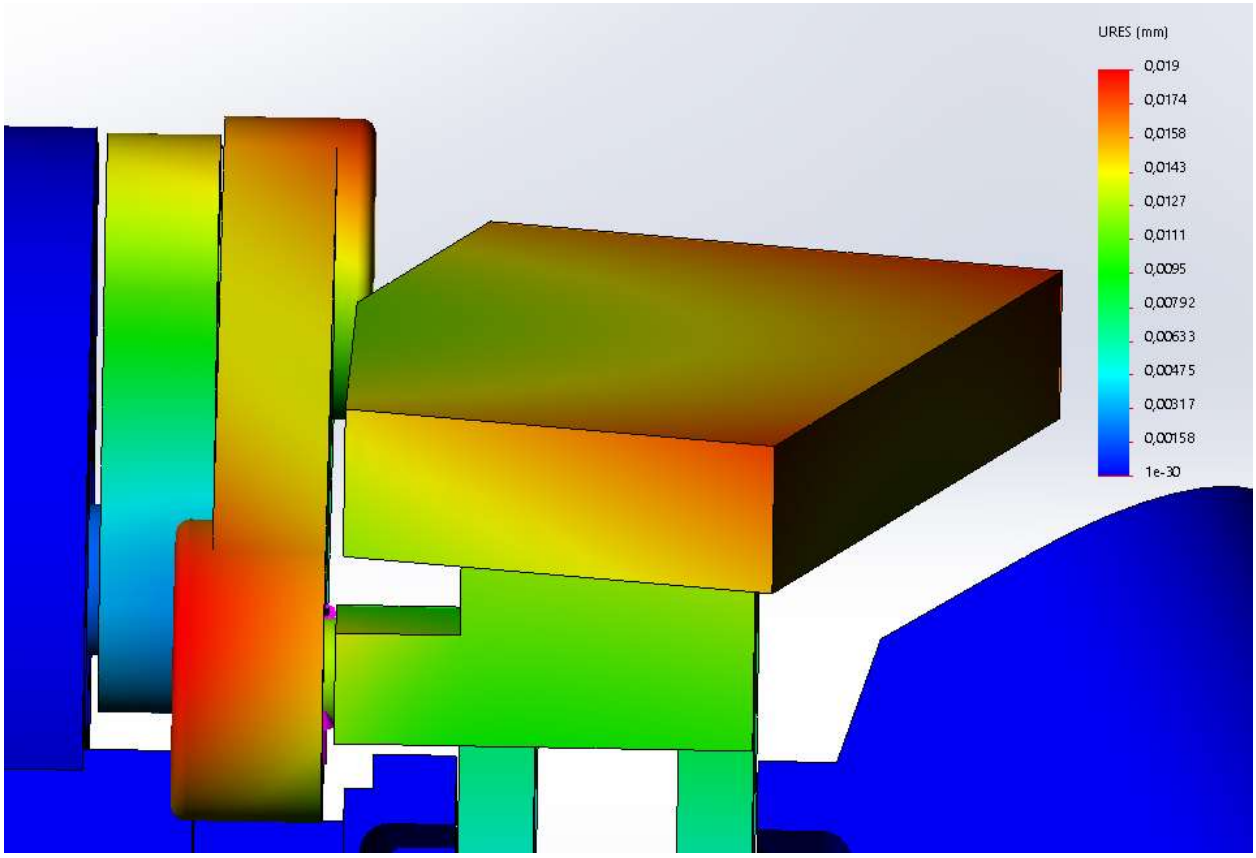

Figure 7.4. Stressed outer linkage

It is necessary to obtain limits for the force that is perpendicular to the bottom joint. From that perspective, less force will be required to cause critical stress. Figure 7.3 shows that 700 N.mm (about 7 N at the edge of the finger) at joint driven by small links of the outer linkage is almost enough for the deformation to occur. For better results, diameter of the joint can be increased, leading to the overall outer linkage proportional growth. From the figures 7.3 and 7.4, it is clear that outer linkage does not bend as well under mentioned stress.

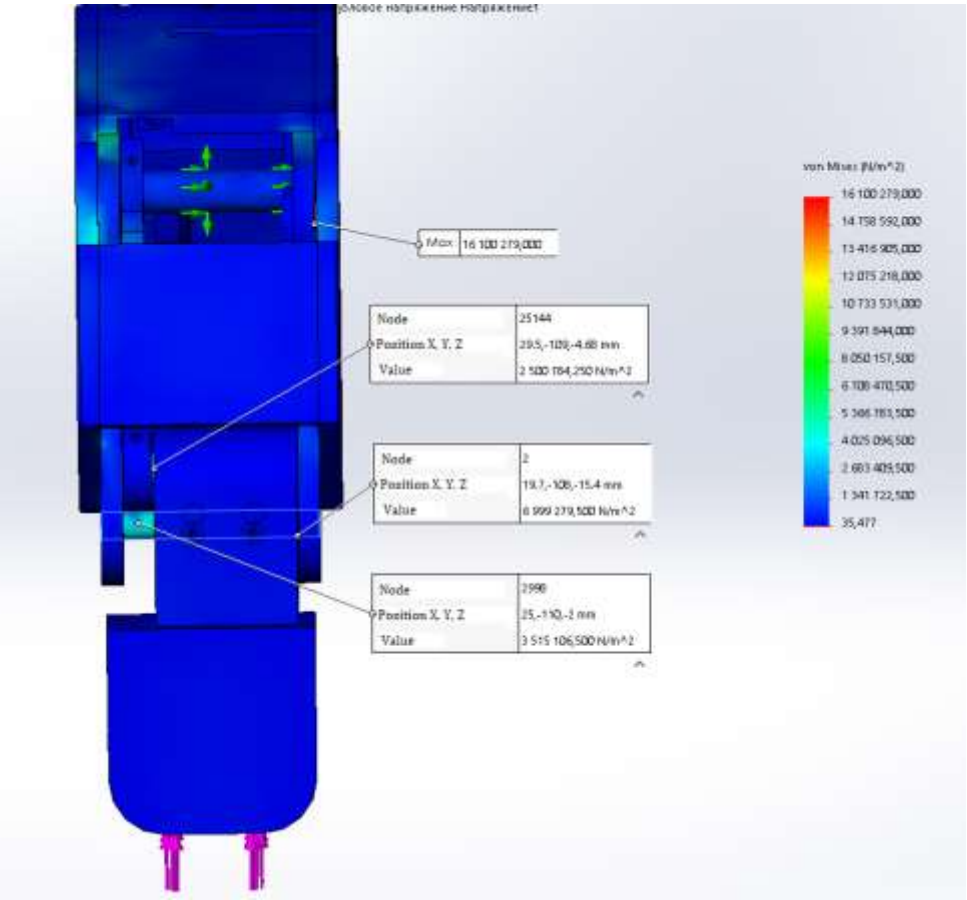

Figure 7.5. Stress during 10 N application

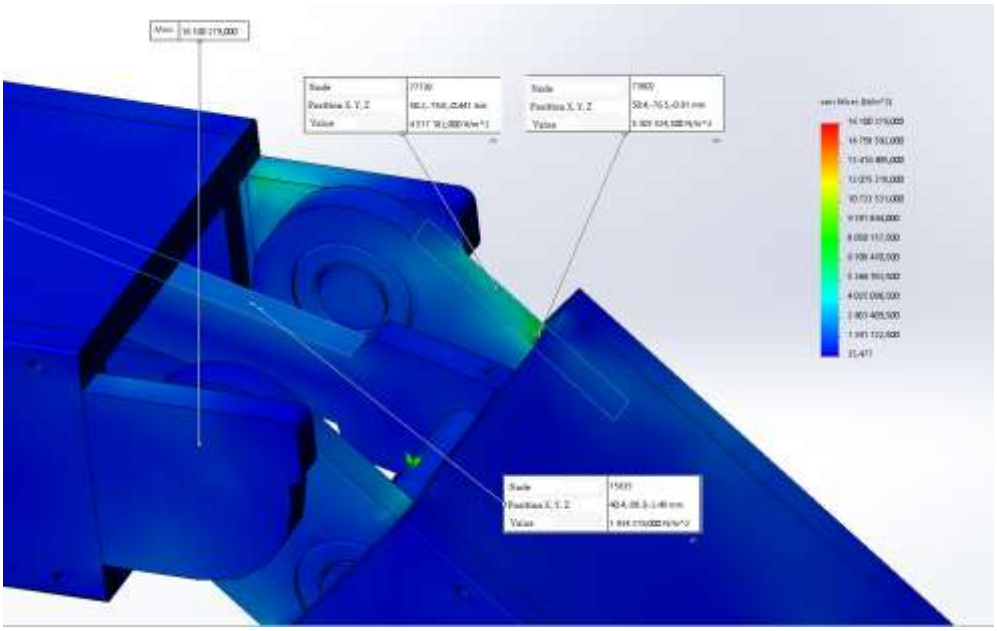

Figure 7.6. Middle phalange and lower phalange joint

Figure 7.5 clearly indicates that the weakest point of the upper part of the thumb is lower phalange and middle phalange common joint. It has shafts that are part of the side plates.

However, insertion of separate steel shafts will lead to disrupted silhouette. Greater performance is not required for the thumb since it not ready to withstand greater force than 10 N. Shifted upper phalange causes unequal torque and force distribution along the finger, which is seen from simulation results.

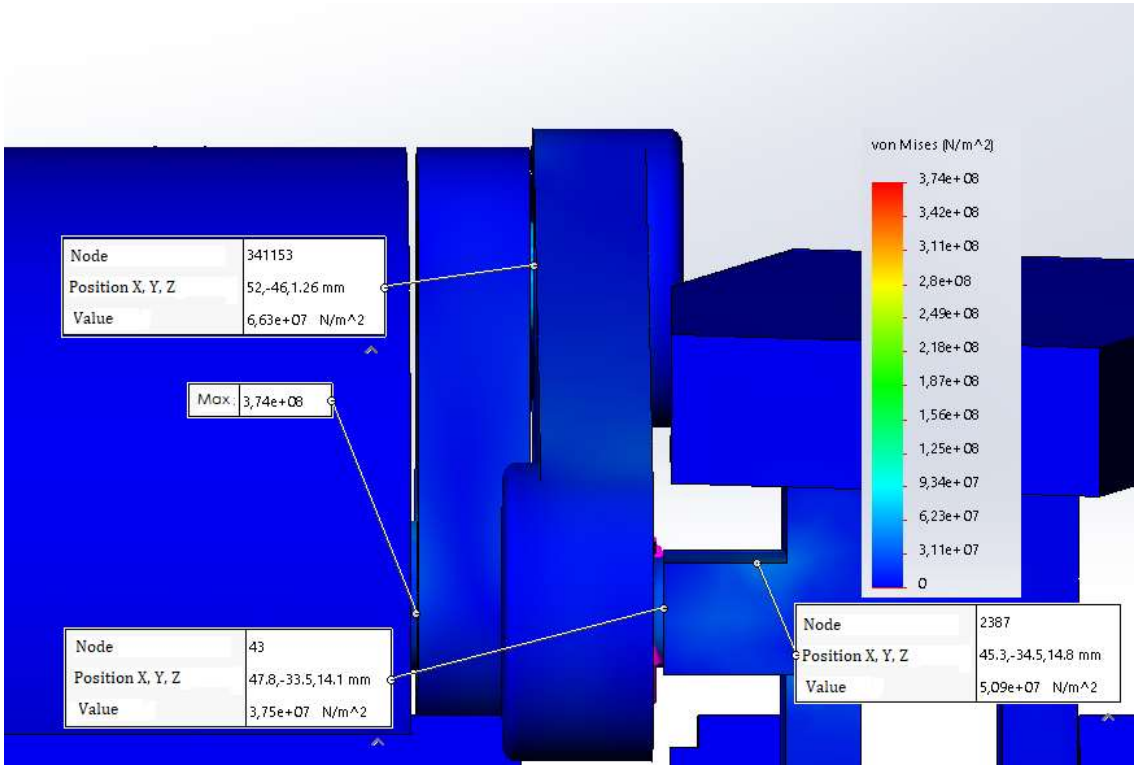

Figure 7.7. Outer linkage is stressed for perpendicular to the bottom joint 10 N at the fingertip

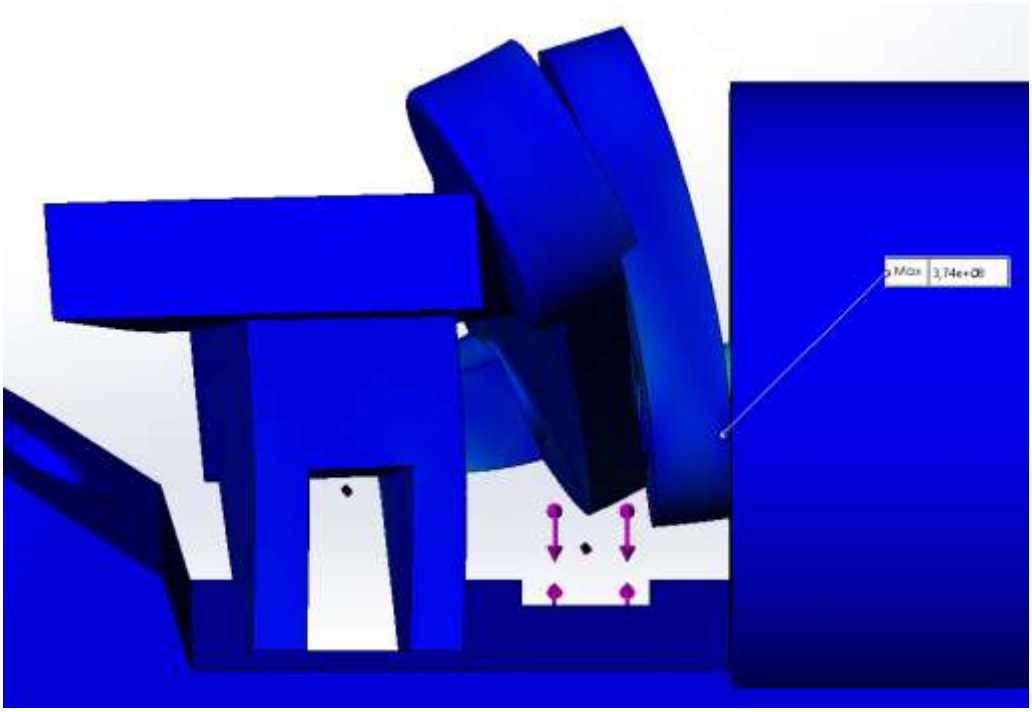

Figure 7.8. Failure of the outer linkage

Figures 7.7 and 7.8 show that driving link fails under 10 N applied to the fingertip when force orientation is perpendicular to the bottom joint. As it was expected, overstepping force limits that were set leads to the mechanism failure.

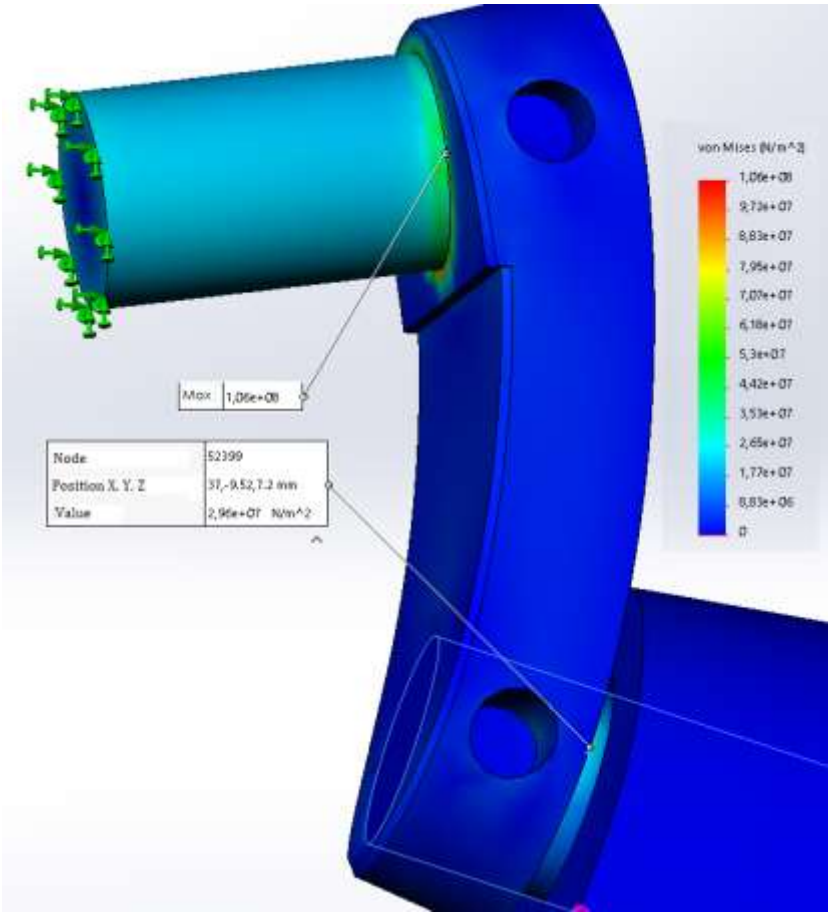

Figure 7.9. 10 N are applied vertically to the thumb's base

The smallest link in the palm raised appropriate concerns regarding its durability and stress resistance at initial stage of designing. In particular, figure 7.9 shows joint's response to vertically applied 10 N to the base of the thumb. It can be seen that performance is acceptable, considering that the metamorphic robotic hand is intended for precision grasping. Furthermore, when manipulating objects, the hand operates with its fingers looking down – this means that inertial impact of other parts of the hand will not influence the joint during, for example, secure power grasp procedure.

7.3. Summary

After major tests were performed, it is now necessary to clarify how the hand can be used. It is understandable that this design cannot be intended for heavy duty job where significant stress impact takes place, but the proposed robotic hand is able to withstand stress of 10 N at each fingertip simultaneously. This conclusion is important and defines force constrains. As chosen actuators are capable of producing 10 N force at each fingertip, this result is satisfying for many applications within the industrial sector.

For reliability increase, the following steps can be reviewed: change of material with higher properties and higher yield withstanding, outer linkage proportions increase. As an alternative, mechanism of the thumb actuation may be revised and different transmission method chosen. Inclusion of pin joints instead of bearing usage can improve the situation. It was also noted that the stress is distributed in fingers unequally, so therefore it is highly advised that the driving crank in the mechanism would be located in the center of the shaft, not on the side.

Chapter 8

Conclusions and Future Work

Designs of scientific robotic hands continue to develop, bringing new ideas and inspiration to robotics field. Identified tendencies of the subject study show that recently there were huge improvements made in terms of design. Soft robotics is very prospective area; it has attracted attention of many scientists that work today on bringing exceptional inventions. While soft robotics evolves, there is still continuous interest in solid designs with high number of DOFs. Implementation of metamorphism in solid designs is prospective and unique opportunity. Current level of actuator technologies does not allow to build efficient metamorphic solid mechanical systems with optimized size and complicated small parts, although this is a subject to changes and future will bring endless relevance to metamorphism in robotics.

As for prosthetic robotic hands that are available to public, due to the high prices of commercial products, more and more popular become low-cost designs or completely open-source models of the robotic hands that can be 3D printed. This trend may influence pricing of existing brand robotic hands and change demand/supply balance in recent future.

Conducted research has fully described properties of the proposed robotic hand, its weaknesses and overall performance. It is not possible to say that inclusion of motors into the palm is completely advantageous – there are certain disadvantages. While motion transmission using gears and linkages is better for accurate manipulations, the mechanical system becomes more vulnerable in terms of structure, weight, shape. Also, it loses compliance.

All in all, proposed design is great for small force operation and when shape of the manipulator is not essential. Metamorphism allows to produce advanced postures and hence objects of complicated shape can be manipulated. Kinematic analysis, numerical simulations and object grasping tests have discovered true nature and benefits of the robotic hand.

The proposed manipulator is able to withstand force of 10 N at each fingertip simultaneously and is considerably resistant to stress, so therefore suitable for industrial applications. However, certain elements of the design can be changed – rivet joints are suggested to replace bearings. If requirements for the manipulator are less strict in terms of force generation, it is advised that the actuators are changed for smaller ones to reduce the overall shape of the manipulator. Linear actuators with partially compliant linkages may be considered to replace gears in case if human interaction is required. The most problematic area of the design is determined to be thumb section. Hence, if the robotic hand is required to be adapted for prosthetics, integrated DC motor into the palm to control thumb should be removed due to inappropriate contribution to the shape of the hand. Nevertheless, designed hand perfectly suits industrial needs and aesthetics is not a necessity in this area. As an additional improvement, it is suggested that the thumb's outer linkage can be revised for better results and general level of design complexity should be decreased for manufacturing purposes.

As a general conclusion, developed manipulator can contribute to both industrial and prosthetics sectors, and its unique structure can serve as a ground for further advancements of robotics.

Overall, future work would involve preparing the developed hand to both markets, industrial and prosthetic. As for the second one, significant changes are implied. It would be wise to contact manufacturing companies and provide detailed schematics of the design to receive an approximate quote. Received suggestions should be reviewed and integrated if necessary.

Strategy of adapting the developed manipulator for prosthetics: 1) using 1 DOF fingers (no DC motor inside the finger), 2) using shorter gearbox (sacrifice the power and improve control of the hand as reduction will decrease) or linear actuators with compliant linkages, 3) thumb would have to be operated by a tendon approach as nothing else is unfortunately applicable. Prosthetics demands high standards of anthropomorphism.

In the end, obtained information from the conducted research would be used as a supplementary material at prototype testing stage. Once prosthetic and industrial versions of the hand are assembled, it is highly recommended that test bench would be used for final tests and design improvements. It is important to see if the robotic hands are able to provide claimed performance and correspond to international standards accepted within the field.

References

1. Wei, G. et al., 'Prehension Analysis and Manipulability of an Anthropomorphic Metamorphic Hand with a Reconfigurable Palm', *2011 IEEE International Conference on Robotics and Biomimetics*, 2011, pp. 1116-1121.
2. Norton, K. M., 'A Brief History of Prosthetics', Amputee Coalition, vol. 17, no. 7, 2007, pp.11-13.
3. Finch, J., 'The Art of Medicine: The Ancient Origins of Prosthetic Medicine', *The Lancet*, vol. 37, 2011, pp. 348–349.
4. Gemma, J., 'How Robots Conquer Industry Worldwide', International Federation of Robotics, Frankfurt, 2017.
5. Schultz, S., 'First Experiences with the Vincent Hand', *MEC 11 MyoElectric Controls/Powered Prosthetics Symposium Fredericton*, New Brunswick, University of Brunswick, 2011.
6. McCarthy, N., *Engineering: A Beginner's Guide*, Oxford, Oneworld Publications, 2012.
7. Sullivan, D., 'i-LIMB Hand wins Prosthetic Product Innovation Award', *Touch Bionics*, 1st December 2008, http://www.touchbionics.com/news-events/news/i-limb-hand-wins-prosthetic-product-innovation-award (Accessed 21st May 2018)
8. Touch Bionics, 'History', *Touch Bionics*, 2018, http://www.touchbionics.com/about/history (Accessed 21st May 2018)
9. RSLSteeper, 'Bebionic v2 Product Brochure', *RSLLIT294*, 2, 2011, pp. 1-23.
10. RSLSteeper, 'Bebionic3 Multi-Flex Wrist Technical Information', Ottobock SE & Co., Duderstadt, 2013.
11. Schultz, S., 'Vincent - Ein innovatives mehrgliedriges Finger- und Handsystem', Ortopädie-Technik, 4/11, 2011, pp. 249-255.
12. Vincent Systems, 'Vincent evolution 2', [website], 2018, http://vincentsystems.de/en/prosthetics/vincent-evolution-2/ (Accessed 21st May 2018)
13. Ottobockus., 'Fascinated. With Michelangelo – Perfect use of precision technology', Ottobock SE & Co., Duderstadt, 2014.
14. Butterfass, J., Grebenstein, M., Liu, H. and Hirzinger, G., 'DLR-Hand II: next generation of a dextrous robot hand', *IEEE International Conference on Robotics and Automation*, 1, 2001, pp. 109-114.
15. Butterfass, J. et al., 'Design and experiences with DLR hand II', *Proceedings World Automation Congress 2004*, Seville, 2004, pp. 105-110.

16. Leidner, D. and Dietrich, A., 'Rollin' Justin', *DLR Institute of Robotics and Mechatronics*, 2016.
17. Butterfass, J., 'Hand II', *DLR Institute of Robotics and Mechatronics*, 2003.
18. Liu, H. et al., 'The Modular Multisensory DLR-HIT-Hand: Hardware and Software Architecture', *IEEE/ASME Transactions on Mechatronics*, vol. 13, no. 4, 2008, pp. 461-469.
19. Liu, H. et al., 'Multisensory Five-Finger Dexterous Hand: The DLR/HIT Hand II', *IEEE/RSJ International Conference on Intelligent Robots and Systems*, 2008, pp. 3692-3697.
20. Meusel, P., 'DLR-HIT Hand II', *DLR Institute of Robotics and Mechatronics*, 2014.
21. Townsend, W., 'The BarrettHand grasper – programmably flexible part handling and assembly', *Industrial Robot: An International Journal*, vol. 27 no. 3, 2000, pp. 181-188
22. Stevens, P., 'The Expanding Options of Partial Hand Prostheses', *The O&P Edge*, April 2015, https://opedge.com/Articles/ViewArticle/2015-04_03 (Accessed 21st May 2018)
23. Advanced Arm Dynamics, 'Finger and Partial Hand Options', [website], 2018, http://armdynamics.com/pages/unique-partial-hand-options (Accessed 21st May 2018)
24. Robotiq, 'Adaptive Grippers', [website], 2018, http://robotiq.com/products/adaptive-robot-gripper/ (Accessed 21st May 2018)
25. Parra, L., 'The DEKA Arm', *BME 281 First Presentation*, 2015.
26. Hruska, J., 'FDA approves the Deka arm, the first commercial mind-controlled prosthetic arm', *ExtremeTech*, 12 May 2014, https://www.extremetech.com/extreme/182202-fda-approves-the-deka-arm-the-first-commercial-mind-controlled-prosthetic-arm (Accessed 21st May 2018)
27. Xu, Z. and Todorov, E., 'Design of a Highly Biomimetic Anthropomorphic Robotic Hand towards Artificial Limb Regeneration', *IEEE International Conference on Robotics and Automation (ICRA)*, 2016.
28. Ackerman, E., 'This Is the Most Amazing Biomimetic Anthropomorphic Robot Hand We've Ever Seen', IEEE Spectrum, 18 February 2016, http://spectrum.ieee.org/automaton/robotics/medical-robots/biomimetic-anthropomorphic-robot-hand (Accessed 21st May 2018)
29. Friedl, W., 'David's Hand', DLR Institute of Robotics and Mechatronics, 2015.
30. Guizzo, E., 'Building a Super Robust Robot Hand', IEEE Spectrum, 25 January 2011, http://spectrum.ieee.org/automaton/robotics/humanoids/dlr-super-robust-robot-hand (Accessed 21st May 2018)

31. Grebenstein et al., 'The DLR Hand Arm System', IEEE International Conference on Robotics and Automation (ICRA), Shanghai, China, 2011, pp. 3175-3182.
32. Elumotion, 'EH 2 – Elumotion Hand 2', [website], http://www.elumotion.com/index.php/portfolio/project-title-1(Accessed 21st May 2018)
33. SHUNK, 'Servo-electric 5-finger Gripping Hand SVH', [website], http://www.schunk-modular-robotics.com/en/home/products/servo-electric-5-finger-gripping-hand-svh.html (Accessed 21st May 2018)
34. King's College London, 'Multifingered Robotic Hand Lab', [website], http://nms.kcl.ac.uk/core/?page_id=2309 (Accessed 21st May 2018).
35. Dai, J. S., Wang, D. and Cui, L., 'Orientation and Workspace Analysis of the Multifingered Metamorphic Hand—Metahand', *IEEE Transactions on Robotics*, vol. 25, no. 4, 2009, pp. 942-947.
36. Palli G. et al., 'Development of robotic hands: The UB hand evolution', I*EEE/RSJ International Conference on Intelligent Robots and Systems*, Vilamoura, 2012, pp. 5456-5457.
37. Homberg, B. S. et al., 'Haptic Identification of Objects using a Modular Soft Robotic Gripper', *IEEE/RSJ International Conference on Intelligent Robots and Systems (IROS)*, 2015, pp. 1698-1705.
38. Diemel, R. and Brock, O., 'A Novel Type of Compliant, Underactuated Robotic Hand for Dexterous Grasping', *The International Journal of Robotics Research*, vol. 35, no. 1-3, 2015, pp. 161-185.
39. Diemel, R. and Brock, O., 'A Novel Type of Compliant, Underactuated Robotic Hand for Dexterous Grasping', *The International Journal of Robotics Research*, vol. 35, no. 1-3, 2015, pp. 161-185.
40. Wei, G. et al., 'DEXDEB - application of DEXtrous robotic hands for DEBoning operation', *Springer Tracts in Advanced Robotics*, 2014, pp. 217-235.
41. Lovchik, S. C. and Diftler, M. A., 'The Robonaut hand: a dexterous robot hand for space' *Proceedings 1999 IEEE International Conference on Robotics and Automation*, vol. 2, 1999, pp. 907-912.
42. Bridgwater, L. B. et al., 'The Robonaut 2 Hand – Designed To Do Work With Tools', 2012 IEEE International Conference on Robotics and Automation, Saint Paul, MN, 2012, pp. 3425-3430.

43. Melchiorri, C. et al., 'Development of the UB Hand IV: Overview of Design Solutions and Enabling Technologies', IEEE Robotics & Automation Magazine, vol. 20, no. 3, 2013, pp. 72-81.
44. SSSA, 'D5.20: First robot hand development', *CogLaboration*, 2012.
45. Cipriani, C., Controzzi, M. and Carrozza, M. C., 'The SmartHand transradial prosthesis', *Journal of NeuroEngineering and Rehabilitation*, vol.8, 2011, doi: 10.1186/1743-0003-8-29.
46. Shadow Robot Company, 'Shadow Dexterous Hand E1 Series', *Shadow Dexterous Hand Technical Specification*, 2013.
47. Buckley, D., 'Hand research', [website], 2012, http://www.davidbuckley.net/RS/HandResearch.htm#shadow (Accessed 21st May 2018)
48. Reichel, M., 'Transformation of Shadow Dextrous Hand and Shadow Finger Test Unit from Prototype to Product for Intelligent Manipulation and Grasping', *International Conference on Intelligent Manipulation and Grasping*, 2004.
49. Quote with tech. specs and pricing issued in August 2009. Ref.Number:P-DH-200908
50. Sivakumar, K. and Priyanka Ch., 'Grasping Objects Using Shadow Dexterous Hand with Tactile Feedback', *IJIRSET*, vol. 4, no. 5, 2015, pp. 3108-3116.
51. Shigley, J. E. and Mischke, C. R., *Standard Handbook of Machine Design*, 2nd edn., New York, McGraw-Hill, 1996.
52. Budynas, R. G. and Nisbett, K. J., *Shigley's Mechanical Engineering Design*, 10th edn., New York, McGraw-Hill Education, 2015.
53. Gordon, C. C. et. al., *1988 Anthropometric Survey of U.S. Personnel: Summary Statistics Interim Report*, Anthropology Research Project, Inc., Ohio, 1989.
54. Methot, J., Chinchalkar, S. J. and Richards, R. S., 'Contribution of the ulnar digits to grip strength', *The Canadian Journal of Plastic Surgery*, vol.18, e10-e14, 2010.
55. Siciliano, B. et al., *Robotics: Modelling, Planning and Control*, London, Springer-Verlag London Ltd, 2010.
56. Craig, J., *Introduction to robotics: Mechanics and control*, 3rd edn., New Jersey, Pearson/Prentice Hall, 2004.
57. Siciliano, B. et al., *Robotics: Modelling, Planning and Control*, London, Springer-Verlag London Ltd, 2010.
58. Craig, J., *Introduction to robotics: Mechanics and control*, 3rd edn., New Jersey, Pearson/Prentice Hall, 2004, p. 68.

59. Gallardo-Alvarado, J., 'Kinematics by means of screw theory', *Multibody System Dynamics*, vol.14, no. 3-4, pp. 345-366.
60. Huang, Z. et al., *Theory of Parallel Mechanisms*, 2013.
61. Jia, Y-B., 'Problem Solving Techniques for Applied Computer Science', *Com S 477/577*, Iowa State University, 2017.
62. Huang, Z. et al., *Theory of Parallel Mechanisms*, 2013.
63. Kumar, V., 'Background, Twists in Kinematics and Wrenches in Statics*', ASME DETC 1998*, 1998.
64. J.Gallardo-Alvarado, *Kinematic Analysis of Parallel Manipulators by Algebraic Screw Theory*, Springer International Publishing, Switzerland, 2006.
65. Gallardo-Alvarado, J., 'Kinematics by means of screw theory', *Multibody System Dynamics*, vol.14, no. 3-4, p. 349.
66. Craig, J., *Introduction to robotics: Mechanics and control*, 3rd edn., New Jersey, Pearson/Prentice Hall, 2004, pp. 173-176.
67. Meredith, M. and Maddock, S., *Real-Time Inverse Kinematics: The Return of the Jacobian*, 2004.
68. Jazar, R. N., *Theory of Applied Robotics*, 2nd edn., Springer Science & Business Media, London, 2010.
69. McCarthy, J. M. and Soh, G. S., *Geometric Design of Linkages*, Springer Science & Business Media, London, 2011.
70. Tsai, L. W., *Robot Analysis: The Mechanics of Serial and Parallel Manipulators*, John Wiley & Sons, New Jersey, 1999.
71. Howard, D., *BEng Dynamics handout*, University of Salford, UK, 2015.
72. Zhu, H., 'Motion Trajectory Planning and Simulation of 6- DOF Manipulator Arm Robot', *Academic Journal of Manufacturing Engineering*, vol. 15(3), 2013.
73. Lynch, K.M. and Park, F. C., *Modern Robotics. Mechanics, Planning, and Control*, Cambridge, Cambridge University Press, 2017.
74. Bakshi, U. A. and Bakshi V. U., *Principles of Control Systems*, Pune, Technical Publications Pune TM, 2009.

Appendix

Version 2 (Different method with the same result). Part of Kinematics position derivation:

$$A\cos x + B\sin x = C$$

$$A\cos x + B\sqrt{1-\cos^2 x} = C \;\rightarrow\; \text{^2}$$

$$A^2\cos^2 x + 2AB\cos x\sin x + B^2 - B^2\cos^2 x = C^2 \;\rightarrow : \cos^2 x$$

$$A^2 + \frac{2AB\sin x}{\cos x} + \frac{B^2}{\cos^2 x} - B^2 = \frac{\mathrm{C}^2}{\cos^2 x}$$

$$A^2 - B^2 + 2AB\tan x = \frac{\mathrm{C}^2}{\cos^2 x} - \frac{B^2}{\cos^2 x}$$

$$A^2 - B^2 + 2AB\tan x = (\mathrm{C}^2 - B^2)\frac{1}{\cos^2 x}$$

$$A^2 - B^2 + 2AB\tan x = (\mathrm{C}^2 - B^2)(1+\tan^2 x)$$

$$A^2 - B^2 + 2AB\tan x = \mathrm{C}^2 + \mathrm{C}^2\tan^2 x - B^2 - B^2\tan^2 x$$

$$A^2 + 2AB\tan x = \mathrm{C}^2 + \mathrm{C}^2\tan^2 x - B^2\tan^2 x$$

$$\mathrm{C}^2\tan^2 x - B^2\tan^2 x - 2AB\tan x + C^2 - A^2 = 0$$

$$(\mathrm{C}^2 - B^2)\tan^2 x - (2AB)\tan x + (C^2 - A^2) = 0$$

$$Let\ A' = \mathrm{C}^2 - B^2,\ B' = -2AB,\ C' = C^2 - A^2$$

$$A'\tan^2 x + B'\tan x + C' = 0$$

$$\tan_{1.2} x = \frac{-B' \pm \sqrt{B'^2 - 4A'C'}}{2A'}$$

$$\tan_{1.2} x = \frac{2AB \pm \sqrt{4A^2B^2 - 4(C^2 - B^2)(C^2 - A^2)}}{2(C^2 - B^2)}$$

$$\tan_{1.2} x = \frac{2AB \pm \sqrt{4A^2B^2 - 4C^4 + 4C^2A^2 - 4A^2B^2 + 4B^2C^2}}{2(C^2 - B^2)}$$

$$\tan_{1.2} x = \frac{2AB \pm \sqrt{4C^2(C^2 + A^2 + B^2)}}{2(C^2 - B^2)}$$

$$\tan_{1.2} x = \frac{2AB \pm 2C\sqrt{C^2 + A^2 + B^2}}{2(C^2 - B^2)}$$

$$x_{1,2} = \tan^{-1}\left(\frac{AB \pm C\sqrt{C^2 + A^2 + B^2}}{(C^2 - B^2)}\right)$$

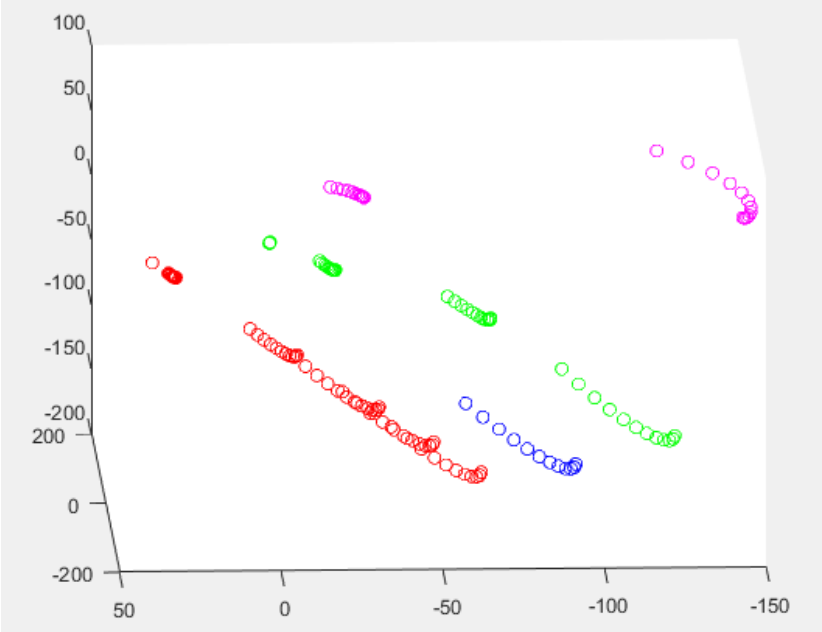

Figure 9.1. Fingertips can be tracked. Pink for thumb, green for index finger, blue and red for middle and ring fingers respectively

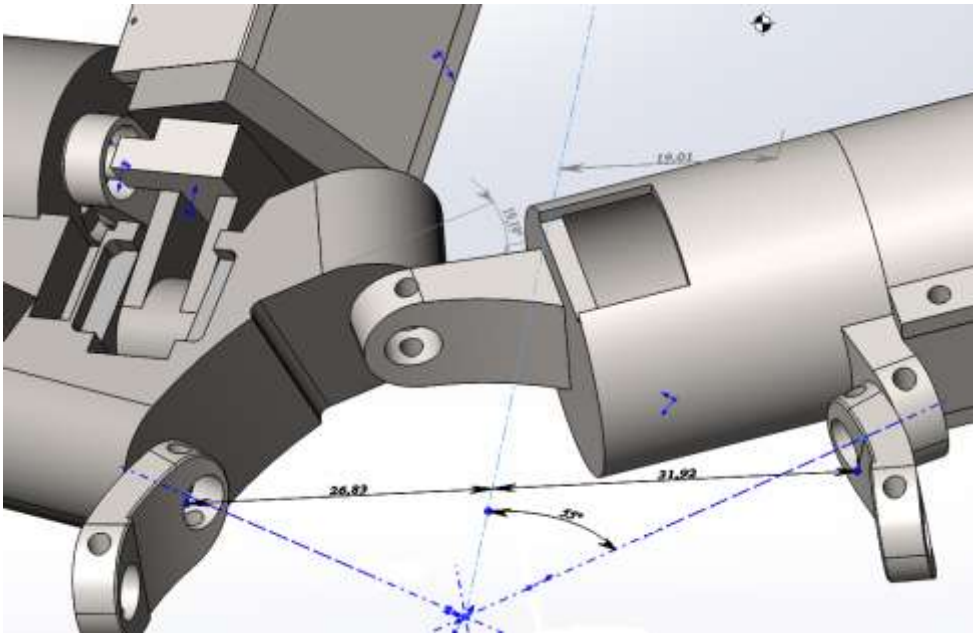

Figure 9.2. Theta 3 is 19.19 deg

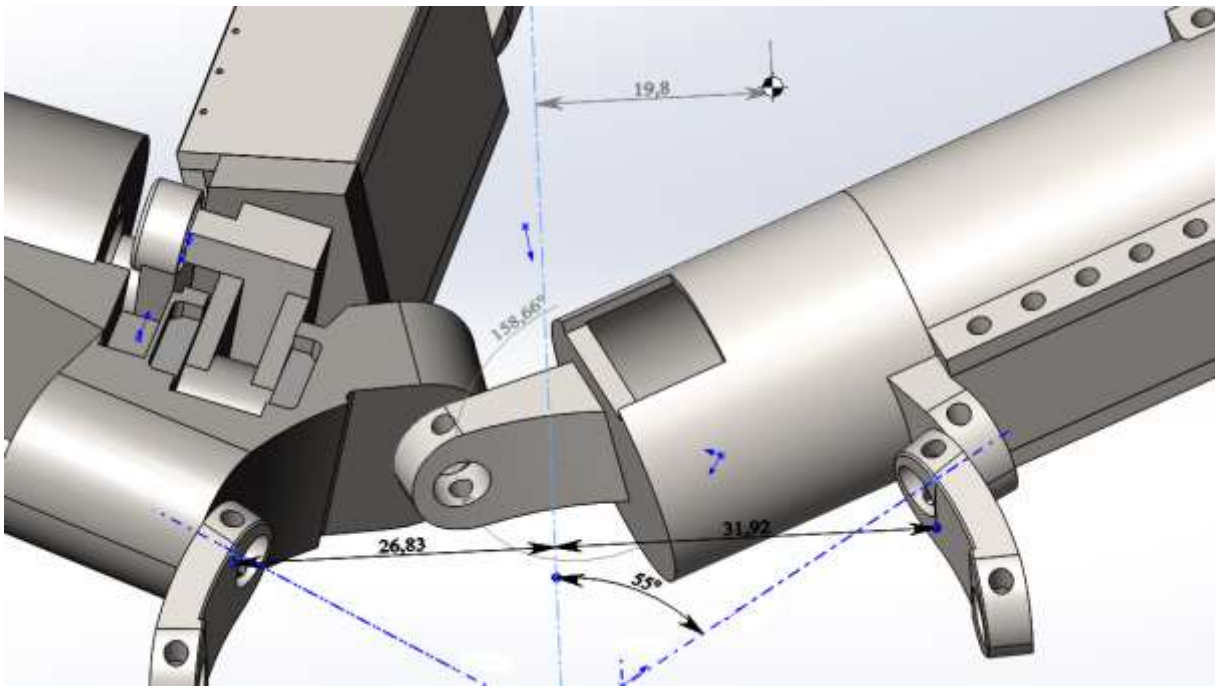

Figure 9.3. Theta 3 is -21.34 deg

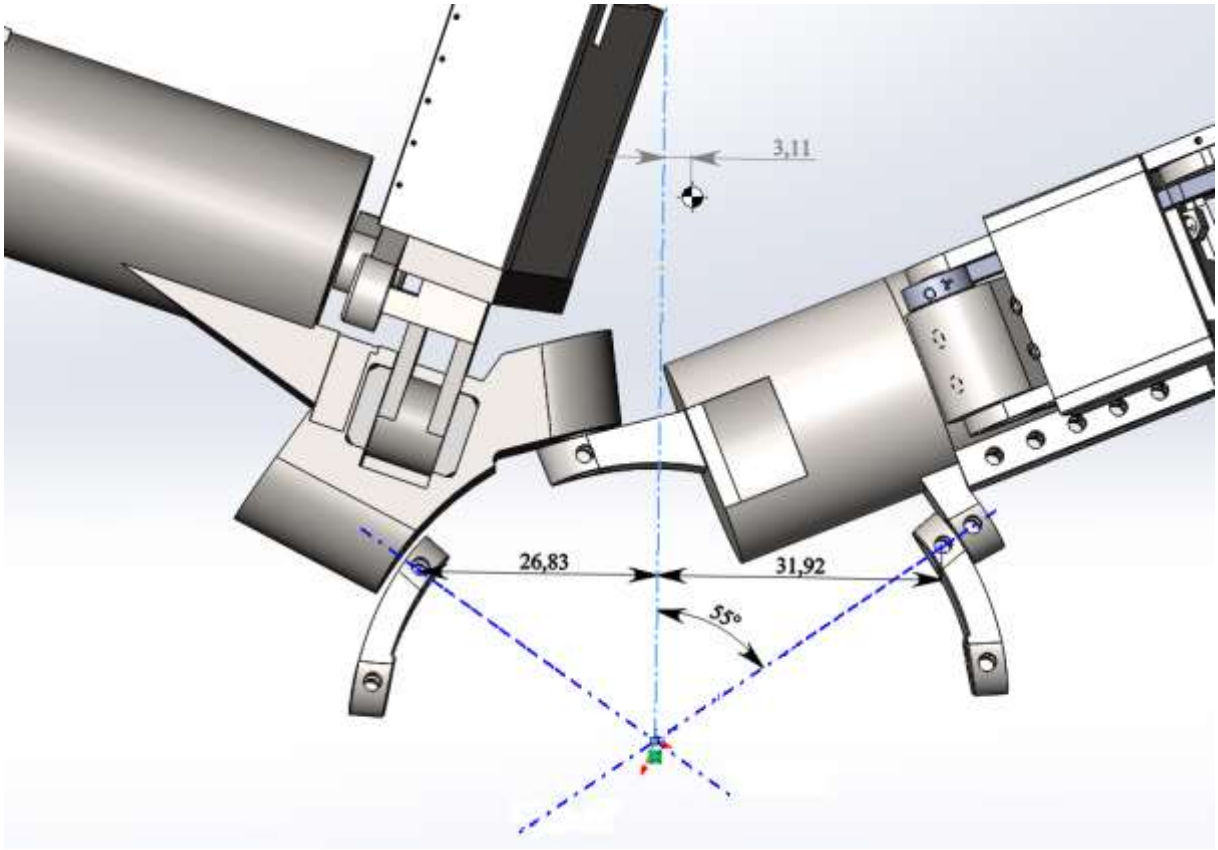

Figure 9.4. Only index is bent

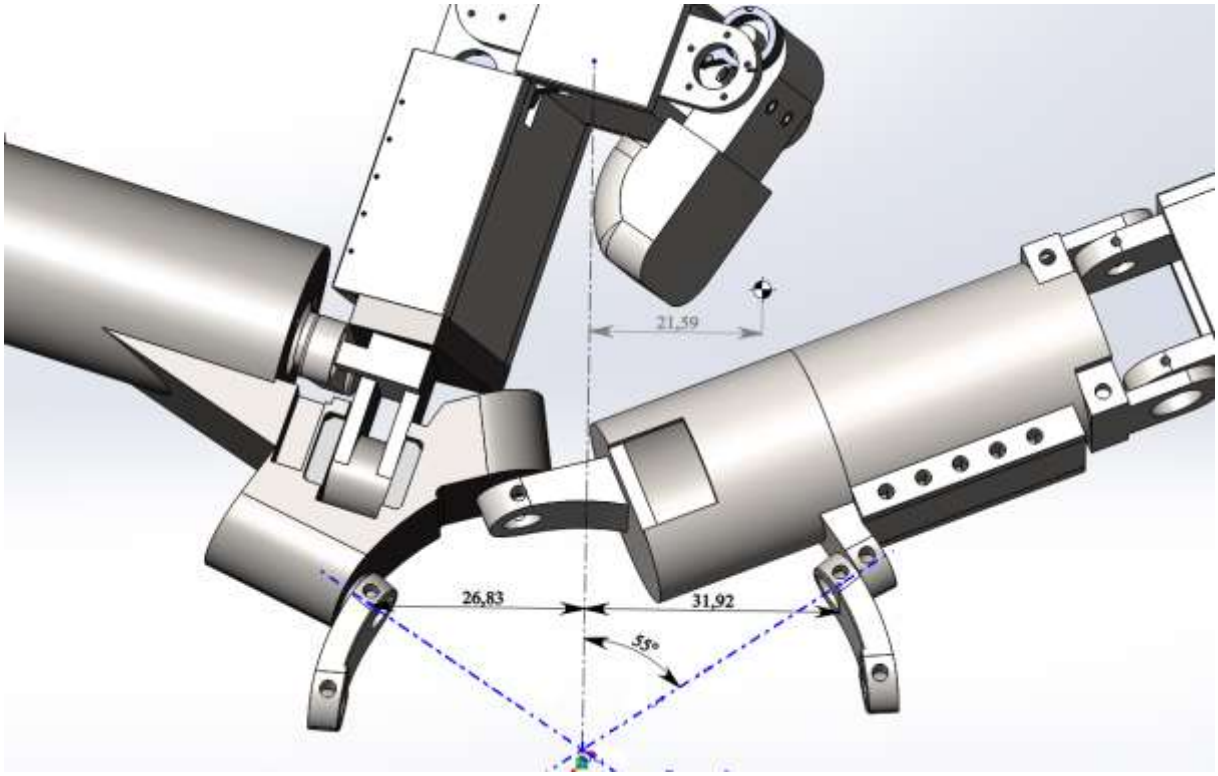

Figure 9.5. Only thumb is bent